Microfluidic Digital ELISA Towards Single Cell Analysis

By
Divya Jyothi Lella
M.S., University of Kansas 2017
M.S., Western Kentucky University, 2014
B.S., Osmania University, India, 2008

Submitted to the graduate degree program in Chemistry and the Graduate Faculty of the University of Kansas in partial fulfillment of the requirements for the degree of Master of Science.

_____

Chair: Dr. Yong Zeng

_____

Dr. Michael Johnson

_____

Dr. Liang Xu

Date Defended: November 28th, 2017

The thesis committee for Divya Jyothi Lella certifies that this is the approved version of the following thesis:

Microfluidic Digital ELISA Towards Single Cell Analysis

Chair: Dr. Yong Zeng

Date Approved: November 28th, 2017

Abstract

Cell-to-cell heterogeneity predicts a multitude of functions for homeostasis and development of disease states. These minute variations can make a massive impact in understanding the main components involved in a disease such as cancer. Tracking the protein expression in single cells is in great need as they enable the study of heterogeneous behaviors, but the main challenges are the requirement of the methodologies that are sensitive enough to detect low copy number of protein molecules within a wide dynamic range. Low copy proteins cannot be neglected as they can provide information about the phenotypic responses involved. Moreover, traditional analog methods are not suitable for detecting such small numbers as they give an average measurement, differentiating unique cells and quantifying population distributions would be problematic. Digital immunoassays have emerged as a robust technology for ultrasensitive detection of proteins. Here we engineered a multiplexed microfluidic digital ELISA platform with microarray structures for analyzing multiple proteins with low sample volume and high sensitivity. Cross communication between individual reactions, diffusing of reagents into bulk solutions and evaporation of solvents could be critical. To address this concern, we have developed a portable, automated instrument for sealing the microwells in the chambers with high pressure for conducting chemi- fluorescent reactions with increased resolution and sensitivity.

With our developed platform, we can detect up to 15 biomarkers. We also applied our digital platforms for the detection of PSA aptamer with biotinylated lectins.

Dedication

To my family for their unconditional support through my entire life and during the pursuit of this dream. Your love and encouragement helped me to make this dream a reality.

To the Department of Chemistry, University of Kansas for all the support.

Acknowledgements

First and foremost, I would like to acknowledge everyone who has contributed to this body of work and helped me mold the person I am today, I would be remiss if I did not recognize a number of individuals.

I would like to thank my advisor, Dr. Yong Zeng for his all-time support and mentorship during this journey. Through thoughtful discussion, Dr. Zeng has motivated me to think critically, developing my ability to analyze and interpret data, as well as equipped me with the knowledge and understanding to develop sound ideas. Because of his mentorship, I am a better scientist, and I'm truly grateful for him. I would like to thank my thesis defense committee members, Dr. Michael Johnson and Dr. Liang Xu for your continued support and assistance in fulfilling my goal and I am very thankful for your dedication and time.

I would like to thank my colleagues, past and present, from the Dr. Zeng research group, Dr. Yuqin Shang, Dr. Peng Zhang, Dr. Hongmei Cao, Dr. Xiaoni Fang, Yang Yang, Xin Zhou, Alexander Kolomaya, and Nick.

Thank you to my family my parents and in-laws for their constant outpouring of love and encouragement during this journey. You all have been my biggest cheerleaders, and I am so grateful for each of you. Last, but certainly not least, I would like to thank my amazing husband, Gangadhar Vuppuluri for being a constant source of strength during this moment in my life. I could not have made it to this point without you by my side. Words could never express how thankful I am for you, for your dedication and love surpasses all understanding. I would like to thank my dearest friends Aishwarya Neti, Yogitha Movva, Dr. Swathi Reddy Pullagurla for their continuous support throughout my journey.

Table of Contents

List of Tables

List of Figures

Chapter 1

1. Introduction

1.1. Background and Significance

Cancer is a leading health issue all over the world mainly, United States. In 2017, there will be an estimated new cancer cases of about 1,688,780 diagnosed and 600,920 cancer deaths in the US.[1] This figure is ascending, as competing causes of death diminish in importance. The fundamental abnormality for the development and growth of cancer is the continuous unregulated proliferation of cancer cells.[2] Usually under normal conditions, cells respond appropriately to the signals that control the cell behavior whereas, cancer cells grow and divide in an uncontrolled manner, invading normal tissues and organs and ultimately spreading throughout the body as shown in Figure 1.[3] The induced loss of growth control shown by cancer cells is the result of accumulated abnormalities in multiple regulatory systems and is reflected in various aspects of cell behavior that can distinguish cancer cells from the normal cells.[4] Most cancers, are mainly associated with poor prognosis due to the asymptomatic nature of the disease, and late diagnosis, thus composing patient care and therapeutic outcome. Therefore, well established and accurate approaches for timely diagnosis of the disease both at early and advanced stages are critical to better assess treatment options, and saving lives. A key challenge in cancer control and prevention is detection of the disease as early as possible, enabling effective interventions and therapies to contribute to reduction in mortality and morbidity.[5]

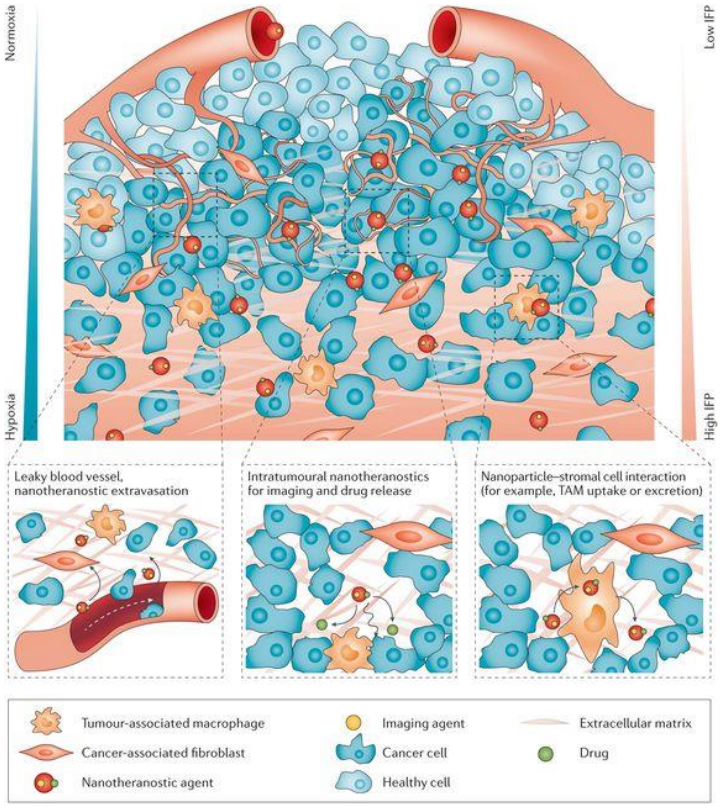

Figure 1: Growth of normal cells vs cancer cells[6]

1.2.Biomarkers

Concentrations of certain biomolecules usually increase in the body during the formation of cancer. These biomolecules, are referred as biomarkers, which need to be accurately measured to detect specific diseases at early stage for better and more decisive prognosis.[7] Biomarkers are important molecular signposts of the physiological state of a cell at a specific time. As a normal cell progresses through the complex pathways of transformation to a cancerous state, biomarkers could provide vital information for the identification of early cancer and people at risk of developing cancer.[8] Identification and detection of cancer by pathological techniques are possible only on microscopic examination of the tumor tissue, long after disease onset. Although these techniques are important for prediction of tumor behavior and prognosis, additional methods are necessary for early detection as shown in Figure 2.[9]

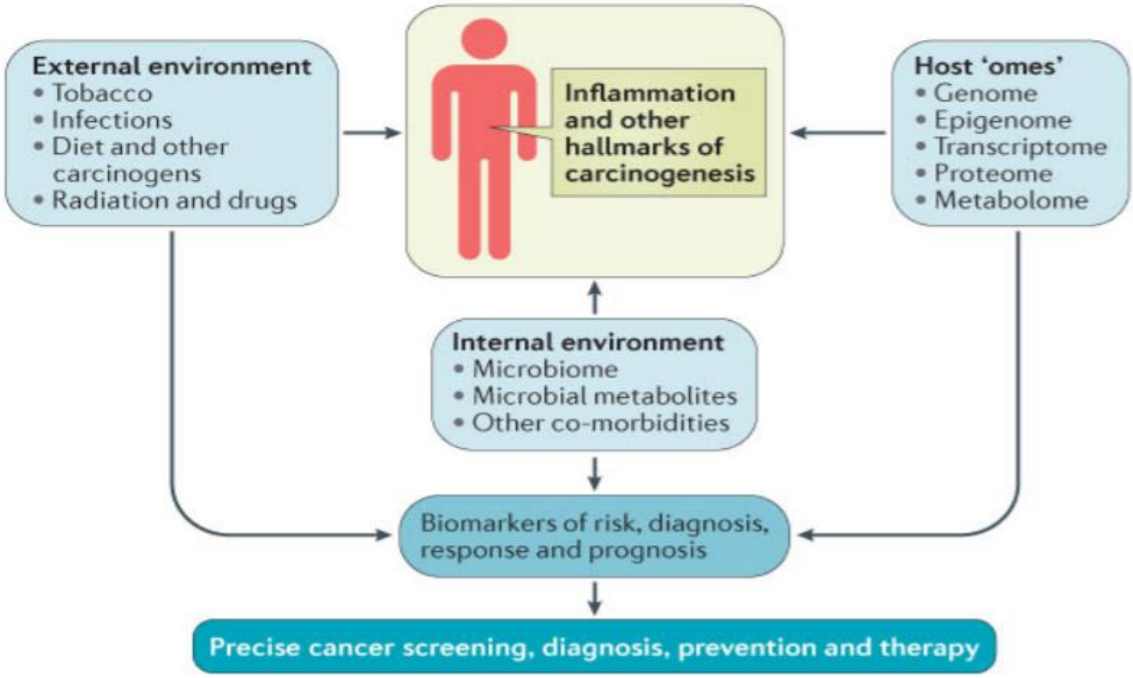

Figure 2: Role of biomarkers for early detection of diseases.[9]

The usefulness of a biomarker lies in its ability to provide early indication of disease or the progression of the disease.[10] Biomarkers should be easy to detect, measurable across populations, and amenable to use in one or more of the following settings: detection at an early stage; identification of high-risk individuals; early detection of recurrence; or as intermediate endpoints in chemoprevention. Many secreted proteins are over-expressed in the blood at very early stages of developing cancers, prior to any possible physical symptoms. Levels of these secreted proteins can indicate the presence or absence of disease. In certain cases, these levels can indicate the stage of cancer as well, and guide therapy.[11-12] These biomarker proteins are usually specific to distinct cancers but do not have high predictive values. For example, prostate specific antigen (PSA), a well-known FDA approved and first clinically used single biomarker protein for prostate cancer has a positive predictive value of ~70%. While this can detect the cancer, it has nonetheless the

potential to detect false positives, and consequently un-required medical treatments and stress. Therefore, it is required to detect cancer with a panel of biomarker proteins specific to that cancer for point-of-care diagnosis and better understanding of the disease.[13]Measuring biomarkers in blood or serum provides essential information that allows prognosis and management of diseases. Moreover, the possibility of detection of low biomarker concentrations allows early diagnosis and plays a key role in increasing the survival rates of the patients. The biomarkers that are most widely used are either nucleic acids or proteins. They can show high abundance in the primary affected organ, but they become diluted when they spread into the body or blood stream, like in the case of cancer.[14] Detection of a disease starting from a blood or serum sample is therefore often the preferred option. There are various proteomic technologies for identifying the cancer biomarkers like mass spectrometry, two-dimensional electrophoresis and many other techniques, but they suffer limitations like sample volume, assay time and sensitivity. On the other hand, having low blood sample consumption is also important, but evidently detecting rare biomarkers in small sample volumes requires techniques with high sensitivity as shown in Figure 3.[11]

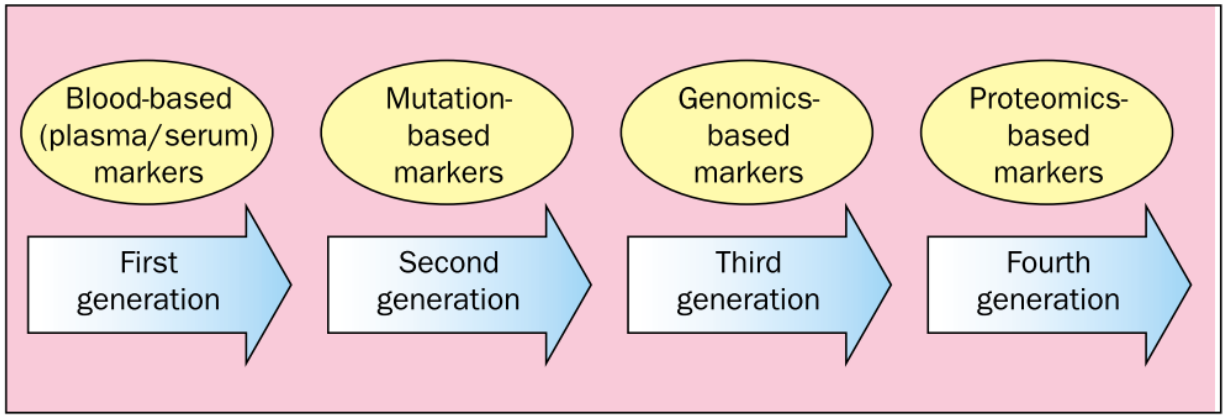

Figure 3:Evolution of biomarkers from first generation to fourth generation.[8]

1.3.Immunoassays

Immunoassays are mainly used for the quantification of proteins and small molecules in many different fields such as medical diagnostics, proteomics, pharmaceutical research and biological research.[15] Immunoassays were classified into main two types: heterogeneous and homogeneous. In heterogeneous immunoassays, antibodies are first immobilized on a solid support and then the antigen interacts at the boundary layer. With the help of this format, unbound antibodies and other reagents can be easily washed. In homogenous immunoassays, the capture antibodies interact with antigens in solution. In this case, the bound and unbound antibodies are differentiated based on physical or chemical changes forming from the binding event. Immunoassays are used to detect target proteins based on the specific interaction and complex formation between a target antigen (Ag) and an antibody (Ab), the latter being an immunoglobulin (Ig) with specific binding sites for the Ag.[16] There are diverse types of assays such as direct, indirect and sandwich based assays. Among them sandwich immunoassays are the most widely used assay formats for protein analysis. In these type of assays, the target Ag is 'sandwiched' between two types of Abs, which are often called capture and detection Ab (cAb and dAb), respectively. In a sandwich immunoassay, first cAbs are immobilized on a substrate, after which the substrate is treated with blocking reagents like bovine serum albumin (BSA) to eliminate non-specific adsorption of molecules and increase the assay selectivity. Afterwards, the cAbs are exposed to an Ag-containing sample solution, after which the formed cAb–Ag complexes are incubated with the dAbs. After formation of the sandwich complex, antigens are detected to labels present on the dAbs. Sometimes, instead of a single dAb, a primary Ab that is specific to the Ag is applied, followed by a secondary Ab that is linked to the detection label as shown in Figure 4.[15]

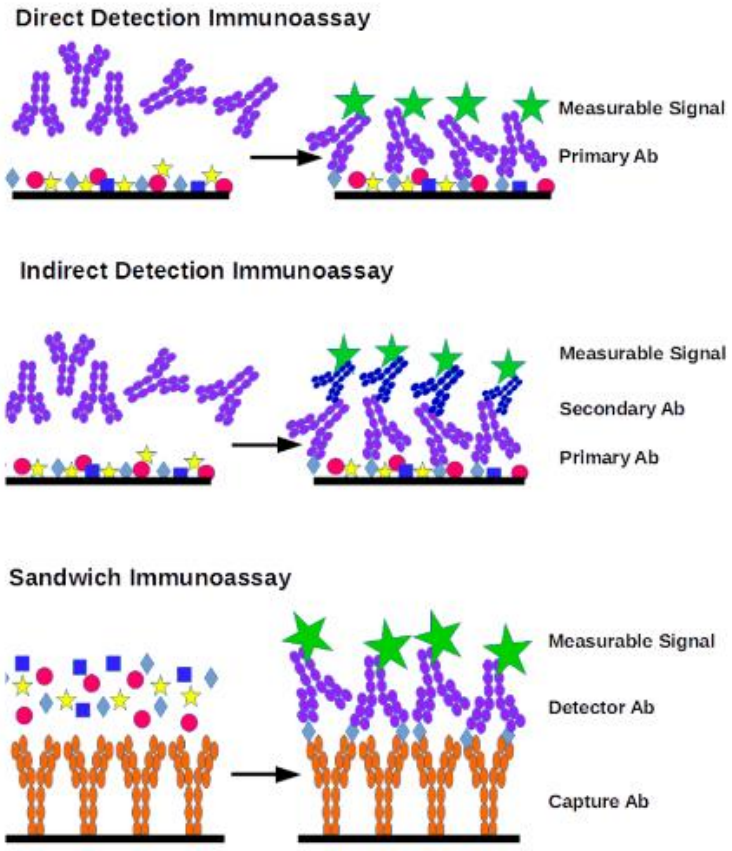

Figure 4: Distinct types of immunoassays: Direct detection, indirect detection and sandwich immunoassays.[15]

Fully automated immunoassay systems represent the gold standard for in vitro diagnostics currently, but at the same time there are several drawbacks that limit their effectiveness in practical use. One drawback is the requirement of large sample volumes, which limits their clinical practical utility. For example, in disease diagnostics, it would be ideal to use a single sample of a patient's serum for studying many different disease markers. But, this can pose problems when 100-200 µL of sample is required for each specific test. Another drawback is the time and cost required for each assay.[15] Analysis can take up to several hours because analyte molecules must diffuse across long distances before they encounter antibodies on the solid phase. Consequently, these

instruments are only feasible in centralized facilities such as hospital reference laboratories, to which samples are transported after collection. Conventional immunoassays are time- and resource-consuming, particularly when extensive automation is not economically beneficial or when portability becomes a predominant requirement. Consequently, there has been a sustained effort in the past decade to develop reliable diagnostic tools while reducing the complexity and associated costs of such assays. With the growing cost of health care, there is a need for decentralized immunodiagnostic tools capable of providing fast, quantitative results in the clinic or at the bedside.[17] The availability of such tools can enable early diagnosis, decrease hospital stays, and eliminate transportation and administrative expenses. The need for decentralized immunodiagnostics has prompted the development of portable assays, and many researchers addressed this challenge by miniaturizing immunoassays using microfluidics. However, to date, a very few number of microfluidic systems have achieved fast, parallel, and highly sensitive detection of biomedically relevant proteins using a single fully functional microfluidic chip.[18]

1.4 Microfluidic Platforms

Microfluidics is the science and engineering of manipulating and controlling the flow of fluids and particles at micron and submicron dimensions. Since its origins in the early 1990s, about when microscale analytical chemistry techniques were gaining popularity and microelectronic technology began to be recognized to fabricate the miniaturized chromatographic and capillary electrophoresis systems, microfluidics has grown tremendously fast and sustained by the promise to revolutionize the conventional laboratory handling, processing, and analytical techniques.[19]While there are many obvious potential applications for microfluidics to significantly reduce sample volumes and to carry out reaction, separation, and detection quickly and sensitively. The main driving force behind the rapid development of microfluidic systems has been its future

to be exploited for a wide range of biological applications such as high-throughput drug screening, single cell or molecule analysis and manipulation, drug delivery and advanced therapeutics, bio sensing, and point-of care diagnostics as shown in Figure 5.[20] The bias in the development of microfluidic devices toward biological-related applications has arisen, due to the search for a cost effective tool that can be imposed as a first user to mitigate the risks and costs associated with the attempt to introduce any modern technology into the commercial market. The need for decentralized immunodiagnostics has been prompted the development of portable assays, and many researchers addressed this challenge by miniaturizing immunoassays using microfluidics. The most common microfluidic paradigm relies on networks of enclosed micron dimension channels. At these small scales, fluids exhibit laminar flow—i.e., fluidic streams flow parallel to each other and mixing occurs only by diffusion.[21] Miniaturizing immunoassays using microfluidics offer at least three main advantages over conventional available methods: (1) The smaller dimensions of microfluidics can often reduce the diffusion times, which result in faster analysis. (2) The small volume of samples used in microfluidics reduces the consumption of expensive reagents and valuable samples, and make it compatible with blood samples, eliminating the need for phlebotomist and lowering the cost per assay. (3) The fluid handling in microfluidic channels can be automated with simple, compact instrumentation, reducing the size and operating cost of test equipment. These advantages can potentially upgrade the clinical utility of automated immunoassays while making them more feasible in a decentralized near-patient setting.[22]

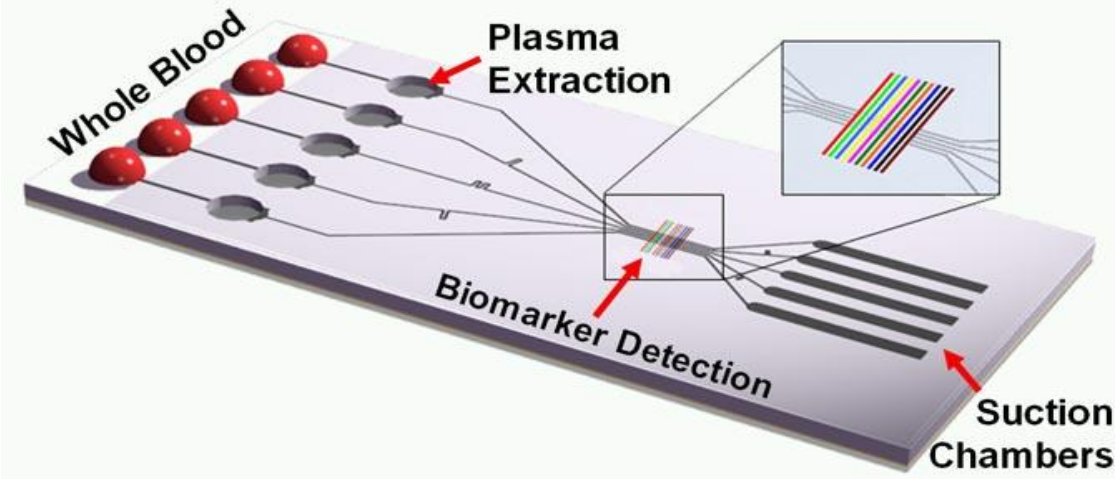

Figure 5: A microfluidic device for point of care diagnostics[23]

However, from a physics point of view, there are several unique features of microfluidic systems, which can distinguish them from their macro-scale counterparts. For instance, the motion of liquid that we typically observe at the macro-scale, such as the flow of water in a river, is largely influenced by inertial forces. On the other hand, the physical fluid phenomena that can be observed in micro-meter to nano-meter scale conduits are different. In such a small scale, liquid transport is mostly governed by viscous forces rather than inertial forces.[24] By taking advantage of this inherent effect, the precise control of 10^{-9} to 10^{-18} liters of liquid in fluidic channels can be performed via electro kinetic effects such as electro-osmosis and electrophoresis.[25] For the fabrication of microfluidic devices, chemistry has been playing the leading role. Traditionally, silicon was the material used for the fabrication of microfluidic devices since micro-fabrication techniques were well established in the semiconductor industry. With advances in material chemistry, scientists today can prepare these devices on glass and polymer substrates using photolithography and soft lithography, respectively, with significantly less effort. Even paper-based fluidic channels have been recently reported that can cost only a few pennies to develop.[26] Chemistry based advances have been essential not only for easier fabrication of the devices but

also for taking more reliable and sensitive quantitative measurements on them. Fluorescence measurement is the most standard one on microfluidic systems although other spectrophotometric techniques such as UV-Vis, FT-IR, and Raman spectroscopy have been also demonstrated on this platform. In addition, electrochemical (coulometry, amperometry voltammetry) and mass spectrometric analyses can be applied to microfluidic devices which makes it a very versatile analytical tool to work with.[27]

1.5 Brief Summary of this dissertation

This thesis is composed of four chapters that focus in two different microfluidic research areas: designing microfluidic devices with two layers, developing chip-based digital enzyme-linked immunosorbent assays (ELISAs) and exploiting their applications for detection of ultrasensitive proteins. For performing a digital immunoassay on a microfluidic device, a sample must be transported in a microchannel by using a separate component such as a pump. While connecting an external pumping system to the device may be the simplest way for introducing solution into a channel. Sealing the microwells is an important parameter for obtaining a digital signal. [28]Thus, it is usually desirable to fabricate a microarray and seal it efficiently, and *Chapter 2* describes the development of such microfluidic devices with microwell compartments and an instrument for sealing the microwells. The application of a microfluidic channel for an enzyme-linked immunosorbent assay (ELISA) is another research area that we have focused on. An ELISA is one of the most standard laboratory techniques in bio-medical fields for the identification and quantitation of antigens or antibodies. While ELISAs are typically performed on a plastic microtiter plate (96 well plate), there are many advantages of carrying out the assays on the microfluidic platform. As an example, using an electric field, it is possible to transport analyte molecules to a specific area within a microfluidic channel and increase the analyte concentration

at the location.[28] We also designed and demonstrated an automated sealing instrument which involved a actuator with stroke length of 25mm, for sealing the femtoliter microcompartments for the digital detection of multiple biomarkers without cross contamination between the microwell compartments. Multiplexed digital ELISAs were also performed on our developed microfluidic devices. *Chapter 3* presents the adaptation of the microfluidic digital assay for sensitive glycoprofiling of cancer biomarkers based on aptamer lectin sandwich assays. This involved the detection of various PSA glycosylation sites with different biotinylated lectins that are specific to the glycans. Finally, in *Chapter 4* future work was discussed which involved the basic design of a microfluidic device and different methods for capturing single cells.

1.6 References

1. Siegel, R. L.; Miller, K. D.; Jemal, A., Cancer statistics, 2017. *CA: A Cancer Journal for Clinicians* **2017,** *67* (1), 7-30.
2. Navin, N. E., Cancer genomics: one cell at a time. *Genome Biology* **2014,** *15* (8), 452.
3. Khan, I.; Steeg, P. S., Metastasis suppressors: functional pathways. *Lab Invest* **2017**.
4. Klein, S.; McCormick, F.; Levitzki, A., Killing time for cancer cells. **2005,** *5*, 573.
5. David, A. R.; Zimmerman, M. R., Cancer: an old disease, a new disease or something in between? **2010,** *10*, 728.
6. Chen, H.; Zhang, W.; Zhu, G.; Xie, J.; Chen, X., Rethinking cancer nanotheranostics. **2017,** *2*, 17024.
7. Ludwig, J. A.; Weinstein, J. N., Biomarkers in Cancer Staging, Prognosis and Treatment Selection. **2005,** *5*, 845.
8. Srinivas, P. R.; Kramer, B. S.; Srivastava, S., Trends in biomarker research for cancer detection. *The Lancet Oncology* **2001,** *2* (11), 698-704.
9. Vargas, A. J.; Harris, C. C., Biomarker development in the precision medicine era: lung cancer as a case study. **2016,** *16*, 525.
10. Manne, U.; Srivastava, R.-G.; Srivastava, S., Keynote review: Recent advances in biomarkers for cancer diagnosis and treatment. *Drug Discovery Today* **2005,** *10* (14), 965-976.
11. Hawkridge, A. M.; Muddiman, D. C., Mass Spectrometry–Based Biomarker Discovery: Toward a Global Proteome Index of Individuality. *Annual review of analytical chemistry (Palo Alto, Calif.)* **2009,** *2*, 265-277.
12. Yang, X.; Tang, Y.; Alt, R. R.; Xie, X.; Li, F., Emerging techniques for ultrasensitive protein analysis. *Analyst* **2016,** *141* (12), 3473-3481.
13. Zhang, H.; Zhao, Q.; Li, X.-F.; Le, X. C., Ultrasensitive assays for proteins. *Analyst* **2007,** *132* (8), 724-737.
14. Rusling, J. F.; Kumar, C. V.; Gutkind, J. S.; Patel, V., Measurement of biomarker proteins for point-of-care early detection and monitoring of cancer. *Analyst* **2010,** *135* (10), 2496-2511.
15. Ng, A. H. C.; Uddayasankar, U.; Wheeler, A. R., Immunoassays in microfluidic systems. *Analytical and Bioanalytical Chemistry* **2010,** *397* (3), 991-1007.
16. Rissin, D. M.; Kan, C. W.; Song, L.; Rivnak, A. J.; Fishburn, M. W.; Shao, Q.; Piech, T.; Ferrell, E. P.; Meyer, R. E.; Campbell, T. G.; Fournier, D. R.; Duffy, D. C., Multiplexed single molecule immunoassays. *Lab on a Chip* **2013,** *13* (15), 2902-2911.
17. Tekin, H. C.; Gijs, M. A. M., Ultrasensitive protein detection: a case for microfluidic magnetic bead-based assays. *Lab on a Chip* **2013,** *13* (24), 4711-4739.
18. Bange, A.; Halsall, H. B.; Heineman, W. R., Microfluidic immunosensor systems. *Biosensors and Bioelectronics* **2005,** *20* (12), 2488-2503.
19. Craighead, H., Future lab-on-a-chip technologies for interrogating individual molecules. *Nature* **2006,** *442* (7101), 387-393.
20. Eyer, K.; Stratz, S.; Kuhn, P.; Küster, S. K.; Dittrich, P. S., Implementing Enzyme-Linked Immunosorbent Assays on a Microfluidic Chip To Quantify Intracellular Molecules in Single Cells. *Analytical Chemistry* **2013,** *85* (6), 3280-3287.
21. Janasek, D.; Franzke, J.; Manz, A., Scaling and the design of miniaturized chemical-analysis systems. *Nature* **2006,** *442* (7101), 374-380.
22. Digital Microfluidics. *Annual Review of Analytical Chemistry* **2012,** *5* (1), 413-440.

23. Pappas, D., Microfluidics and cancer analysis: cell separation, cell/tissue culture, cell mechanics, and integrated analysis systems. *Analyst* **2016,** *141* (2), 525-535.
24. Faley, S. L.; Copland, M.; Wlodkowic, D.; Kolch, W.; Seale, K. T.; Wikswo, J. P.; Cooper, J. M., Microfluidic single cell arrays to interrogate signalling dynamics of individual, patient-derived hematopoietic stem cells. *Lab Chip* **2009,** *9*.
25. Dutta, D.; Ramsey, J. M., A microfluidic device for performing pressure-driven separations. *Lab on a Chip* **2011,** *11* (18), 3081-3088.
26. Yeo, L. Y.; Chang, H.-C.; Chan, P. P. Y.; Friend, J. R., Microfluidic Devices for Bioapplications. *Small* **2011,** *7* (1), 12-48.
27. Wei, W.; Shin, Y. S.; Ma, C.; Wang, J.; Elitas, M.; Fan, R.; Heath, J. R., Microchip platforms for multiplex single-cell functional proteomics with applications to immunology and cancer research. *Genome Medicine* **2013,** *5* (8), 75.
28. Yuan, Y.; Wu, W.; Xu, S.; Liu, B., A biosensor based on self-clickable AIEgen: a signal amplification strategy for ultrasensitive immunoassays. *Chemical Communications* **2017,** *53* (38), 5287-5290.

Chapter 2
Multiplexed Microfluidic Digital ELISA for Detection of Biomarkers using an Automated Sealing system

2.1 Introduction

2.1a. Digital ELISA concept

Development of bioassays with high sensitivity has gained a significant importance. Various efforts have been made based on different signal amplification techniques for improving the sensitivity of bioassays. [1] A digital assay set up requires a high-density array of small containers to ensure that enough wells are occupied at low concentration. In comparison to conventional bioassays that are frequently performed in a single reactor (tubes, microtiter plates, etc.), the reaction solution is partitioned into many microreactors in digital bioassays, allowing most compartments to be filled with either 0 or 1 target molecule.[2] The operation of digital bioassays involves partitioning reaction solutions into micrometer-sized compartments. Instead of quantifying the absolute intensity of ensemble signals from tubes or microtiter plates, in digital bioassays, only the fraction of microcompartments showing positive signals is counted. Because of the unique binary property of the system, it is called the "digital" bioassay.[3] Isolating single molecules into small volume containers has several advantages, including higher resolution and sensitivity, low sample and reagent volume requirements, low cost, and shorter analysis times. An additional advantage of using small containers is the ability to confine individual molecules for single-molecule studies.

The traditional analog readout systems require a huge volume of the analyte molecules that could dilute reaction product, which would need millions of enzyme labels to generate the required signals that are easily detectable utilizing conventional plate readers. Sensitivity is therefore limited to the picomolar (pg/mL) range and above.[4] Whereas, single molecule measurements are

digital in which each molecule amplifies a signal that can be counted as shown in Figure 6. It is much easier to measure the presence or absence of signal than to detect the absolute whole amount of signal. For example, early stage detection of many types of cancer is associated with improved patient outcomes, but the serum concentration of proteins that reliably indicate the presence of disease is expected to be picomolar (10^{-12} M) or lower.[2] Most immunoassays, the traditional detection method for disease-associated proteins, cannot measure such low concentrations. Digital immunoassays utilizing single-molecule detection approaches have pushed the theoretical limit of detection down by several orders of magnitude into the attomolar (10^{-18} M) range.

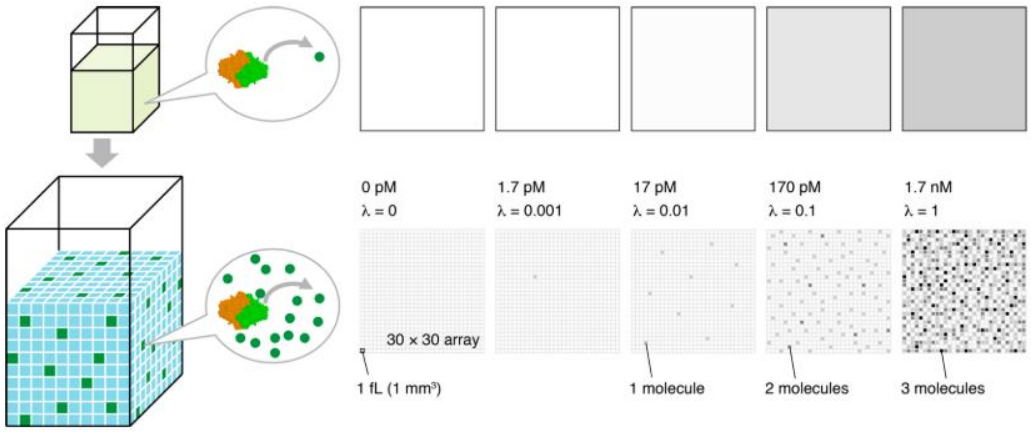

Figure 6: Concept of the digital bioassay. A schematic comparison between analog measurement and digital counting is shown. In digital bioassays (bottom part), the bulk reaction solution is partitioned into extremely small compartments to rapidly concentrate the reaction product. In conventional tube-based assays (top part), the reaction product diffuses very quickly, making a highly diluted product difficult to detect.[3]

Because some of the biomolecules like proteins cannot be amplified like DNA, detecting a single molecule per microcompartment is more challenging. This problem has been addressed by the development of digital ELISA. The type of ELISA used in the digital bioassay is usually sandwich enabling the target analyte to be sandwiched between the two antibodies. The sensitivity

achieved by digital ELISA in some cases is in good agreement with theoretical sensitivity derived from parameters such as concentration, time, and affinity, making it possible to approach the theoretical limit of detection via an appropriate experimental setup.[5] There are diverse ways in performing a digital ELISA, once such type is Single Molecule Array technology (Simoa). Simoa employs a bead suspension to carry out the entire binding and labeling process. The first step of digital ELISA is binding the target analyte onto beads conjugated to capture antibodies. Beads and the target analyte are mixed together so that the quantity of beads is more than the analyte molecules. The beads are then loaded on to the wells and further sealed and the wells containing beads that carry an enzyme molecule begin to build up fluorescent product as shown in Figure 7.[6]

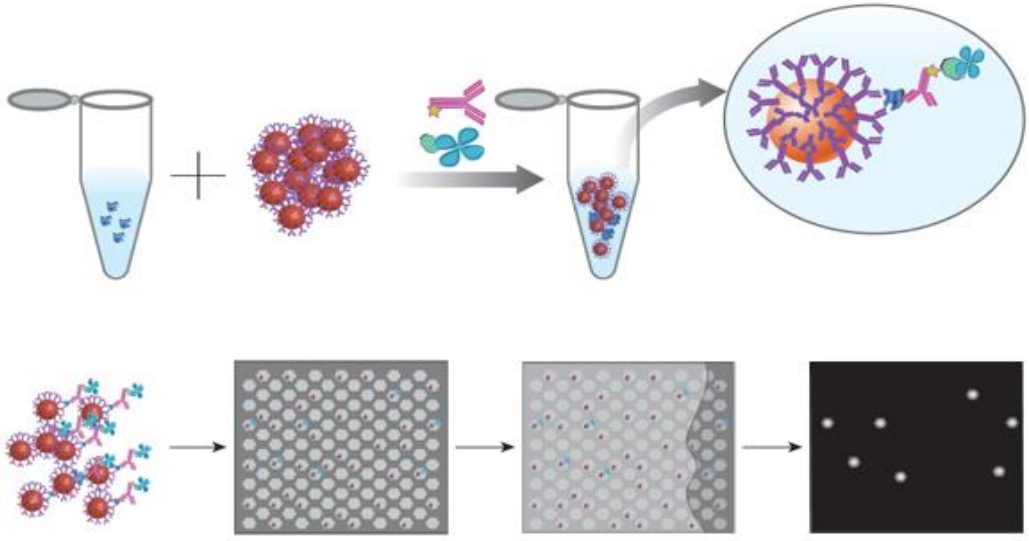

Figure 7: Digital ELISA. (a) A sample containing a target analyte is incubated with beads coated with capture antibodies. The beads are then consecutively incubated with biotinylated detection antibodies and SβG to form a single-enzyme–labeled immunocomplex on the bead. (b) The beads are resuspended in RGP and loaded onto a microwell array such that only one bead fits into each well. The array is then sealed with oil, and wells containing beads that carry an enzyme molecule begin to build up fluorescent product. Fluorescent images of the array are obtained to locate the beads inside the wells and to identify beads labeled with enzyme.[6]

2.1b. Digital Determination of Protein concentration with Poisson Distribution

A digital bioassay is composed of several identical and independent reactions, with each showing either a positive or a negative signal (i.e., exactly two possible outcomes), satisfying the prerequisites of Bernoulli trials (or binomial trials); therefore, the digital bioassay should be modeled using Poisson distribution.[7] At low ratios of enzyme to microwells, when there are a statistically significant number of beads with no enzymes, by measuring the fraction of active wells in a population it is possible to determine the bulk analyte concentration because the binding probability of a population of analyte molecules to a population of microwells is defined by the Poisson distribution. The Poisson distribution (eq.1) describes the likelihood of a number of events occurring if the average number of events is known. If the expected average number of occurrences is λ, then the probability that there are exactly k occurrences (k being a non-negative integer, k = 0, 1, 2, 3,…) is equal to

$$P\ (X = k) = e^{-\lambda}\frac{\lambda^k}{k!} \text{.....(eq.1)}$$

At very low ratios of labeled analyte to microwells (less than about 0.1 enzyme labels per well), most wells have either zero or one labeled analyte molecule and the percentage of active wells increases approximately linearly with increasing analyte concentration. As the fraction of active wells becomes larger (> 0.1), Poisson statistics show that there are a considerable number of wells with multiple enzyme molecules as shown in Table 1. If the fraction of active wells is plotted against concentration, linearity is lost at high target concentrations because active wells that have multiple enzyme molecules bound contribute the same 'digital' signal as an active well that has one enzyme bound.

Table 1: Examples of probability calculation by Poisson Distribution.[3]

expected value λ	number of occurrences k	probability $P(X = k)$, %
1	0	36.8
	1	36.8
	2	18.4
	3	6.13
	4	1.53
	5	0.307
0.1	0	90.5
	1	9.05
	2	0.905
0.01	0	99.0
	1	0.990

In digital ELISA, λ is equal to the ratio of bound labeled proteins to the number of microwells, and k is the number of enzyme-labeled proteins carried by each sub-population of microwells (i.e., 0, 1, 2, 3, etc.). The aim of the digital assay experiment is to determine λ which is equal to average molecule per microwell and use it as the quantitative parameter to determine protein concentration. In the digital mode of analysis where microwells are identified as being either "on" or "off", then k = 1, 2, 3 are indistinguishable and characterized as "on" beads. The probability for positive and negative wells is equal to 1.[8]

$$P_{positive} + P_{negative} = 1 \quad \text{(eq. 2)}$$

$P_{positive} = 1 - P_{negative}$ where $P_{negative}$ means P (0) fraction of off wells.

Due to this broad distribution, only occurrences of k = 0 can by determined as the fraction of "off" wells ($P_\lambda(0)$). Using eq.1 to determine $P_\lambda(0)$, and the fact that the fraction of "on" wells is equal to one minus the fraction of "off" wells, it is possible to determine λ from f_{on} (the fraction of "on" beads or % active) from (eq.4).

$$P_{positive} = 1 - P_\lambda (k=0)$$

From eq.1 $P_\lambda (k=0) = e^{-\lambda}$

$$P_{positive} = 1 - e^{-\lambda}$$

$$e^{-\lambda} = 1 - P_{positive} \ldots\ldots \text{(eq.3)}$$

By applying logarithm (ln) on both sides of (eq.3)

$$\lambda = -\ln (1 - P_{positive}) \text{ or } \lambda = -\ln (1 - f_{on}) \ldots\ldots\ldots\ldots\ldots\ldots\ldots\ldots\ldots\ldots \text{(eq.4)}$$

2.1c. Importance of Sealing

High-density arrays of compartments fL - nL volume offer an excellent platform for performing parallel biochemical measurements to obtain statistically meaningful results for single-molecule reactivity and cellular heterogeneity in a population sealing the containers is very important to achieve digital readout as it is critical to prevent evaporation, eliminate diffusion of the contents into bulk solution, and reduce transfer of product between containers.[9] For example, If the captured molecule is an enzyme that acts on a fluorogenic substrate that is also in solution, enzyme activity will result in a fluorescent product that will reach a high concentration within sealed containers Whereas, containers in which no enzyme is present will maintain background levels of fluorescence intensity a shown in Figure 8.[10] Instead of relying on the total amount of fluorescent product formed as is the case for bulk measurements, this approach has a digital readout, with the percentage of positive containers. Therefore, sealing is the main step for digital measurement of single molecules. The challenges for effective sealing of the compartments on a microarray platform is to prevent solvent evaporation, diffusion of reagents into bulk solution, and more importantly cross-communication between individual reactions. This is where my project comes in to develop an effective sealing method for detection of single molecule reactions where we developed an automated sealing system for closing the microwells which is discussed in experimental section.

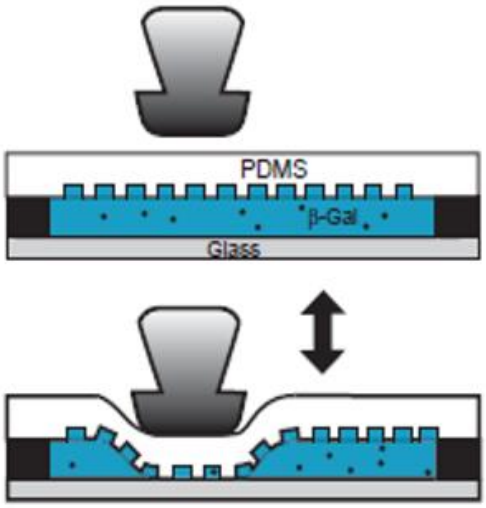

Figure 8: Sealing plays a vital role in obtaining digital signal. By pressing a small area of the PDMS sheet with a glass needle, successive opening/closing rounds could be performed, allowing the exchange of the content of each chamber.[10]

2.1d. Different Biomarkers

a) CEA Protein

Carcino Embryonic Antigen (CEA) is a heavily glycosylated cell-surface glycoprotein and one of a large family of immunoglobulins. Almost, thirty-six different glycoproteins have been identified in the CEA family, and they are derived from eight genes localized on chromosome 19 in two clusters. CEA is a non-mucinous, 180kDa glycoprotein secreted by the epithelial cells of the digestive tract in the normal fetus and in adult cancers.[11] A carcinoembryonic antigen (CEA) test is a blood test used to help diagnose and manage certain types of cancers, especially cancers of the large intestine and rectum.[12]

b) EGFR

The Epidermal Growth Factor Receptor (EGFR) subfamily of receptor tyrosine kinases comprise four members: EGFR (also known as HER-1, ErbB1, or ErbB), ErbB2 (Neu, HER-2),

ErbB3 (HER-3), and ErbB4 (HER-4). EGFR signaling regulates multiple biological functions including cell proliferation, differentiation, motility, and apoptosis.[13] All EGFR family members are transmembrane glycoproteins with an extracellular ligand binding domain and a cytoplasmic domain containing a membrane-proximal tyrosine kinase domain followed by multiple tyrosine autophosphorylation sites with a molecular weight of 95kDa.[14]

c) CA-125

The Cancer Antigen (CA125) antigen, also called as MUC16, is a mucin protein that is found in type I transmembrane or present in secreted forms that are used monitor the progress of epithelial ovarian cancer therapy.[15] Expression of isoforms, proteolytic cleavage, and heavy N- and O- linked glycosylation produce forms of human CA125 that can vary from 200-5000 kDa in size. It inhibits natural killer NK cell activity, which is thought to contribute to immune evasion in peritoneal cancer and pregnancy.[16]

d) IL-6

IL-6 (Interleukin-6) is a cytokine with molecular weight of 21kDa, that acts in the acute phase reaction, inflammation, hematopoiesis, bone metabolism, and cancer progression.[17] It contributes to chronic inflammation in obesity, insulin resistance, inflammatory bowel disease, arthritis, sepsis, and atherosclerosis. In addition, the increased IL-6 serum levels were known to be associated with metastasis and poor prognosis mainly in prostate, ovarian and gastrointestinal cancers.[18]

e) IL-8

Interleukin- 8 (IL-8) is an 8.4 kDa protein belonging to the chemokines family that is well characterized by two important cysteine residues, and also separated by a third amino acid in between. [19]There are two major forms of IL-8, one is the 72-amino acid monocyte-derived form,

which is very predominant in cultures of monocytes and macrophages, and the other is the endothelial form, which has five extra N-terminal amino acids, and predominant in cultures of tissue cells such as endothelial cells and fibroblasts.[18]

2.2 Experimental

2.2.1 Chemicals and Reagents

The following reagents were used as received: 1 phosphate buffered saline solution 1 PBS (> 98.5, Mediatech, Inc.), Superblock T20 blocking buffer (PBST) (Thermo Scientific), fluorescein di B D galactopyranoside (FDG) (Invitrogen), Streptavidin Beta galactosidase conjugate (SBG) (Invitrogen), 2- propanol (IPA) (> 99.5%; Sigma Aldrich), ethanol (100% Decon laboratories Inc.), carcino embryonic antigen, human EGFR Duoset ELISA kit (R&D Systems), human CEACAM-5 Duoset ELISA kit (R&D Systems), human CA-125 Duoset ELISA kit (R&D Systems), Human IL-6 Duoset ELISA kit (R&D Systems), human IL-8 Duoset ELISA kit (R&D Systems), 2mM MgCl2 (Fluka Analytical), bovine serum albumin (BSA) (Sigma Aldrich), 3 glycidyloxy propyl trimethoxy silane (GPS) (Sigma Aldrich), anhydrous toluene (>99.8%;Alfa Aesar), N,N,N',N'- tetramethylethylenediamine (TEA) (Sigma Aldrich), SU-8 2010 (Microchem), biotinylated BSA (Thermofisher)

2.2.2 Micro Fabrication and device assembly

The microfluidic fabrication was performed to prepare the SU-8 molds on silicon wafers using a multi-layer soft lithography approach because there are two layers that were aligned together as shown in Figure 9. The Si mold for the pneumatic layer was fabricated using SU-8 2025 (Micro Chem) with a final thickness of ~ 30 µm, following the recommended procedure by the manufacturer. The mold for the fluidic layer was fabricated by the two-step lithography. Briefly, the 25 µm thick channel features with a reaction volume of 0.1 µL was first patterned with

SU-8 2025 photoresist following the same procedure as above. The micropost array was patterned on top of the first layer by spin-coating SU-8 2010 at 4500 rpm for 60 s. The wafer was first prebaked at 65˚C for 2 min and at 95˚C for 4 min, and exposed for 10 s for total exposure energy of 110 mJ cm^{-2}. The wafer was then post-baked at 65˚C for 1 min and at 95˚C for 4 min, followed by a 2 min development and hard-baking at 200 ˚C for 2h. Before making PDMS chips, all Si molds were treated with trimethylchlorosilane by gas phase silanization under vacuum for overnight.[20]

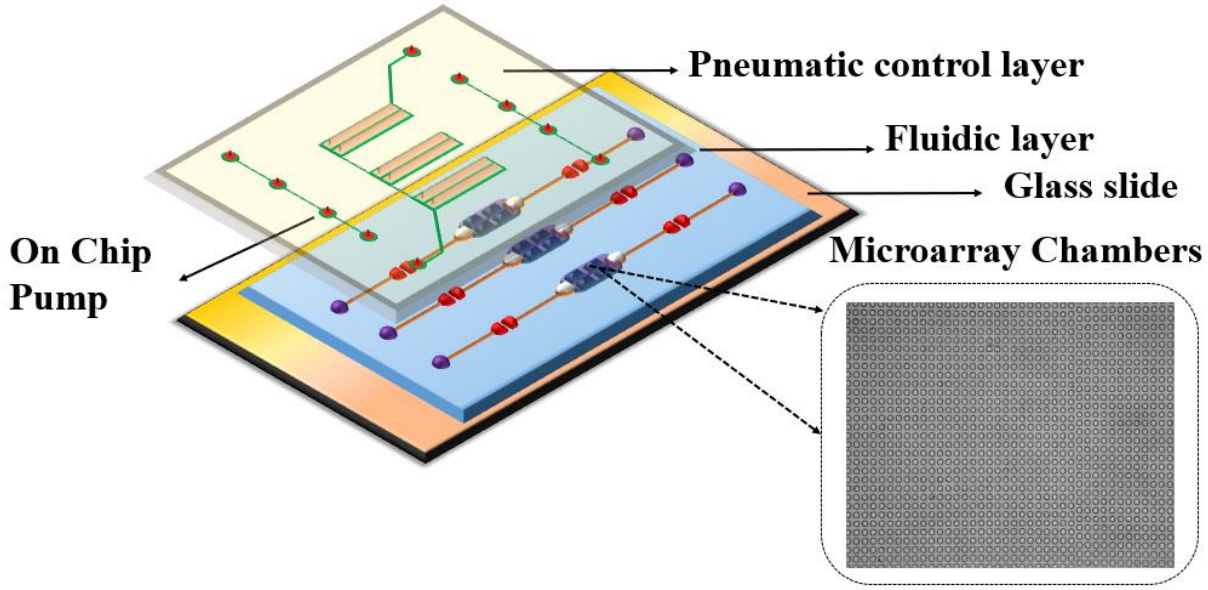

Figure 9: Schematic representation of the design and assembly of a double layer microfluidic device. The two-layer microfluidic device integrates three parallel units each containing two channels with microarray compartments with top layer as pneumatic control and bottom layer as fluidic control.

The silicon wafers were used as molds for making PDMS devices. For the pneumatic layer, PDMS (Dow Corning, USA) mixture at a 8 (base material): 1 (curing agent) ratio was mixed thoroughly, degassed in vacuum chamber, then poured on to the mold and cured in the oven at 70˚C for 40 min. The cured PDMS slab was then peeled off from the mold and cut into rectangular

pieces. Access holes were punched in the PDMS replica of the pneumatic layer for pneumatic connections. Meanwhile, 5 g PDMS mixed at a ratio of 20:1 was spin coated over the mold at 300 rpm for 30 s twice and cured on a 70°C hotplate for 30 min to make the fluidic membrane layer. The pneumatic layer was then manually aligned with the aligner as shown in Figure 10 under a stereomicroscope and permanently bonded with the bottom fluidic layer by baking in the 70°C oven overnight. The assembly was then removed from the mold and the holes were punched for fluid access.

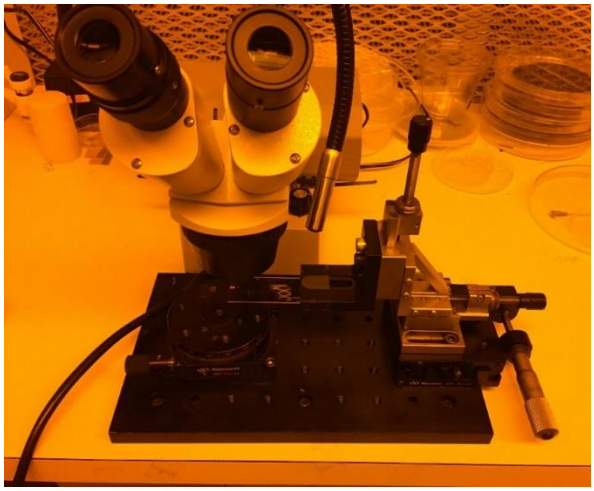

Figure 10: Aligner for pneumatic and flow channel alignment from our research lab.

2.2.3 Surface patterning

The glass substrates were patterned with 3- glycidyloxy propyl trimethoxy silane (GOPS) through silanization to enhance the surface adsorption of capture antibody within the area of the assay detection chamber. Before this step the glass slides (76.2 mm × 25.4 mm, Fisher Scientific) were first cleaned with freshly prepared piranha solution (3:1 mixture of concentrated H_2SO_4 with H_2O_2) for 15 min or overnight, rinsed twice thoroughly with deionized water, and dehydrated by baking on a 95°C hotplate for 30 min. Hot piranha is extremely dangerous and should be handled with appropriate personal protection in a fume hood free of organic chemicals. The specific area

of the glass was then patterned by 2% GOPS in anhydrous toluene with 0.2% TEA by shaking for 1 h. To remove the adsorbed excessive silane the glass slides were washed twice with toluene and isopropanol. GOPS patterned glass slides were then cured at 80°C for 2h to cross link the monolayer.[21]The epoxy silane has been shown to form a dense homogenous and complete monolayer when compared with other silanes. The epoxide ring which is the terminal group of GOPS reacts with nucleophilic reagents like amines to form a neutral oxygen-hydrogen bond. The interaction between the nonbonded electron pair on the nitrogen of amine group and the carbon atom of the epoxy ring lead to the sequential processes of ring opening, electron rearrangement, and then formation of a neutral oxygen hydrogen bond as shown in the Figure 11. The neutral oxygen hydrogen bond further reacts covalently with the amino terminus of the capture antibodies. PDMS device was cleaned with ethanol and isopropanol. The GOPS patterned glass slide and PDMS device were with UV Ozone (UVO-Cleaner1 42, Jelight Company Inc.) for 5 min. The cleaned PDMS assembly was aligned and reversibly bonded with the APTES patterned glass resulting in permanent bonding between glass and PDMS making the device ready for experiment.

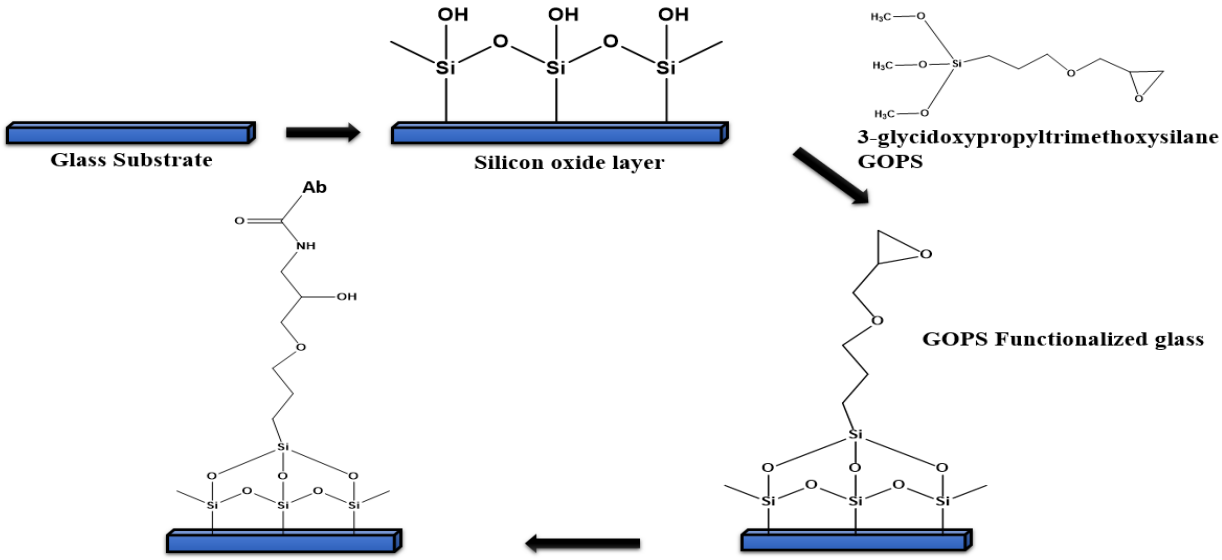

Figure 11: Schematic of the GOPS structure and its interaction with the silanol groups on glass. The epoxide ring which is the terminal group of GOPS reacts with nucleophilic reagents like amines to form a neutral oxygen-hydrogen bond.

2.2.4 Microfluidic Pumping

A crucial factor in solid-phase immunoassay was effective affinity capture of protein targets. Using our device, we could easily program on-chip pumping to control the sequential fluidic delivery of the antibodies and antigens for the sandwich immunoassay. Moreover, the integrated pneumatic pumps and valves allowed us to monitor and control the flow delivery and mass transport actively.[21] Here a five-step stop-flow pumping method that we developed in our lab by other lab colleagues was adapted with a very slight modification and the on-chip pump was operated at 0.45Hz with four consecutive valve actuation steps set to 0.5 s each and a pulse step of 2 s. The flow rate was controlled by adjusting the closing pressure while simultaneously holding the opening vacuum at −80 kPa for valve actuation. The optimal volumetric flow rate was determined to be ~0.4 μL/min generated at 50 kPa closing pressure, which was in concordance with the previous study of our lab colleagues with the geometries factored in and the flow rate range predicted by numerical simulation.[20] In addition to controlling flow delivery, the valves were

aligned on the top of each assay chamber were actuated briefly to generate convective mixing to facilitate affinity binding. The microwell chambers were used as reaction chamber as well.

2.2.5 Sealing Manifold

a) Manual

The manual sealing manifold was used initially to press down the pneumatic channel under pressure as shown in the Figure. But the results were not as expected and there was leakage between the channels. So intense work was put to develop an automated sealing instrument as shown in the Figure 12.

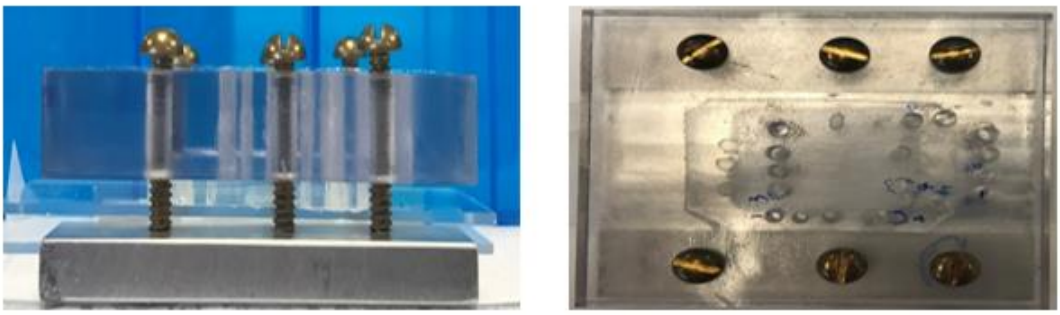

Figure 12: Side view and top view of the manual sealing manifold. There is a sliding place for placing the glass slide with PDMS device and then the screws were pushed down manually.

b) Automated Sealing Instrument

The automated sealing instrument was designed to facilitate the pressing of microwells for achieving the successful digital signal. Actuator was used with a stroke length of about 25mm so that it is portable to place on the microscope stage so that it would be easier to carry the signal amplification step under fluorescence microscope as shown in Figure 13.

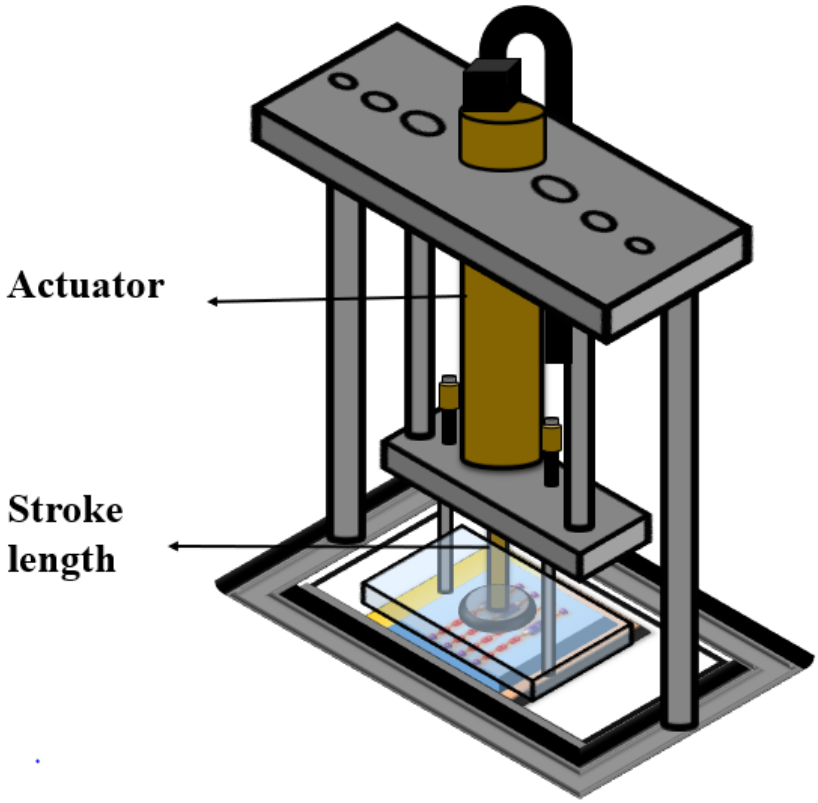

Figure 13: Schematic illustration of automated sealing instrument which included a conex actuator with 25mm travel distance for digitalizing multiple biomarkers in micro compartments.

2.2.6 Photobleaching experiment

To test the sealing performance 100 µM fluorescein was passed through the channels and allowed to bleach at different time intervals by turning the laser on. The time interval was 20 min and the images were taken every 20 min up to 80 min to see if there was any diffusion between the burnt spot and the surrounding area.

2.2.7 Free enzyme Assay

For the free enzyme assay, SβG of various concentrations (1 – 100ng/ml) and FDG 500 µM were mixed as shown in Figure 14 and filled in the chip by on-chip pumping and the assay chambers were pushed down with a 55 kPa pressure applied to the pneumatic channel immediately.

The microscope was adjusted to focus on the microwells and the fluorescence images were taken 15 min after the closure of the chamber with an exposure time of 5000 ms.

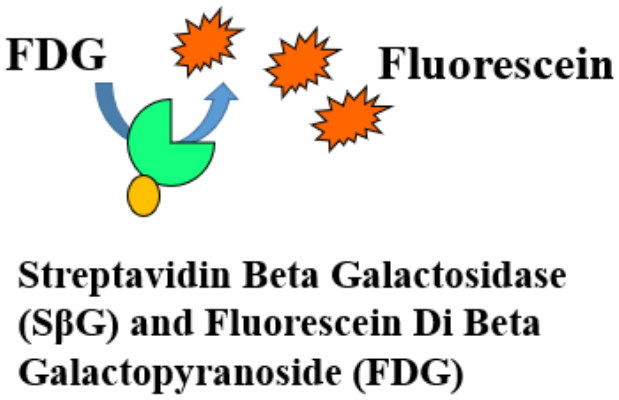

Figure 14: Schematic representation of free enzyme solution SβG and FDG. SβG of various concentrations (1 – 100ng/ml) and FDG 500 µM were mixed.

2.2.8 Testing the sealing efficiency with single layer device with pressor

For testing the sealing efficiency and effectively have more pressure in the detection area another PDMS pressor was added during the fabrication of the PDMS devices. The pressor was aligned manually in the detection area to have more pressure on the microwells. The Si mold was spin coated with PDMS mixture. The single layer device was prepared same as pneumatic layer as mentioned above, pressor and PDMS device were aligned together as one piece. The PDMS piece with pressor was reversibly bonded on to the glass slide as shown in the Figure 15.

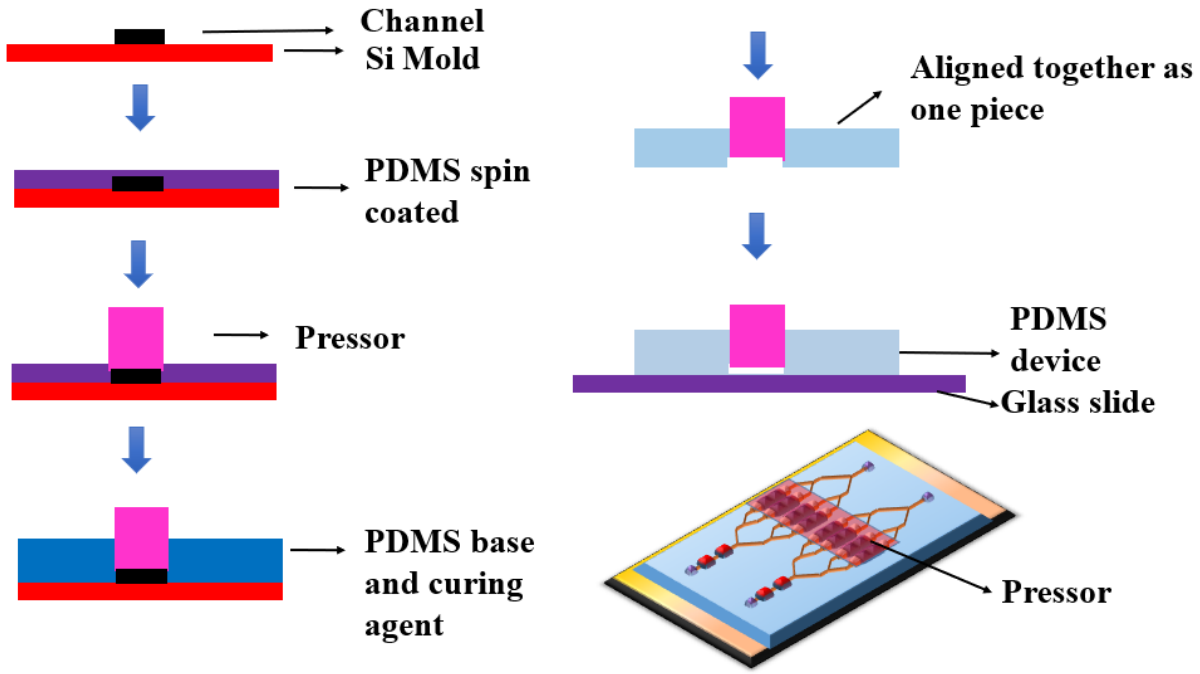

Figure 15: Schematic representation of the fabrication of single layer device with pressor which is used for testing the sealing efficiency and effectively have more pressure in the detection area another PDMS pressor was added during the fabrication of the PDMS devices.

2.2.9 CEA Assay

The workflow of sandwich ELISA was shown in Figure 16. First, 8µg/mL capture antibody was pumped through the chip, incubated for overnight and then washed with PBS. The channels were then blocked with 5% BSA for 30min and washed with PBS Various concentrations of CEA protein (0 -1ng/mL) in PBS were added and incubated for 1h and then washed with PBS. Then 0.2 µg/ mL detection antibody was pumped through the chip and incubated for 1h, then washed with PBS. 0.1 µg/mL SβG in PBSW was added and incubated for 20 min and then washed with PBS. 0.5 mM FDG was added as the final step and incubated for various time intervals. The channels were pressed down with the actuator. The signal was measured under fluorescent microscope, with 470nm wavelength and exposure time is 8000ms.

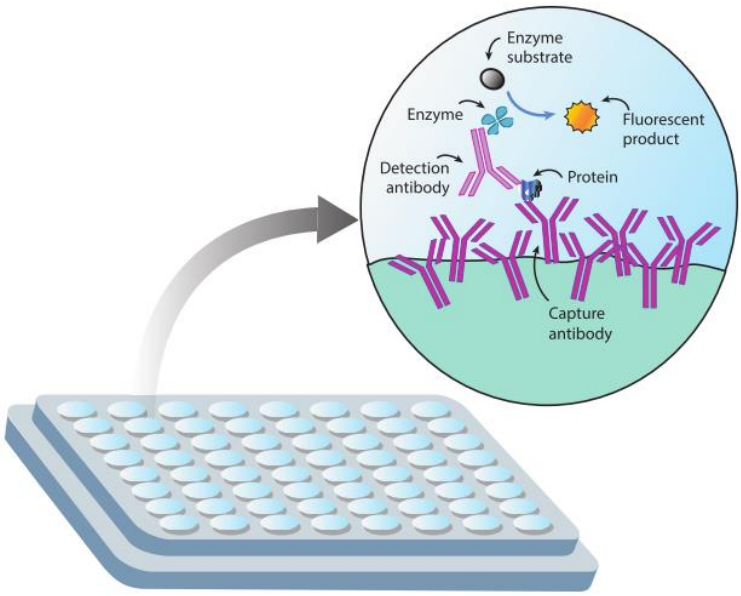

Figure 16: Scheme for a sandwich ELISA. A capture antibody specific to a target analyte is adsorbed onto a microtiter plate. A sample containing the target analyte is incubated with the adsorbed capture antibodies, which results in binding of the target analyte. The enzyme turns over a substrate that generates a detectable signal, such as a fluorescent or chemiluminescent product. The intensity of signal increase is related to the amount of target analyte that is bound.[6]

2.2.10 Capture Efficiency comparison with and without PDMS membrane on glass slide

To enhance the capture efficiency with the automated sealing instrument a different fabrication method with PDMS membrane was developed as shown in the Figure 17. The protocol involved in bonding the PDMS membrane to the glass slide before patterning the glass slides with GOPS. The desired size of PDMS membrane was cut and the cover on one side was removed, treated with UV and then bonded to the glass slide which was later cured in 70˚C for overnight. Then the glass slides along the PDMS membrane were coated with GOPS as mentioned above. PDMS device was treated with UV and then bonded onto the PDMS membrane glass slide. Then the CEA assay was performed on this set up.

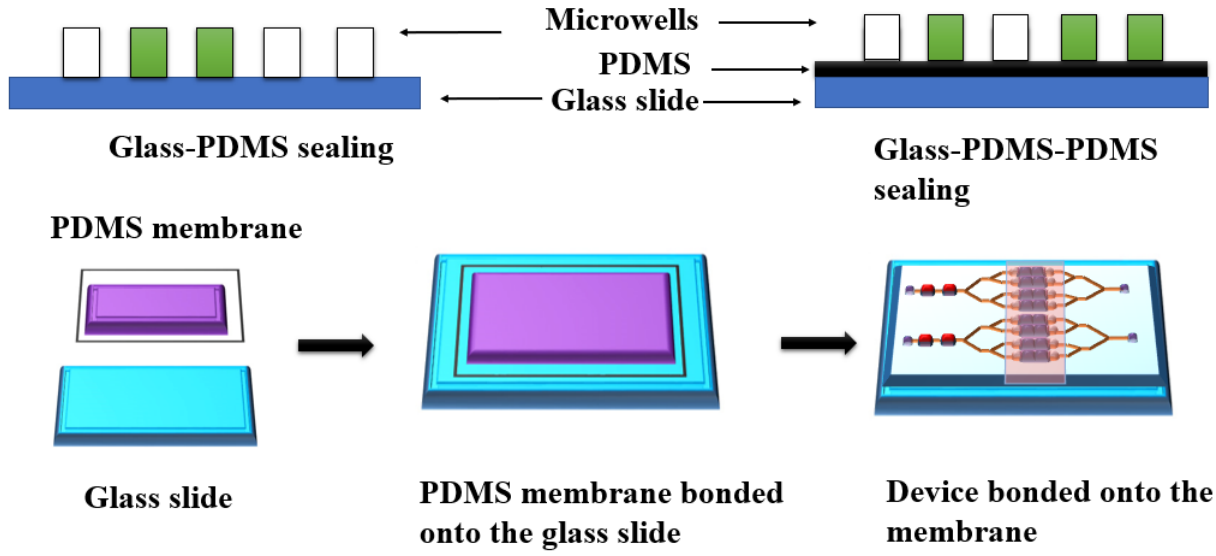

Figure 17: Schematic workflow of the fabrication steps of glass slides with PDMS membrane. To enhance the capture efficiency with the automated sealing instrument a different fabrication method with PDMS membrane was developed.

2.2.11 EGFR assay

The glass slides were immobilized with GOPS as mentioned in the surface patterning section and then the PDMS device was bonded permanently on the patterned glass slides. First, 1 µg/mL capture antibody was pumped through the chip, incubated for overnight and then washed with PBS. The channels were then blocked with 5% BSA for 1h and washed with PBST. Various concentrations of EGFR protein (0 -200 pg/mL) in PBS were added and incubated for 2h and then washed with PBST. Then 0.36 µg/ mL detection antibody was pumped through the chip and incubated for 2h, then washed with PBST. 0.2 µg/mL SβG in PBSW was added and incubated for 20 min and then washed with PBS. 500 µM FDG was added as the final step and incubated for various time intervals and the optimized time was 20 min. The channels were pressed down with the actuator. The signal was measured under fluorescent microscope, with 470nm wavelength and exposure time is 8000ms.

2.2.12 Digital ELISA for different biomarkers

The glass slides and PDMS device preparation were same as mentioned under section 2.2.9. Different biomarkers like CA-125, CEACAM-5, IL-6 and IL-8 were tested on our developed digital ELISA platforms. For the CA-125 assay, 1 μg/mL capture antibody, various concentrations of CA-125 protein (0 -3 pg/mL) in PBS, 0.36 μg/ mL detection antibody, 0.2 μg/mL SβG in PBSW and 500 μM FDG were used. For the CEACAM-5 assay, 4 μg/mL capture antibody, various concentrations of CEACAM-5 protein (0 -2 pg/mL) in PBS, 0.05 μg/ mL detection antibody, 0.2 μg/mL SβG in PBSW and 500 μM FDG were used. For the IL-6 assay, 4 μg/mL capture antibody, various concentrations of IL-6 protein (0 -6 pg/mL) in PBS, 0.05 μg/ mL detection antibody, 0.2 μg/mL SβG in PBSW and 500 μM FDG were used. For the IL-8 assay, 4 μg/mL capture antibody, various concentrations of IL-8 protein (0 -2 pg/mL) in PBS, 0.02 μg/ mL detection antibody, 0.02 μg/mL SβG in PBSW and 500 μM FDG were used. For all the above assays the channels were pressed down with the actuator. The signal was measured under fluorescent microscope, with 470nm wavelength and exposure time is 8000ms.

2.2.13 Multiplexed ELISA

As the above biomarker assays were successful the next step was to put all these biomarkers into one device by performing the detection of multiple analytes at the same time. To achieve the multiplexed ELISA, we designed a patterning device for immobilization of capture antibodies of different biomarkers.

a) Patterning Device for immobilization of capture antibodies

The Si wafer was patterned with photolithography process with five different channels for immobilizing five different antibodies as shown in the Figure 18. The PDMS device was fabricated same as pneumatic as discussed above with 8:1 ratio of PDMS mixture and later curing for 2 h at

70˚C. The patterning device was then bonded temporarily by treating with UV Ozone for 2 min and placed reversibly on the glass slide. There was no cross talking between the channels as shown in the Figure which was tested with different food color solutions. The concentrations of the capture antibodies were same as used above in the ELISA protocols. Three different biomarkers were immobilized in alternate channels having two channels for EGFR and IL-6 and one channel in the center for CA-125. Two other inlets were used for fluorescent BSA which would help in dividing the channels in five parts later in the detection chip. The patterning device after loading the capture antibodies was placed in the 4˚C refrigerator overnight. Then the channels were washed with PBST thoroughly and the device was carefully peeled off. The glass slide was washed with deionized water and dried under N_2 gas. Now the detection chip was bonded onto the above treated glass slide as shown in Figure 19.

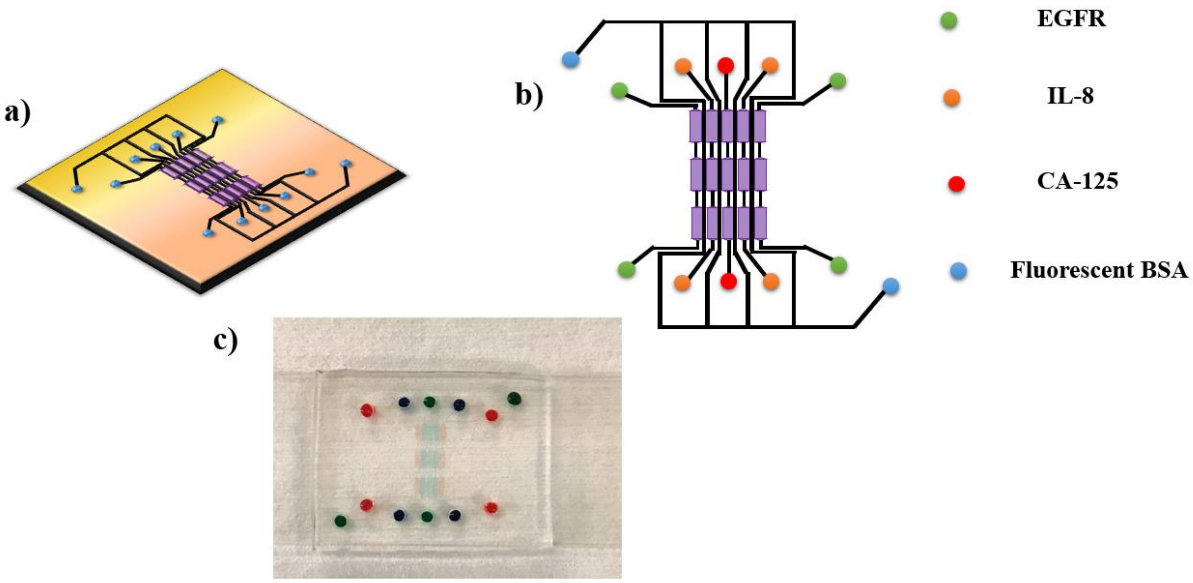

Figure 18: Schematic of patterning device for patterning different capture antibodies; a) three-dimensional representation of the patterning device on glass slide; b) two-dimensional representation of five different channels where first channel and last channel were used for EGFR represented in green color, second and fourth channel for IL-8 represented in orange color, and the third channel for CA-125 represented in red color. The two-thin channel at the extreme were used

for fluorescent BSA represented in blue color; c) Real image of the patterning device on glass slide with different food color dye solutions.

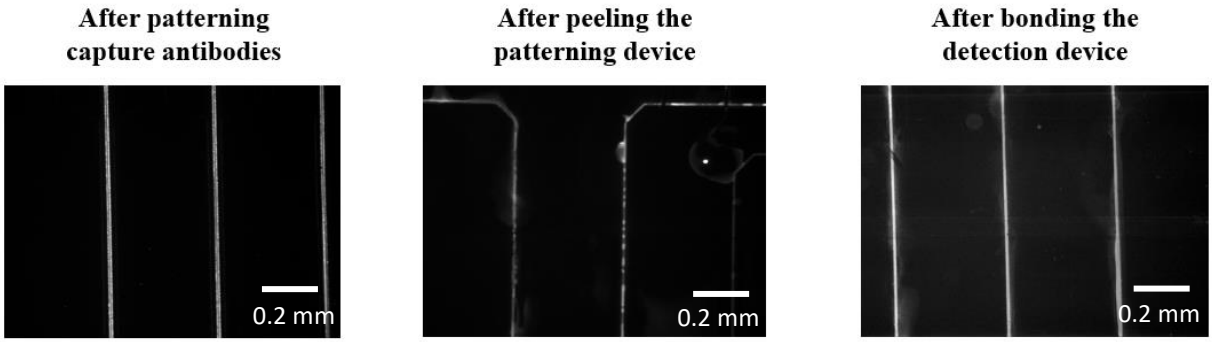

Figure 19: Typical fluorescence images of three different cases where the fluorescence resulted from fluorescent BSA a) after patterning the capture antibodies, b) after peeling the patterning device, c) after bonding the detection device.

b) Specificity test

As we were running the multiplexed ELISA on one device we were concerned about the cross interactions between the channels. The specificity test was used to confirm that there were no interferences between different channels as shown in Table 2. This was carried out by using each inlet in the device for each biomarker that means first channel for CA-125, second for IL-6 and third for EGFR. Optimized ELISA protocol was performed through these channels but while introducing the target antigen only the specific antigen could pass through the channels. So, in the first channel only CA-125 antigen was used, in the second channel IL-6 antigen and in the third channel EGFR antigen. In that way only, the antibody that was specific to the target antigen was interacted but not with other target antigens.

Table 2: Specificity test with three biomarkers CA-125, IL-8, EGFR. This was carried out by using each inlet in the device for each biomarker that means first channel for CA-125, second for IL-6 and third for EGFR.

	EGFR	IL-8	CA-125	IL-8	EGFR
CA - 125	✖	✖	✓	✖	✖
IL-8	✖	✓	✖	✓	✖
EGFR	✓	✖	✖	✖	✓

2.2.14 ELISA protocol

As the above biomarker assays were successful the next step was to put all these biomarkers into one device by performing the detection of multiple analytes at the same time. To achieve the multiplexed ELISA, we designed a patterning device for immobilization of capture antibodies of different biomarkers as discussed above. The workflow of the multiplexed ELISA was shown in the Figure 20.

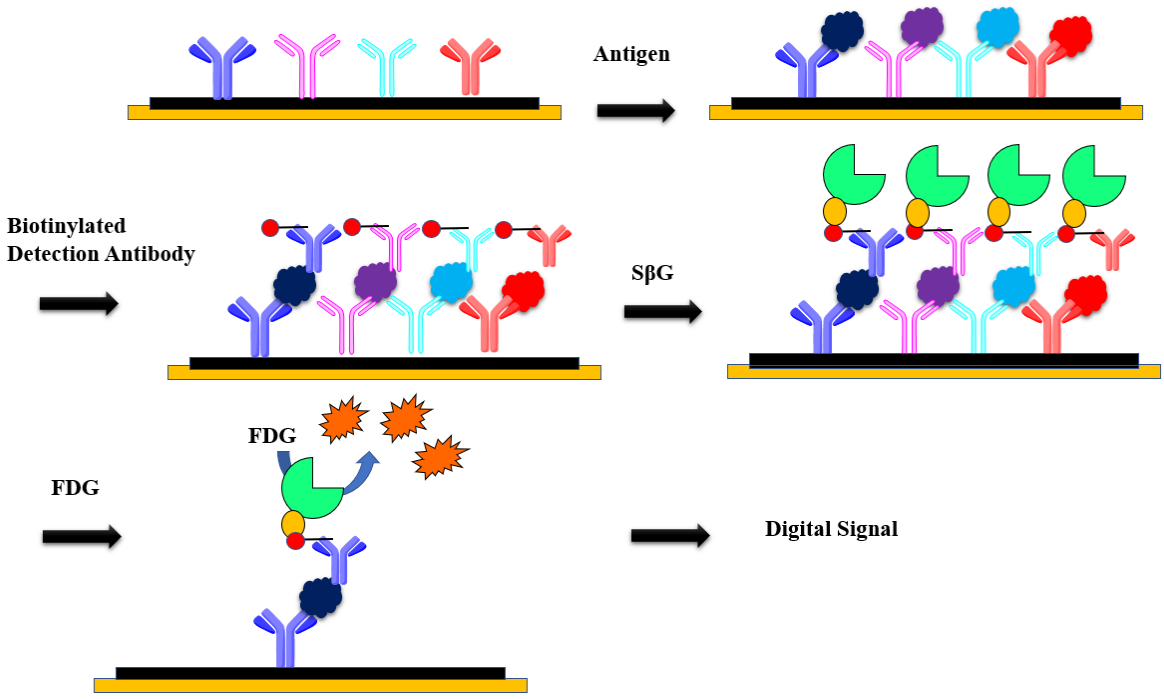

Figure 20: Schematic workflow of multiplexed digital ELISA. After the immobilization of capture Abs, the target antigens and detection Abs were added. Then SβG and FDG were added in the last step and the channels were pushed down.

Once the detection device was ready for the further ELISA steps. The channels were blocked with 1% BSA for 1h. Then the channels were washed with PBST. The target antigens with specific concentrations were prepared as a mixture, pumped through the channels and incubated for 1.5h. The channels were washed with PBST. Now the detection antibodies mixture was prepared with specific concentrations, pumped through the channels and incubated for 1.5h. 0.2 µg/mL SβG in PBSW was added and incubated for 20 min and then washed with PBS. 500 µM FDG was added as the final step and incubated for various time intervals and the optimized time was 20 min. The channels were pressed down with the actuator. The signal was measured under fluorescent microscope, with 470nm wavelength and exposure time is 8000ms.

2.3 Results and Discussion

2.3.1 Photobleaching Experiment

Photobleaching experiment was performed with 100µM fluorescein to see the sealing performance and if there is any diffusion between the bleached area and unbleached area. There are specific conditions that may affect the re-radiation of light by an excited fluorophore, and thus reduce the intensity of fluorescence. This reduction of emission intensity is generally called fading or photobleaching. As shown in the Figure 21 the images were taken with a 20-min time interval up to 80 min. The images clearly depicted that there was no diffusion between the bleached and unbleached area and the sealing performance with the automated instrument was successful.

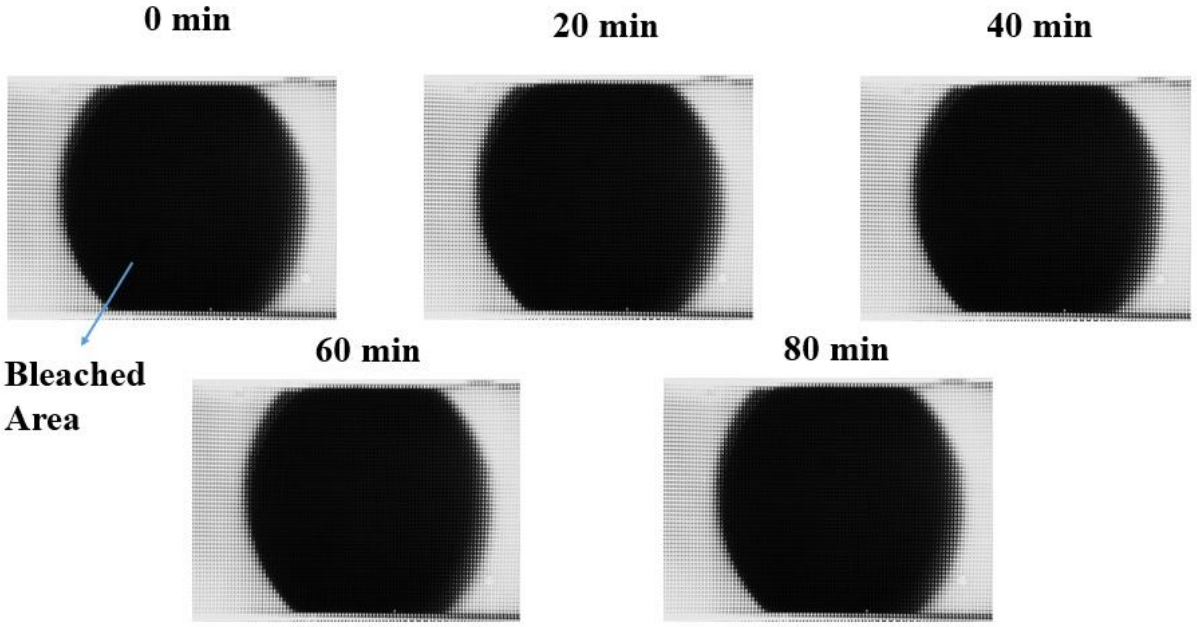

Figure 21: Photobleaching experiment was performed and the typical fluorescence images were taken at different time intervals starting from 0 min to 80 min respectively.

2.3.2 Free Enzyme Assay

For testing performance of the microwell-assisted microfluidic chemifluorescence detection, a free enzyme assay was implemented to detect the beta galactosidase. A typical fluorescence image was presented in the Figure 22 for various concentrations of 0 and 100 ng/mL respectively, showing the successful detection of beta galactosidase. Fluorescence intensity across an array of wells were measured for a serial 10-fold dilution of beta galactosidase, which showed constant fluorescence intensity across the microwells as shown in the Figure. It was also observed that the signal levels in the microwells increased with the target concentration. With the successful results of free enzyme assay we further proceeded to CEA assay.

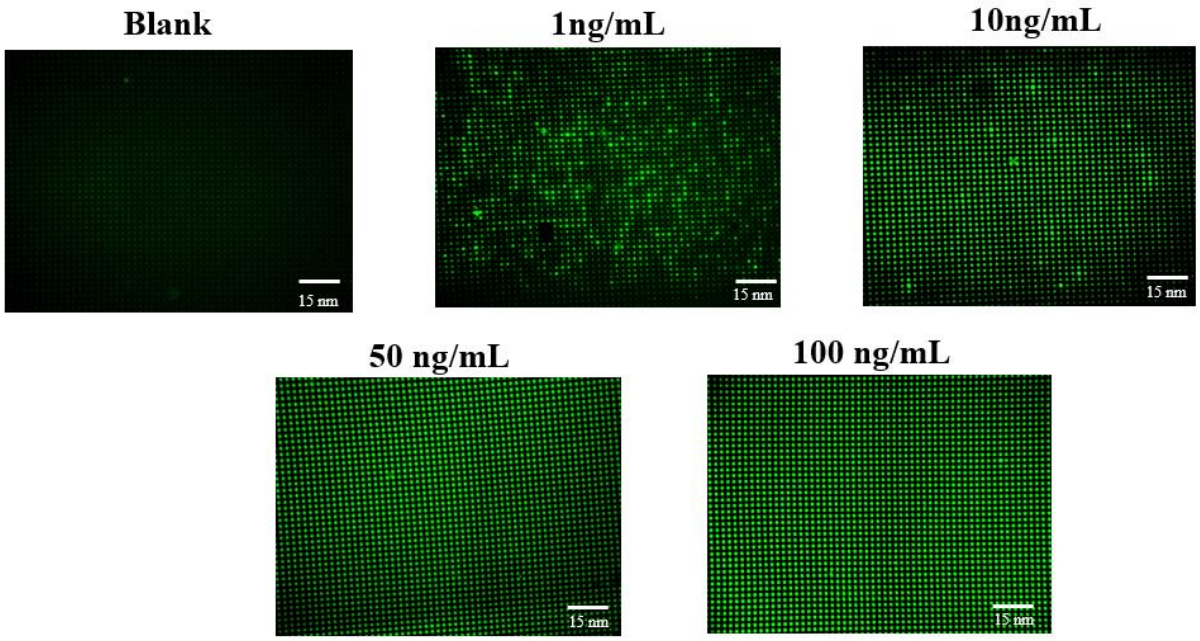

Figure 22: For testing the performance of the microwell-assisted microfluidic chemifluorescence detection various concentrations of SBG and FDG were mixed and allowed to pass through the channels.

2.3.3 Digital Counting of positive well with Image J

First the images were captured with fluorescence inverted microscope and saved in tiff format. Then the images were opened with Image J software and converted into 32-bit format by clicking image tab on Image J. Then the background was subtracted by choosing subtract background under process tab. The background was corrected with image calculator under edit process tab, by using the background mage which was the plain glass slide image taken under the same conditions. Then the image was inverted by choosing edit tab and the threshold was adjusted by choosing image tab as shown in the Figure 23. Then the image was processed by clicking the process tab and clicking the binary tab, mask was created by selecting the fill in the holes. Later the image was analyzed by choosing the analyze particles under measure tab and clicking the add to manager command. In that way, the positive wells were selected and were counted as number. Based on the total number of wells per image and positive wells the percentage of wells was calculated for each concentration in each experiment.

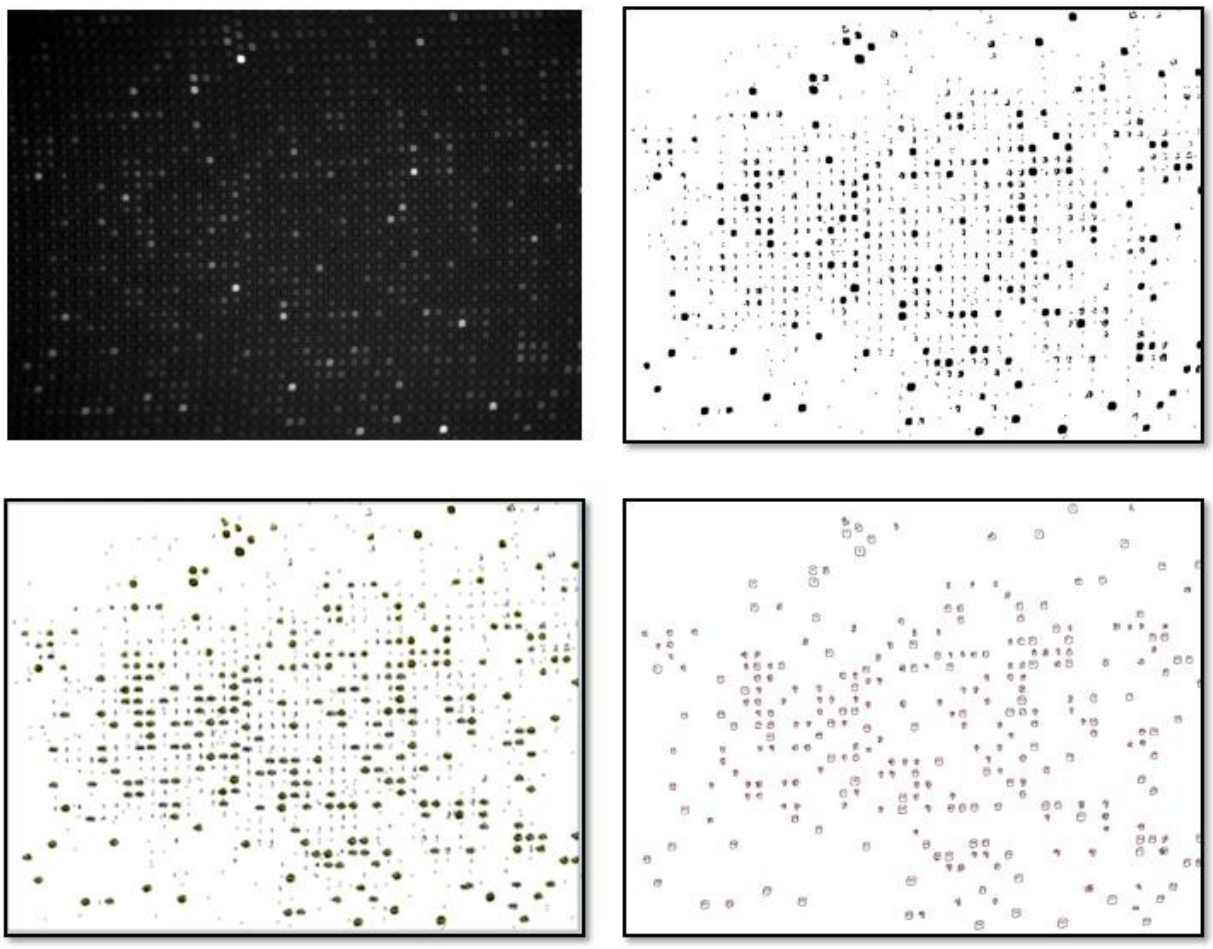

Figure 23: Steps followed for digital counting by using Image J software.

2.3.4 CEA Assay

CEA assay was performed as mentioned in the above protocol and various concentrations of target antigen were used in the assay starting from 0 – 1 ng/mL. The fluorescence images acquired for different concentration standards such as control, 0.01, 0.1, 1 pg/mL were displayed in Figure 24, which showed a very low background level for the blank control. The percentage of positive microwells were plotted as a logarithmic function of CEA concentration. The percentage of positive microwells showed a linear increase along with the CEA concentration. The quantitative detection of CEA was achieved over a dynamic range of 10 fg/mL which had 4.55% of positive wells to 1 ng/mL with 55% of positive microwells. From this experiment we could not

achieve better digital detection due to the microcompartment sealing issues and also the capture efficiency was not that good.

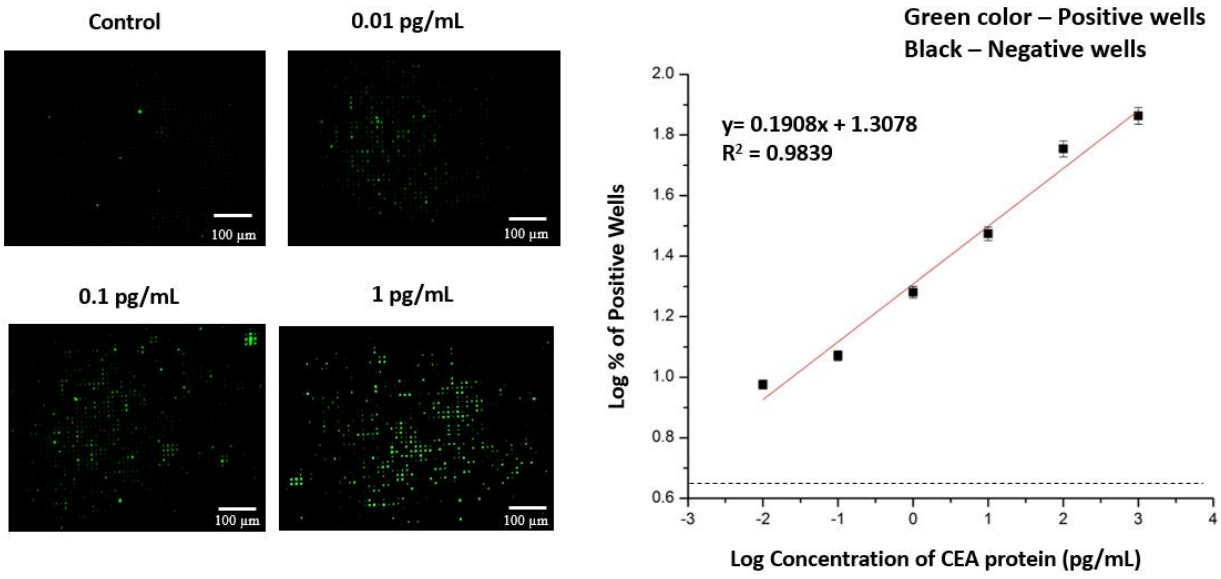

Figure 24: Microfluidic ELISA for CEA protein. Typical fluorescence images (false color) showing a very low background level for the blank control and increased number of positive wells with the CEA concentration. Quantitative detection of CEA was achieved over a dynamic range of 10 fg/mL to 1ng/mL. Error bars are standard deviations of three replicate experiments.

2.3.5 Capture Efficiency comparison with and without PDMS membrane on glass slide

To enhance the capture efficiency and better sealing performance with the automated sealing instrument a different fabrication method with PDMS membrane was developed as shown in the Figure. CEA assay was performed on this modified device as mentioned in the above protocol and various concentrations of target antigen were used in the assay starting from 0 – 1ng/mL as shown in the Figure 25. Using the optimized conditions, we calibrated the microfluidic ELISA combined with the microwell assisted chemifluorescence detection for quantitative detection of CEA protein. The fluorescence images acquired for different concentration standards were displayed in Figure, which showed a very low background level for the blank control and the

percentage of positive microwells increased along with the CEA concentration. The capture efficiency did not improve as expected when compared to previous assay with 9.46% positive wells for 10 fg/mL and 73% positive wells for 1 ng/mL. The interaction between glass- PDMS was much better when compared to PDMS - PDMS as shown in the Figure 26.

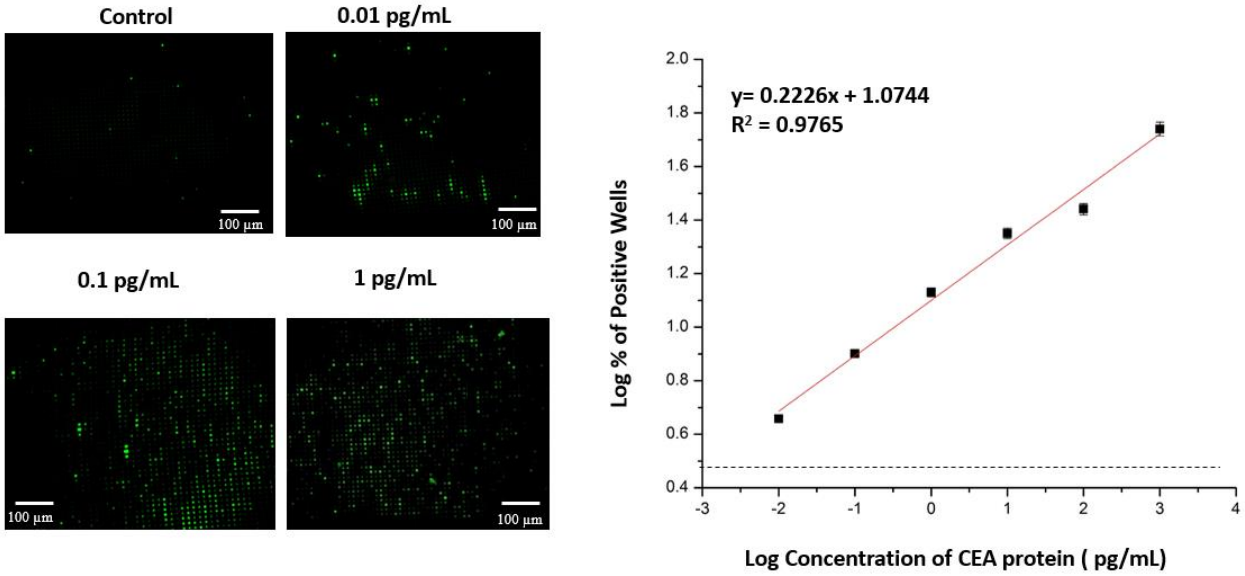

Figure 25: Microfluidic ELISA for CEA protein on modified device set up. Typical fluorescence images (false color) showing a very low background level for the blank control and increased number of positive wells with the CEA concentration. Quantitative detection of CEA was achieved over a dynamic range of 10 fg/mL to 1ng/mL. Error bars are standard deviations of three replicate experiments.

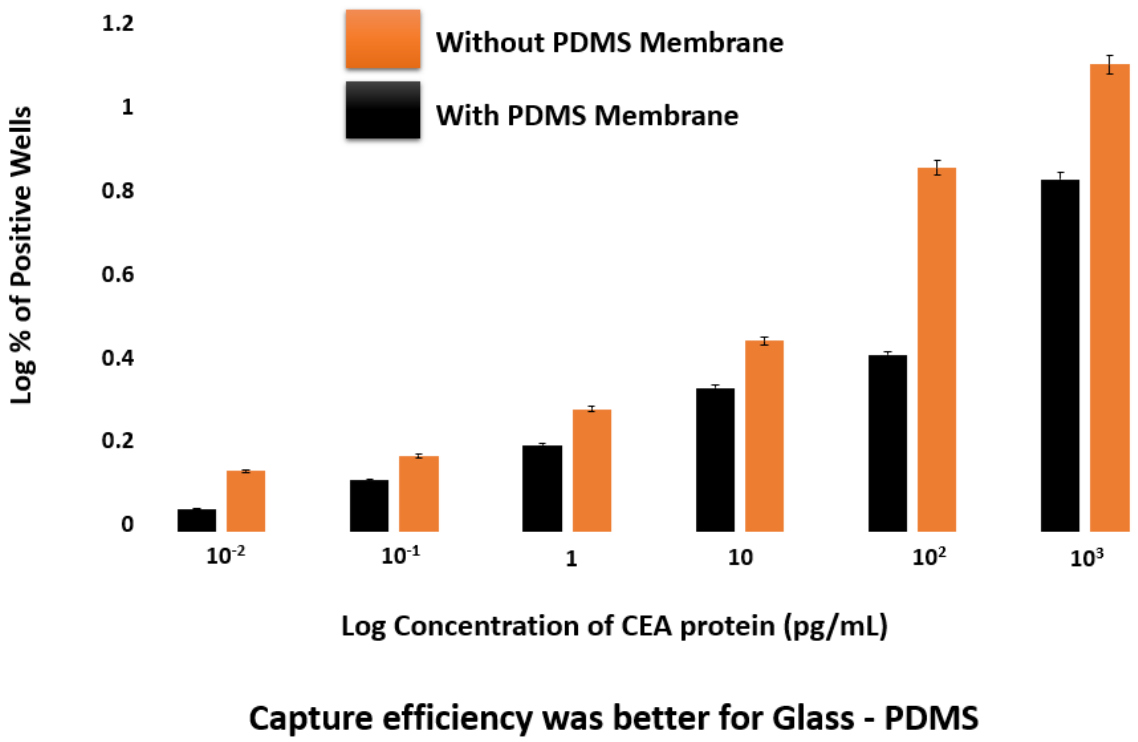

Figure 26: Comparison between two different devices set up that is with PDMS membrane on glass slide and without PDMS membrane. The interaction between glass -PDMS was much better when compared to PDMS- PDMS.

2.3.6 EGFR Assay

EGFR assay was performed as mentioned in the above protocol and various concentrations of target antigen were used in the assay starting from 0 – 200pg/mL. The fluorescence images acquired for different concentration standards 0.002 pg/mL and 0.2 pg/mL were displayed in Figure 27, which showed a very low background level for the blank control and the percentage of positive microwells increased along with the EGFR concentration. The percentage of positive microwells were plotted as a logarithmic function of EGFR concentration.

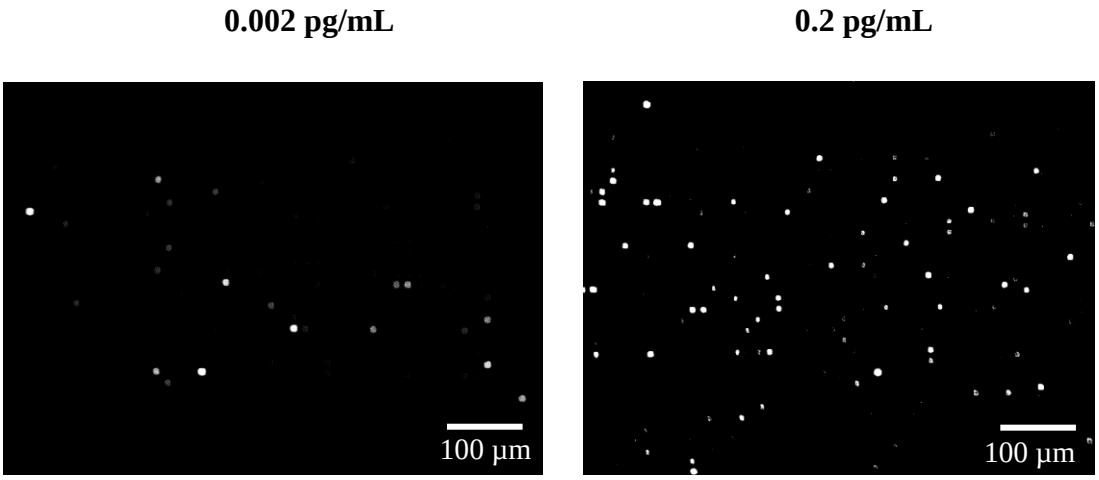

Figure 27: EGFR assay was performed with various concentrations of target antigen from 0 – 200pg/mL. Here we showed typical fluorescence images for 0.002 pg/mL and 0.2 pg/mL.

The percentage of positive microwells increased with that of the EGFR concentration. As shown in the Figure 28 we clearly experienced a linear increase in the percentage of positive wells within the concentration range of 0, 0.002, 0.02, 0.2, 2 pg/mL with 0.55%, 0.85%,1.48%, 2.87%, 12.7% respectively. We also compared the log – log calibration plot with % active wells and concentration of EGFR which showed a semi linear increase as shown in Figure 29 and 30. As shown in the Figure 31 we saw a straight increase after the assay reached a saturation point. The working concentration range for digital assay was between 0 – 2 pg/mL with $R^2 = 0.9923$ whereas from 20 pg/mL the assay slightly deviated from the linear increase to saturation phase where it was no more a digital signal as most of the wells were having fluorescent signal. The assay performance was much better when compared with CEA assay by resulting in low background and high detection limit of 1.05 fg/mL.

The λ value which is the average number of molecules per well was calculated using (eq.4) for each concentration based on the positive wells as shown in Table 3. The Table clearly showed

that the λ increased with the increase in positive wells which increased along with the concentration of EGFR.

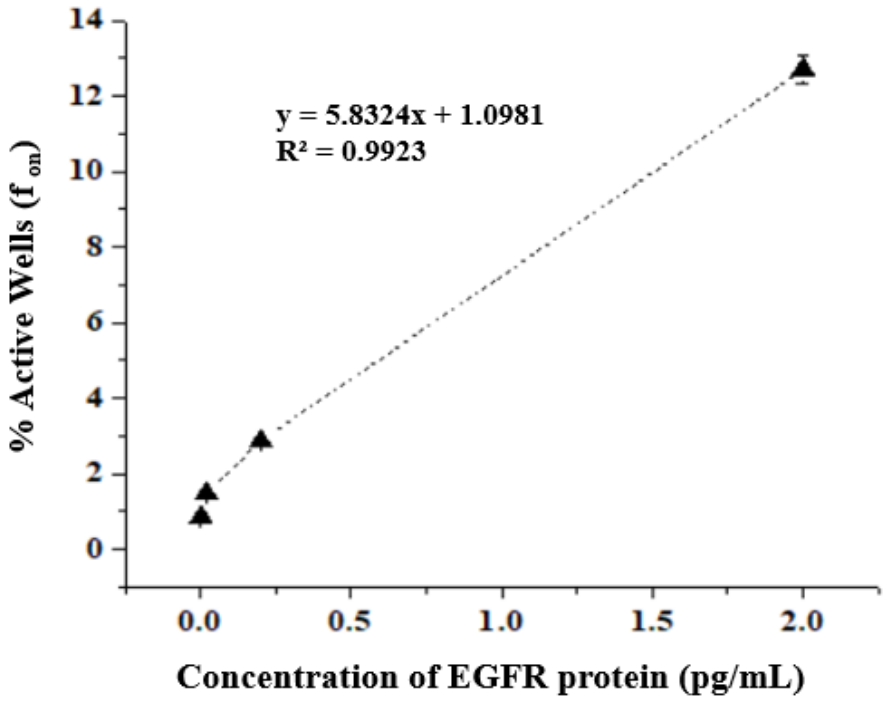

Figure 28: Quantitative detection of EGFR was achieved over a dynamic range of 2 fg/mL to 2 pg/mL with $R^2 = 0.9923$ with a detection limit LOD of 1.05 fg/mL calculated from the value of blank signal plus three standard deviations. Error bars are standard deviations of three replicate experiments.

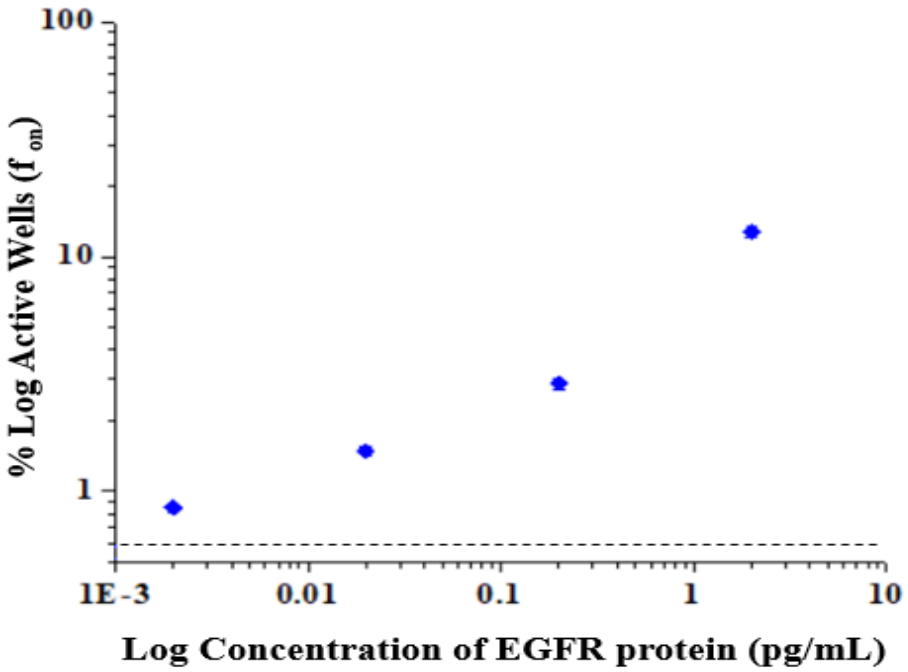

Figure 29: Comparison with log % active wells with log concentration of EGFR range 0.002-20 pg/mL with a detection limit LOD of 1.05 fg/mL calculated from the value of blank signal plus three standard deviations. Error bars are standard deviations of three replicate experiments.

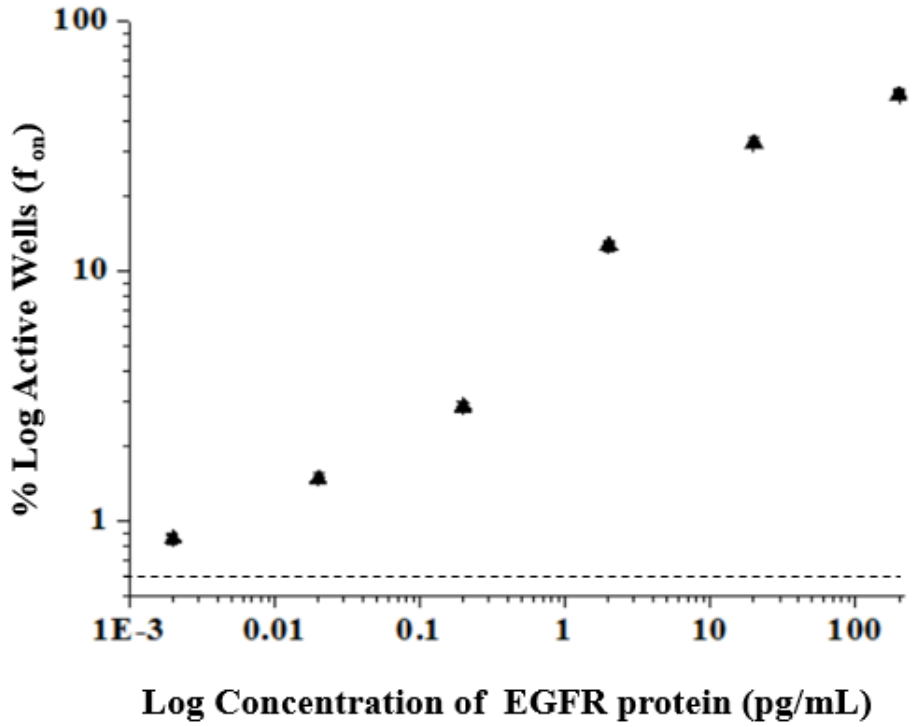

Figure 30: Comparison with log % active wells with log concentration of EGFR range 0.002-200 pg/mL with a detection limit LOD of 1.05 fg/mL calculated from the value of blank signal plus three standard deviations. Error bars are standard deviations of three replicate experiments.

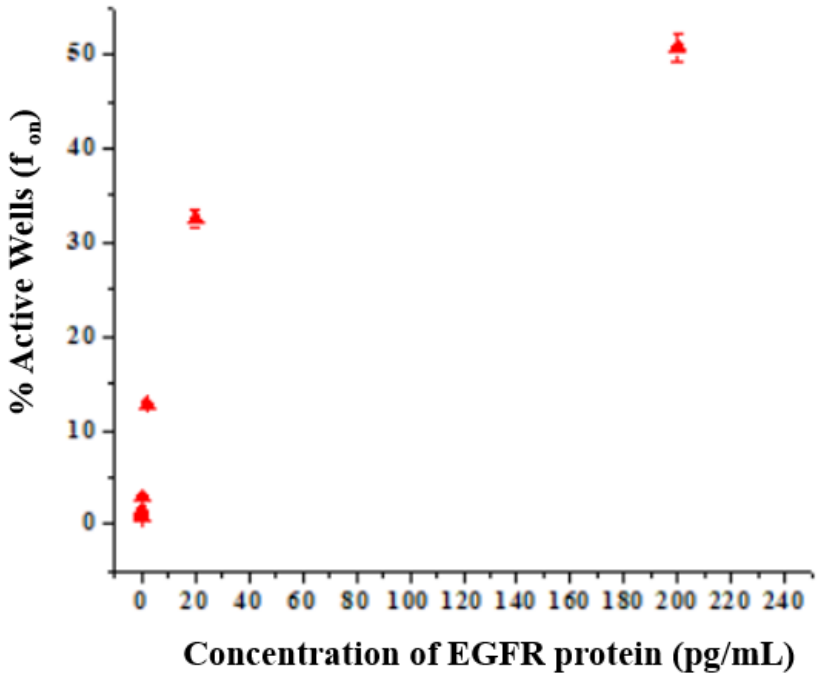

Figure 31: Quantitative detection of EGFR was achieved over a dynamic range of 0.002 to 200 pg/mL. Error bars are standard deviations of three replicate experiments. The working concentration range was between 0 – 2 pg/mL whereas from 20 pg/mL the assay slightly deviated from the linear increase to saturation phase.

Table 3: Calculation of λ (average number of molecules per well) values from % active wells for EGFR concentration range. The Table clearly showed that the λ increased with the increase in positive wells which increased along with the concentration of EGFR.

EGFR concentration (pg/mL)	f on % active wells	λ
0	0.55	0.005
0.002	0.85	0.008
0.02	1.48	0.014
0.2	2.87	0.03
2	12.7	0.13
20	32.54	0.3
200	50.8	0.7

2.3.9 Digital ELISA for different biomarkers

Digital ELISA assays were performed as mentioned under section 2.2.12. For the CA-125 assay we observed that the working range for the digital assay was from 0 – 3 pg/mL which would be further used for carrying the multiplexed ELISA. As an example, the typical fluorescence image for 3 pg/mL was displayed in Figure 32, which showed a very low background level for the blank control and the percentage of positive microwells increased along with the CA-125 concentration. The percentage of positive microwells increased with that of the CA-125 concentration for 0, 0.3, 3 pg/mL with 1.85%, 3.14%, 10.71% respectively. The λ value which is the average number of molecules per well was calculated using (eq.4) for each concentration based on the positive wells as shown in Table 4. The Table clearly showed that the λ increased with the increase in positive wells which increased along with the concentration of CA-125.

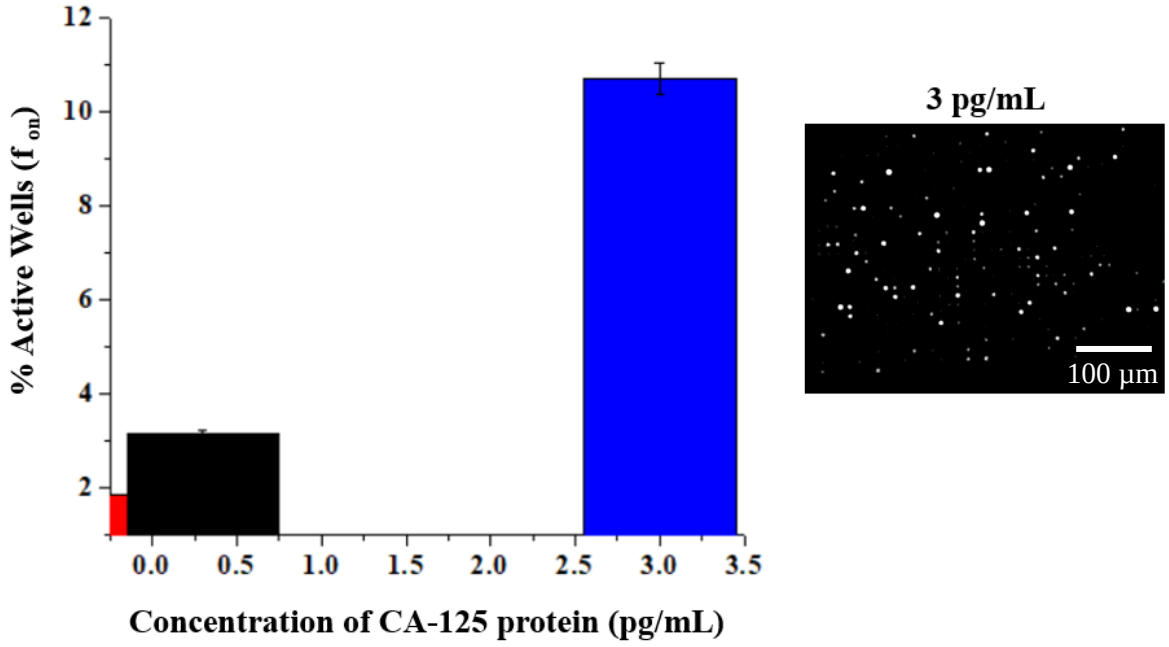

Figure 32: Typical fluorescence image of 3 pg/mL was shown as an example of digital image. A working concentration range for digital assay for CA-125 protein was between 0.3 to 3 pg/mL. Error bars are standard deviations of three replicate experiments.

Table 4: Calculation of λ (average number of molecules per well) values from % active wells for CA-125 concentration range. The Table clearly showed that the λ increased with the increase in positive wells which increased along with the concentration of CA-125.

Concentration (pg/mL)	f on % Active Wells	λ
0	1.85	0.020
0.3	3.14	0.031
3	10.71	0.113

For the CEACAM-5 assay we observed that the working range for the digital assay was from 0 – 2 pg/mL. As an example, the typical fluorescence image for 0.2 pg/mL was displayed in Figure 33 which showed a very low background level for the blank control and the percentage of positive microwells increased along with the CEACAM-5 concentration. The percentage of positive microwells increased with that of the CEACAM-5 concentration for 0, 0.2, 2 pg/mL with 2.35%, 4.50%, 11.05 % respectively which was more when compared with CA-125 including the control. The Table 5 clearly showed that the λ increased with the increase in positive wells which increased along with the concentration of CEACAM-5.

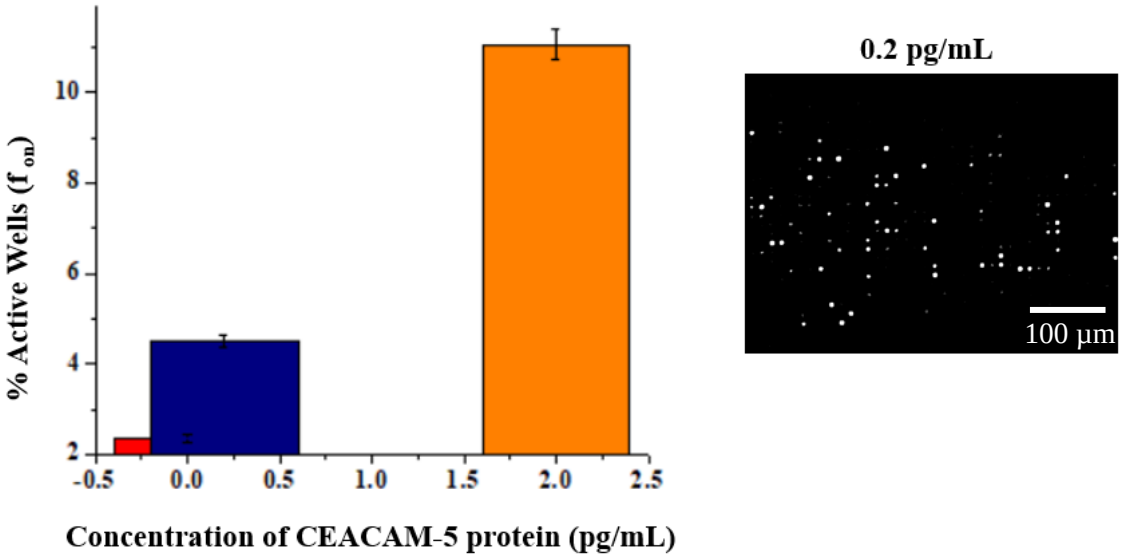

Figure 33: Typical fluorescence image of 0.2 pg/mL was shown as an example of digital image. A working concentration range for digital assay of CEACAM-5 protein was between 0.3 to 3 pg/mL. Error bars are standard deviations of three replicate experiments.

Table 5: Calculation of λ (average number of molecules per well) values from % active wells for CEACAM-5 concentration range. The Table clearly showed that the λ increased with the increase in positive wells which increased along with the concentration of CEACAM-5.

Concentration (pg/mL)	f on % Active Wells	λ
0	2.35	0.02
0.2	4.50	0.04
2	11.05	0.1

For the IL-6 assay we observed that the working range for the digital assay was from 0 – 6 pg/mL. As an example, the typical fluorescence image for 0.6 pg/mL was displayed in Figure 34 which showed a very low background level for the blank control and the percentage of positive microwells increased along with the IL-6 concentration. The percentage of positive microwells

increased with that of the IL-6 concentration for 0, 0.6, 6 pg/mL with 2.05%, 3.75%, 10.25 % respectively which was like that of CA-125 including the control. The Table 6 clearly showed that the λ increased with the increase in positive wells which increased along with the concentration of IL-6.

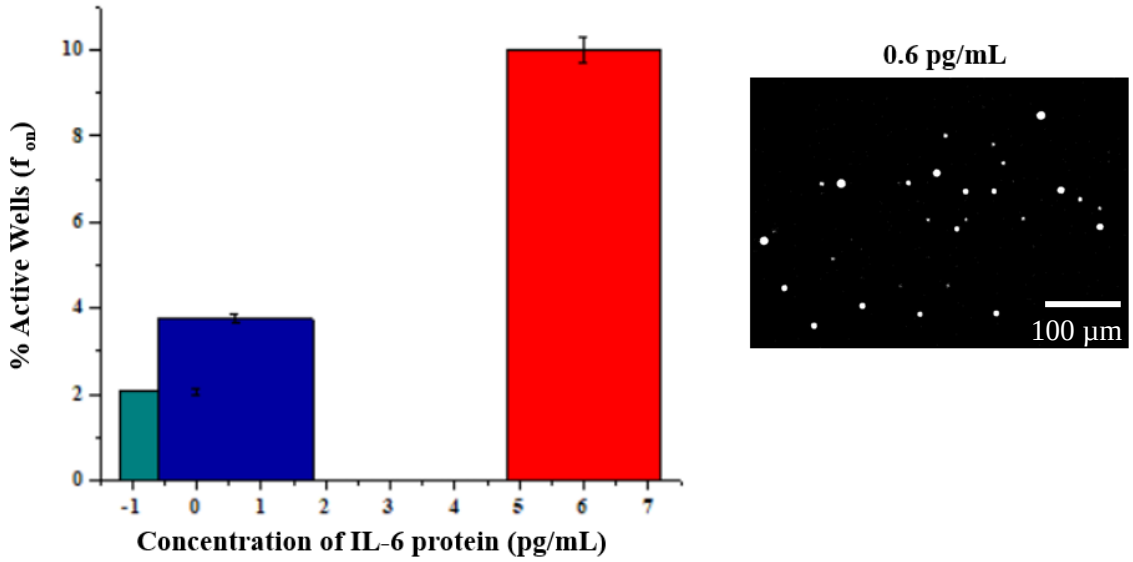

Figure 34: Typical fluorescence image of 0.6 pg/mL was shown as an example of digital image. A working concentration range of IL-6 protein for digital assay was between 0.6 to 6 pg/mL. Error bars are standard deviations of three replicate experiments.

Table 6: Calculation of λ (average number of molecules per well) values from % active wells for IL-6 concentration range. The Table clearly showed that the λ increased with the increase in positive wells which increased along with the concentration of IL-6.

Concentration (pg/mL)	f on % Active Wells	λ
0	2.05	0.020
0.6	3.75	0.038
6	10.25	0.10

For the IL-8 assay we observed that the working range for the digital assay was from 0 – 2 pg/mL. As an example, the typical fluorescence image for 0.2 pg/mL was displayed in Figure 35 which showed a very low background level for the blank control and the percentage of positive microwells increased along with the IL-8 concentration. The percentage of positive microwells increased with that of the IL-8 concentration for 0, 0.2, 2 pg/mL with 1.56%, 2.59%, 9.80 % respectively which was like that of IL-6 with less background. The Table 7 clearly showed that the λ increased with the increase in positive wells which increased along with the concentration of IL-8.

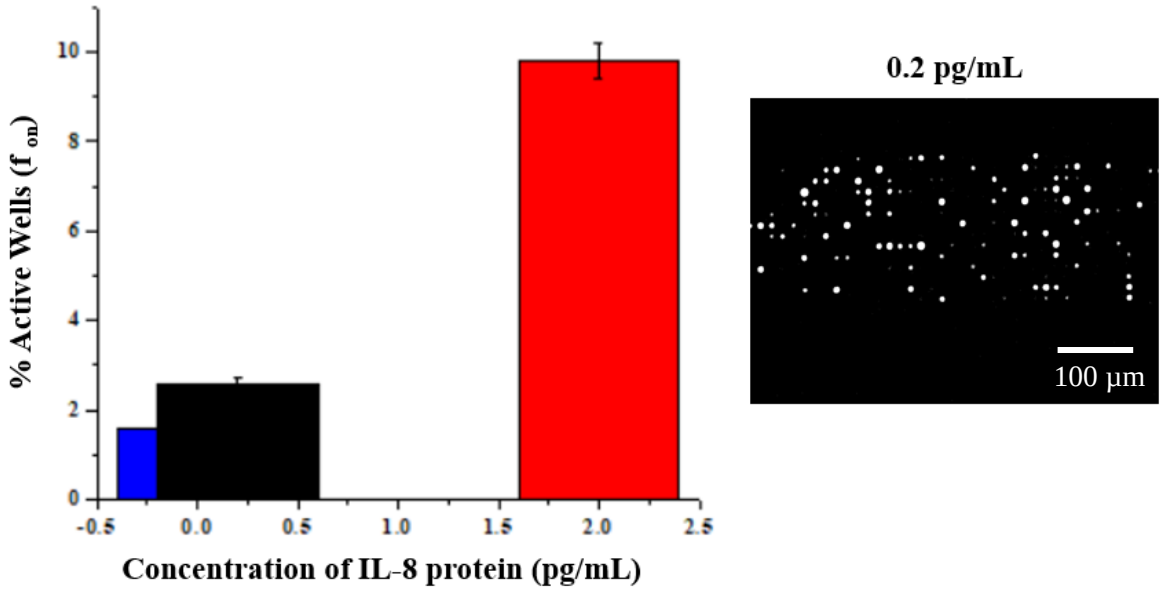

Figure 35: Typical fluorescence image of 0.2 pg/mL was shown as an example of digital image. A working concentration range of IL-8 protein for digital assay was between 0.2 to 2 pg/mL. Error bars are standard deviations of three replicate experiments.

Table 7: Calculation of λ (average number of molecules per well) values from % active wells for IL-8 concentration range. The Table clearly showed that the λ increased with the increase in positive wells which increased along with the concentration of IL-8.

Concentration (pg/mL)	f on % Active Wells	λ
0	1.56	0.015
0.2	2.59	0.026
2	9.80	0.10

2.3.10 Multiplexed Digital ELISA for detection of 3 different biomarkers on one Device

Here we performed multiplexed ELISA with three different biomarkers CA-125, EGFR and IL-8. As we were running the multiplexed ELISA on one device we were concerned about the cross interactions between the channels. The specificity test was used to confirm that there were no interferences between different channels as shown in Table under 2.2.13. With the help of this developed device each channel was divided into five parts where two parts had EGFR biomarker, two parts had IL-8 biomarker and one part had CA-125. We achieved the successful detection of three different biomarkers with different concentrations on just one microfluidic device as shown in the Figure 36.

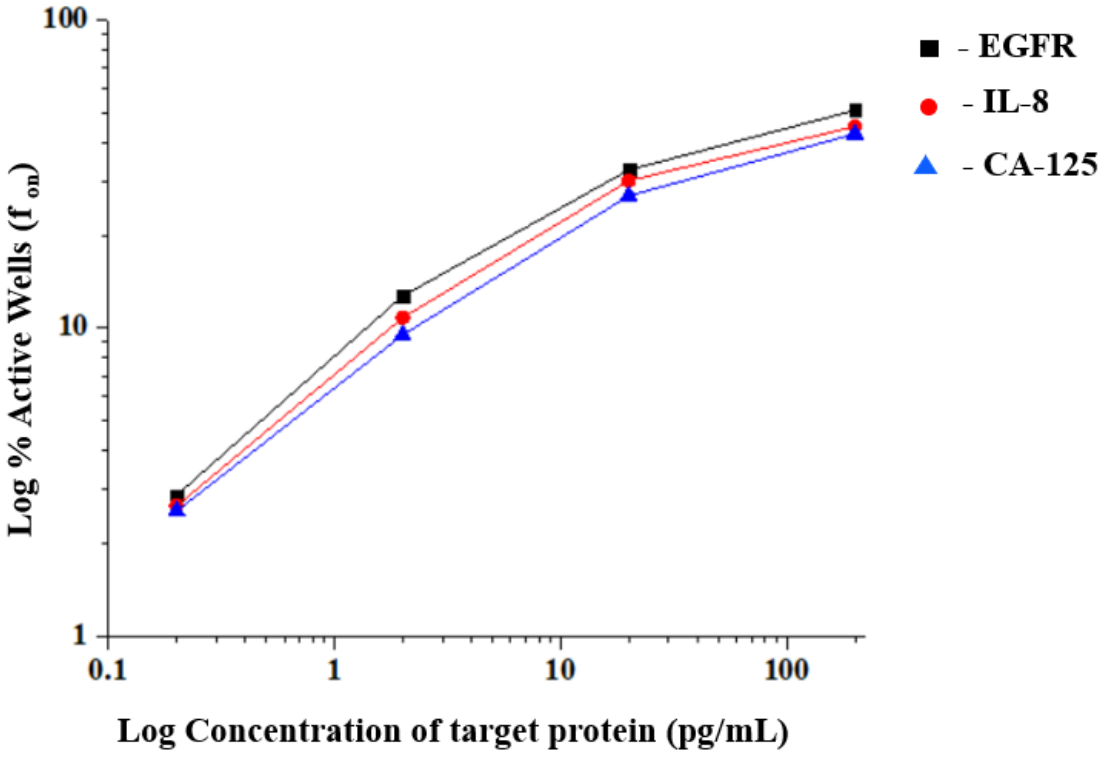

Figure 36: Multiplexed ELISA for three biomarkers was performed. Quantitative detection of three biomarkers CA-125, IL-6 and EGFR was achieved over a working dynamic range of 0.1 to 100 pg/mL. Error bars are standard deviations of three replicate experiments. EGFR showed higher expression levels when compared to IL-8 and CA-125.

The percentage of positive microwells increased with that of the protein concentration. As shown in the Figure 36 we clearly experienced a linear increase in the percentage of positive wells within the concentration range of 0-2 pg/mL and slight deviation from 10 – 100 pg/mL.

2.4. Conclusion

Here we successfully developed an integrated multiplexed microfluidic system for rapid and ultrasensitive ELISA detection of protein biomarkers. When compared with other existing microfluidic devices for solid-phase immunoassays, our system could perform flow through immuno-capture in an open channel and subsequently chemifluorescence detection in a reduced

volume, by improving the analytical sensitivity. Using this novel method, we demonstrated the quantitative detection of three biomarkers, which showed better performance than the commercial ELISA kits. We can also detect fifteen biomarkers with just a single drop of blood which would allow us to just use only one device for the detection of multiple biomarkers. The ability of our assay to quantitatively detect protein biomarkers across a broad dynamic range will be beneficial for the clinical utilities as the target concentration can vary significantly in patients at different disease states. Moreover, the adaptation of the femtoliter microwell pattern in our design opens opportunity to develop the next-generation microfluidic platforms that integrate and automate both digital and analog immunoassays to facilitate the advance of proteomics.

2.5 References

1. Choi, K.; Ng, A. H. C.; Fobel, R.; Wheeler, A. R., Digital Microfluidics. *Annual Review of Analytical Chemistry* **2012,** *5* (1), 413-440.
2. Mok, J.; Mindrinos, M. N.; Davis, R. W.; Javanmard, M., Digital microfluidic assay for protein detection. *Proceedings of the National Academy of Sciences* **2014,** *111* (6), 2110-2115.
3. Zhang, Y.; Noji, H., Digital Bioassays: Theory, Applications, and Perspectives. *Analytical Chemistry* **2017,** *89* (1), 92-101.
4. Scientific Principle of Simoa™ (Single Molecule Array) Technology. *Quanterix Corporation* **2013**.
5. Decrop, D.; Pardon, G.; Brancato, L.; Kil, D.; Zandi Shafagh, R.; Kokalj, T.; Haraldsson, T.; Puers, R.; van der Wijngaart, W.; Lammertyn, J., Single-Step Imprinting of Femtoliter Microwell Arrays Allows Digital Bioassays with Attomolar Limit of Detection. *ACS Applied Materials & Interfaces* **2017,** *9* (12), 10418-10426.
6. Cohen, L.; Walt, D. R., Single-Molecule Arrays for Protein and Nucleic Acid Analysis. *Annual Review of Analytical Chemistry* **2017,** *10* (1), 345-363.
7. Samiei, E.; Tabrizian, M.; Hoorfar, M., A review of digital microfluidics as porTable platforms for lab-on a-chip applications. *Lab on a Chip* **2016,** *16* (13), 2376-2396.
8. Rissin, D. M.; Fournier, D. R.; Piech, T.; Kan, C. W.; Campbell, T. G.; Song, L.; Chang, L.; Rivnak, A. J.; Patel, P. P.; Provuncher, G. K.; Ferrell, E. P.; Howes, S. C.; Pink, B. A.; Minnehan, K. A.; Wilson, D. H.; Duffy, D. C., Simultaneous Detection of Single Molecules and Singulated Ensembles of Molecules Enables Immunoassays with Broad Dynamic Range. *Analytical Chemistry* **2011,** *83* (6), 2279-2285.
9. Zhang, H.; Nie, S.; Etson, C. M.; Wang, R. M.; Walt, D. R., Oil-sealed femtoliter fiber-optic arrays for single molecule analysis. *Lab on a Chip* **2012,** *12* (12), 2229-2239.
10. Rondelez, Y.; Tresset, G.; Tabata, K. V.; Arata, H.; Fujita, H.; Takeuchi, S.; Noji, H., Microfabricated arrays of femtoliter chambers allow single molecule enzymology. *Nat Biotech* **2005,** *23* (3), 361-365.
11. Duffy, M. J., Carcinoembryonic Antigen as a Marker for Colorectal Cancer: Is It Clinically Useful? *Clinical Chemistry* **2001,** *47* (4), 624-630.
12. Garcia, M.; Seigner, C.; Bastid, C.; Choux, R.; Payan, M. J.; Reggio, H., Carcinoembryonic Antigen Has a Different Molecular Weight in Normal Colon and in Cancer Cells due to N-Glycosylation Differences. *Cancer Research* **1991,** *51* (20), 5679-5686.
13. Frederick, L.; Wang, X.-Y.; Eley, G.; James, C. D., Diversity and Frequency of Epidermal Growth Factor Receptor Mutations in Human Glioblastomas. *Cancer Research* **2000,** *60* (5), 1383.
14. Sharma, S.; Sharma, M. C.; Sarkar, C., Morphology of angiogenesis in human cancer: a conceptual overview, histoprognostic perspective and significance of neoangiogenesis. *Histopathology* **2005,** *46*.
15. Hoon H. Sunwoo, M. R. S., Cancer Markers. *The immunoassay Handbook, Elsevier Science* **2013**.
16. Scholler, N.; Urban, N., CA125 in Ovarian Cancer. *Biomarkers in medicine* **2007,** *1* (4), 513-523.
17. Akira, S.; Taga, T.; Kishimoto, T., Interleukin-6 in biology and medicine. *Adv Immunol* **1993,** *54*.
18. Guo, Y.; Xu, F.; Lu, T.; Duan, Z.; Zhang, Z., Interleukin-6 signaling pathway in targeted therapy for cancer. *Cancer Treat Rev* **2012,** *38*.

19. Todorović-Raković, N.; Milovanović, J., Interleukin-8 in Breast Cancer Progression. *Journal of Interferon & Cytokine Research* **2013,** *33* (10), 563-570.
20. Wang, T.; Zhang, M.; Dreher, D. D.; Zeng, Y., Ultrasensitive microfluidic solid-phase ELISA using an actuaTable microwell-patterned PDMS chip. *Lab on a Chip* **2013,** *13* (21), 4190-4197.
21. Shang, Y.; Zeng, Y.; Zeng, Y., Integrated Microfluidic Lectin Barcode Platform for High-Performance Focused Glycomic Profiling. **2016,** *6*, 20297.

Chapter 3
Detection of Prostate Specific Antigen using Aptamer – Lectin based Assay

3.1 Introduction

3.1a. Protein glycosylation

Glycosylation, one of the most prevalent post-translational modifications (PTM) found in proteins, and play a significant role in a varied set of biological processes such as the cellular regulation and immune response. Glycosylation is also a best indicator of environmental effects that are observed during cellular processes.[1] It has been proved that glycosylation is involved in many signaling pathways associated mainly with the transformation of a cell under normal conditions into a cancer cell. The process of glycosylation has been closely associated with cancer, for example, glycosylation can affect the tumor antigen interactions with receptors, e.g. CA125 with galectin.[2] Protein glycosylation is one of the challenging process to analyze due to its aggressive and heterogeneous nature caused by the non-templated biosynthesis. There are also several types of glycosylation. The most currently seen are N- linked glycosylation and O-mannosylation as shown in Figure 37.[3] Human plasma proteins are usually present within a dynamic concentration range of about 10 orders of magnitude.

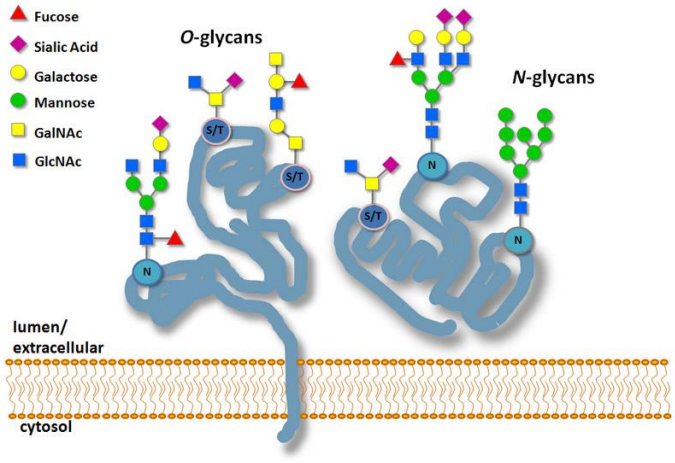

Figure 37: Representative mammalian O-linked and N-linked glycans. Proteins can be glycosylated by N-linkage to asparagine residues or O-linkage to serine or threonine residues. [4]

Whereas, the glycoproteins of interest, such as cancer biomarkers, are generally present at very low concentration levels which makes it extremely challenging to accurately measure their glycan changes.[5] Presently, mass spectrometry (MS) is a powerful technology which is widely used for structural analysis of glycoproteins and has been the gold standard method in glycomics since long time. However, glycan analysis by MS methods usually require large sample volumes and multi-step process for sample preparation.[6] Due to the tedious and time-consuming process this method compromises the quantification accuracy and eventually limits the throughput for large-scale clinical studies to correlate the glycosylation process. Serum is the most common diagnostic fluid, but there is currently a lack of global methods for the characterization of glycoproteins, the 'glycoproteome'. [7]

3.1b. Lectin Microarray

In the recent times, lectin microarray has been emerged as an effective platform that can overcome the challenges faced by MS-based methods for glycomic studies. The lectin microarray technology has been very attractive and increasing attention of not only glycoscientists but also researchers in other fields. This is mainly, because the method enables the direct analysis of crude samples containing glycoproteins, without liberation of glycans, unlike conventional methods.[8]

Lectins are defined as proteins that have the unique feature to recognize and bind to the carbohydrate complexes that protrude from glycolipids and glycoproteins. The term lectin is derived from the Latin word "legere" meaning "to choose", and has been generalized to envelope all the non-immune carbohydrate specific agglutinins regardless of blood type source or specificity.[9] The interaction of lectins with carbohydrates can be as specific and strong as the interaction between those of antigen-antibody or substrate-enzyme. Lectins bind not only to oligosaccharides on cells but they also bind to free-floating glycans including monosaccharides.[10]

The interactions of lectin and monosaccharide however, are relatively weak with dissociation constants often on the order of micromolar to millimolar range.[8] There are many applications of lectins where they can be used to detect specific glycans in a biomarker like PSA. One of the commonly used format is the lectin microarray. In this format, a series of lectins and carbohydrate-binding antibodies with different carbohydrate-binding specificity are immobilized on a glass slide which are treated with appropriate surface chemistry, like an epoxy functional group which bind to the lectin proteins.[11] After the immobilization procedure, surface areas containing residual activated groups are treated with appropriate blockers, such as glycan-free serum albumin. Binding of the target glycans can be detected either directly through the labeling with fluorescent reagents or indirectly by overlaying the target glycoprotein with biotinylated antibody and fluorescently labeled streptavidin as shown in Figure 38.[12] One of the limitation is that the interaction between lectin and glycan is very weak when compared to antigen and antibody. To, improve the sensitivity and specificity, extremely long durations of incubation (usually overnight) and rapid sample processing are required for lectin-glycan assay.[4, 7]

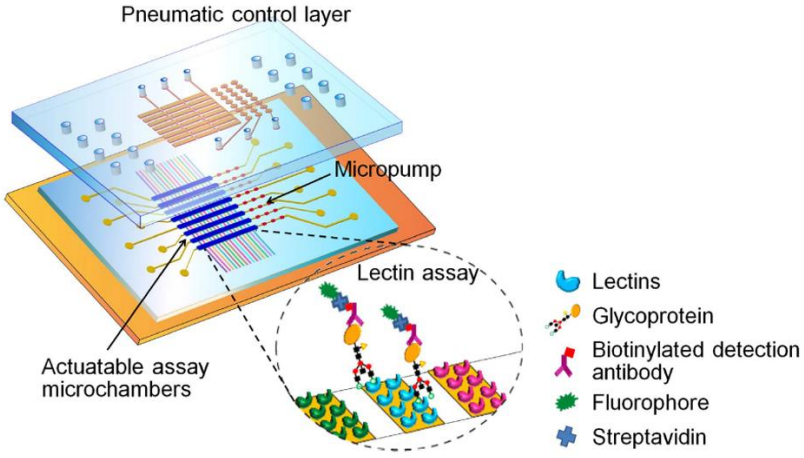

Figure 38: Schematic illustration of the chip design and the scheme of antibody-lectin sandwich assay. The two-layer PDMS chip integrates eight parallel units each consisting of a three-valve pump and an actuatable assay chamber.[7]

Here, we employed microfluidic platforms for the lectin bioassay due to their immense advantages such as low sample volume, portable and simple experimental set up as discusses in chapter 1.

3.1c. PSA Glycosylation

Prostate Cancer also known as glandular cancer of the prostate gland, is one the most challenging medical issue worldwide.[13] The prostate is a walnut shaped structure which is located under bladder and play a significant role in the male reproduction system. PSA is a 33 kDa serine protease (kallikrein-3) secreted by the prostate gland.[14] The physiological function of the prostate is to involve in the ejaculation through the secretory gland and it is a major secretor of the glycoproteins almost all the types.[15] The development and the maintenance of these roles are dependent upon the signals from the androgen receptor (AR). One of the principle role of the prostate is to produce prostate – specific antigen (PSA) which is a serine protease that can liquify semen and thereby enhances the sperm motility.[16] PSA is a glycoprotein and the serum levels of PSA have been widely used as a biomarker of prostate cancer because during the initial stages the disruption of the prostatic epithelium allows the PSA to leak into the blood circulation. PSA has a N-glycosylation site at asparagine (Asn) – 69 which has been the main target of multiple studies. The possible glycan structures that are attached to PSA are mainly the four biantennary glycans and are estimated to comprise almost 80% of the total number of PSA bound glycans. These all have Hex 5 subunits consisting of three mannose and two galactose subunits or Hex – N-acetylglucosamine (NAc) which has four β-N-acetylglucosamine [GlcNAc] subunits with either one or two sialic acid residues and the presence of core fucose moieties as shown in the Figure 39.[17]

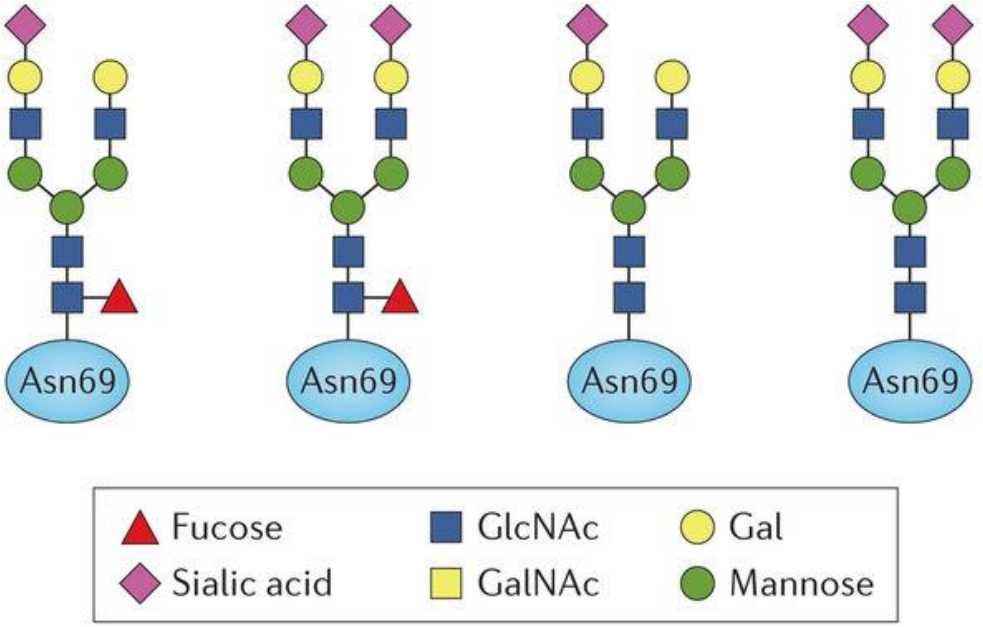

Figure 39: The four most common biantennary N-linked glycan structures detected on PSA asparagine – 69. These all have Hex 5 subunits consisting of three mannose and two galactose subunits or Hex – N- acetylglucosamine (NAc) which has four β-N-acetylglucosamine [GlcNAc] subunits with either one or two sialic acid residues and the presence of core fucose moieties.[17]

Here in this work we have used different biotinylated lectins like SNA, AAL, Con A, DSL and jacalin based on their respective specificities to different glycans a shown in the Table.

3.1d. Aptamers over Antibodies

It is well known that ELISA assays usually depend on antibodies which have various downsides. In addition, to batch-to-batch variations in the production of antibody, it is very tedious and challenging to generate specific monoclonal antibodies, mainly against non-immunogenic molecules.[18] To overcome these challenges there is an immense need for an alternative to antibodies to improve the ELISA method, and, among the different options, commutable replacement of the target capturing agent with a more suitable probe is an optimal approach.[14] This alternative molecular recognition element (MRE) is termed as 'aptamer', which has the potential

to complement the role of antibodies in ELISA, thereby resulting in an improved ELISA which is called as enzyme-linked apta sorbent assay (ELASA). Aptamers are also known as the chemical antibodies which are either single- stranded DNA or RNA that can bind to a wide range of molecules with high specificity and affinity. DNA aptamers and RNA aptamers are not different from each other in terms of specificity or affinity, except that DNA aptamers have greater intrinsic chemical stability.[19-20] It is also difficult to use antibodies for glycoprofiling because the capture antibodies are also glycosylated and there is a high possibility for misleading results because the lectins can bind to the glycans on capture antibodies rather than on antigens. Therefore, it is much better to use aptamers as capture probes. The most significant feature of using the aptamers is that they have dissociation constants that can reach as low as the picomolar–femtomolar range which thereby increases the sensitivity of the biomarker detection and can also handle the cross reactivity issues which are usually observed in glycoprofiling.[14] Therefore, aptamers could be used as a potential tool for multi glycan profiling of biomarkers with high sensitivity and selectivity. At the same time, aptamers are easy to maintain, and they can also be reused which reduces the cost.[18, 21]

Here, we used PSA aptamer for profiling the PSA expression with different biotinylated lectins.

3.2 Experimental

3.2.1 Chemicals and Reagents

The following reagents were used as received: 1 phosphate buffered saline solution 1 PBS (> 98.5, Mediatech, Inc.), Superblock T20 blocking buffer (PBST) (Thermo Scientific), fluorescein di B D galactopyranoside (FDG) (Invitrogen), Streptavidin Beta galactosidase conjugate (SBG) (Invitrogen), 2- propanol (IPA) (> 99.5%; Sigma Aldrich), ethanol (100% Decon laboratories Inc.), All lectins were ordered from (Vector Labs) and (EY Labs). RNase A and B

from bovine pancreas were purchased (Sigma-Aldrich), 3 glycidyloxy propyl trimethoxy silane (GPS) (Sigma Aldrich), anhydrous toluene (>99.8%; Alfa Aesar), N,N,N',N'-tetramethylethylenediamine (TEA) (Sigma Aldrich), SU-8 2010 (Microchem), protein free PBS (Thermo Scientific).

3.2.2 Micro Fabrication and device assembly

The microfluidic fabrication was performed as mentioned under section and the same device with GOPS patterning was used for aptamer based assays which will be discussed further.

3.2.3 RNAse Assay

The glass slides were immobilized with GOPS as mentioned in the surface patterning section and then the PDMS device was bonded permanently on the patterned glass slides. RNase Aptamer 5 µM in water immobilized onto the glass slide and incubated for 2 h at room temperature. The channels were then washed with PBST. The channels blocked with protein free PBS and incubated for 1 h at room temperature. Then RNase B protein (Positive control) and RNase A (Negative control) 0.1 µg/mL and 1 µg /mL diluted in PBS with Mg^{2+} and Ca^{2+} were added into channels and incubated for 1.5 h at room temperature. Then biotinylated ConA 0.2 µg/mL in 10mM HEPES buffer with Ca^{2+}, Mg^{2+}, Mn^{2+} was added into channels and incubated for 1 h at room temperature. Then SBG – 0.2 µg/mL was added into channels and incubated for 30 min. 500 µM FDG was added as the final step and incubated for various time intervals and the optimized time was 20 min. The channels were pressed down with the actuator. The signal was measured under fluorescent microscope, with 470nm wavelength and exposure time is 8000ms.

3.2.6 PSA assay

The glass slides were immobilized with GOPS as mentioned in the surface patterning section and then the PDMS device was bonded permanently on the patterned glass slides. PSA

Aptamer 5 µM in water immobilized onto the glass slide and incubated for 2 h at room temperature. The channels were then washed with PBST. The channels blocked with protein free PBS and incubated for 1 h at room temperature. Then PSA protein 0, 10 pg/mL, 100 pg/mL diluted in PBS were added into channels and incubated for 1.5 h at room temperature. Then biotinylated PSA antibody 0.8 µg/mL in PBS was added into channels and incubated for 1 h at room temperature. Then SβG – 0.2 µg/mL was added into channels and incubated for 30 min. 500 µM FDG was added as the final step and incubated for various time intervals and the optimized time was 20 min. The channels were pressed down with the actuator. The signal was measured under fluorescent microscope, with 470nm wavelength and exposure time is 8000ms.

3.2.7 Detection of PSA with different biotinylated lectins

For the detection of PSA with different lectins the glass slides and devices were prepared as mentioned under section 3.2.6. For all the PSA assays we used 5 µM of single stranded PSA DNA aptamer. PSA protein concentrations of 0 – 100 pg/mL were diluted in PBS, then SβG – 0.2 µg/mL was added into channels and incubated for 30 min. 500 µM FDG was added as the final step and incubated for various time intervals and the optimized time was 20 min. The channels were pressed down with the actuator. The signal was measured under fluorescent microscope, with 470nm wavelength and exposure time is 8000ms. The concentration of biotinylated lectins varied accordingly. For PSA assay with the biotinylated lectins SNA - 0.2 µg/mL, jacalin - 0.5 µg/mL, AAL – 0.1 µg/mL, DSL - 0.2 µg/mL and Con A – 0. 0.1 µg/mL in PBS were used as shown in the Figure 40.

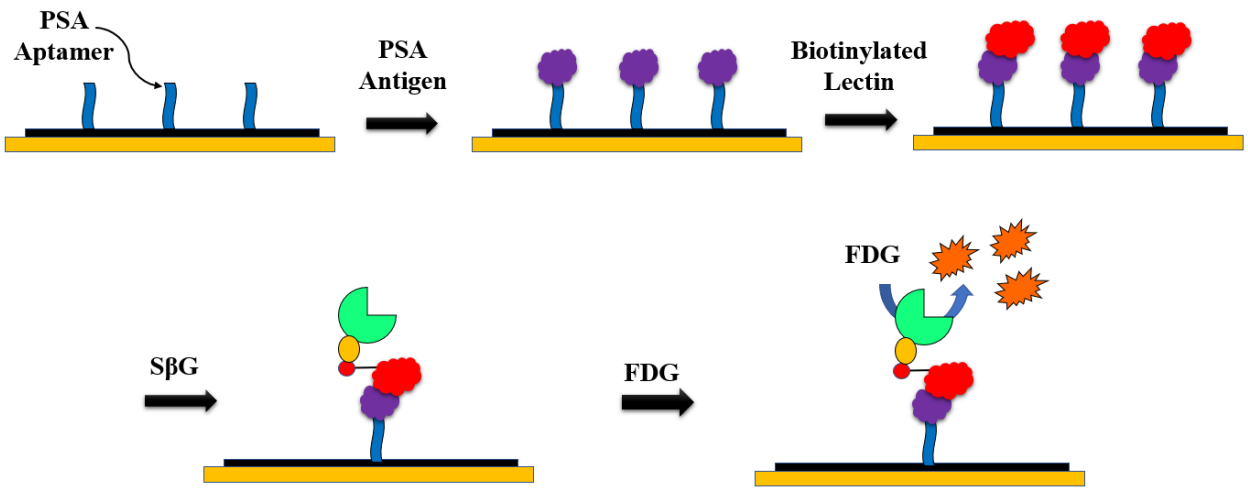

Figure 40: Schematic representation of Aptamer lectin based assay. PSA Aptamer 5 µM in water immobilized onto the glass slide. PSA protein concentrations of 0 – 100 pg/mL diluted in PBS were added into channels and incubated. Then biotinylated lectins with varied concentration in PBS were added into channels and incubated. Then SβG – 0.2 µg/mL was added into channels and incubated. 500 µM FDG was added as the final step and incubated for various time intervals and the optimized time was 20 min.

3.3 Results and Discussion

3.3.1 RNAse Assay

RNase assay was performed as mentioned in the above protocol and various concentrations of RNase A and RNase B were used in the assay starting from 0, 0.1, and 1 µg/mL. Here, we demonstrated the microfluidic assay combined with the microwell assisted analog chemifluorescence detection for quantitative detection of RNase protein. The fluorescence images acquired for different concentration standards were displayed in Figure 41, which showed a very low background level for the blank control. The averaged fluorescence intensities for RNase B was high 201.19 for 1 µg/mL and 99.78 for 0.1 µg/mL which was a positive control as expected and RNase A was having lower intensities 28.18 for 1 µg/mL and 12.58 for 0.1 µg/mL as expected because it was used a negative control and for the blank it was 11.32. This assay was performed to test the working of the lectin assay protocol as shown in Figure 41.

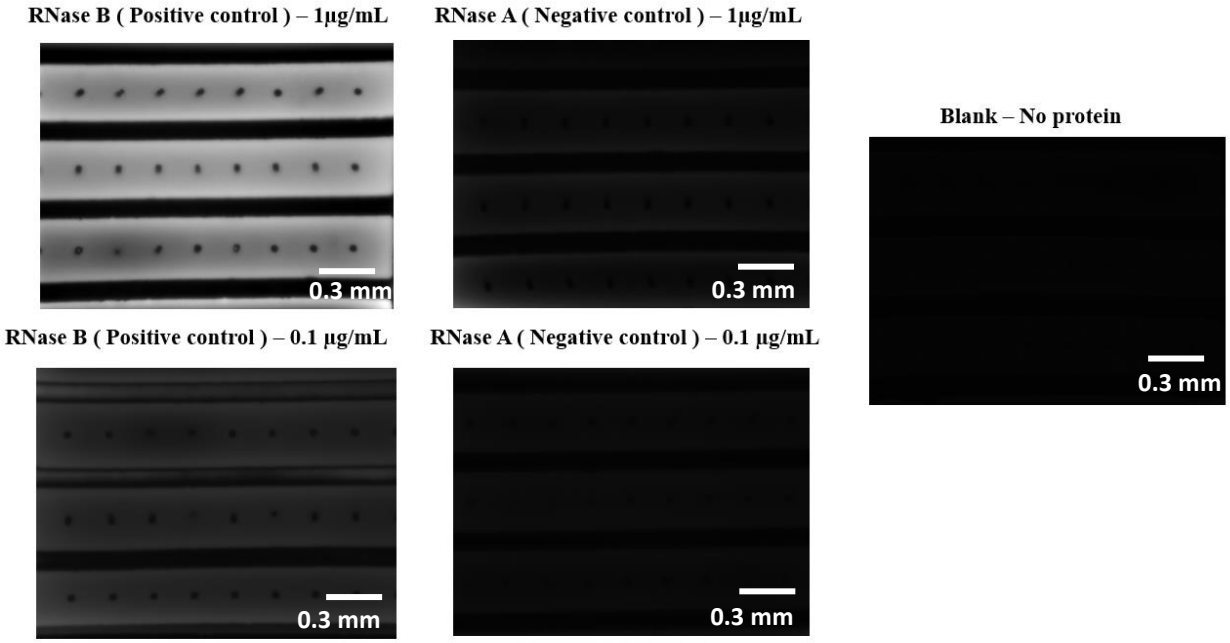

Figure 41: For testing the performance of the microwell-assisted microfluidic chemifluorescence detection of lectins various concentrations of RNase A and B were passed through the channels. A typical fluorescence image was presented in the Figure for various concentrations of 0, 0.1, 1, 10, 100 µg/mL respectively.

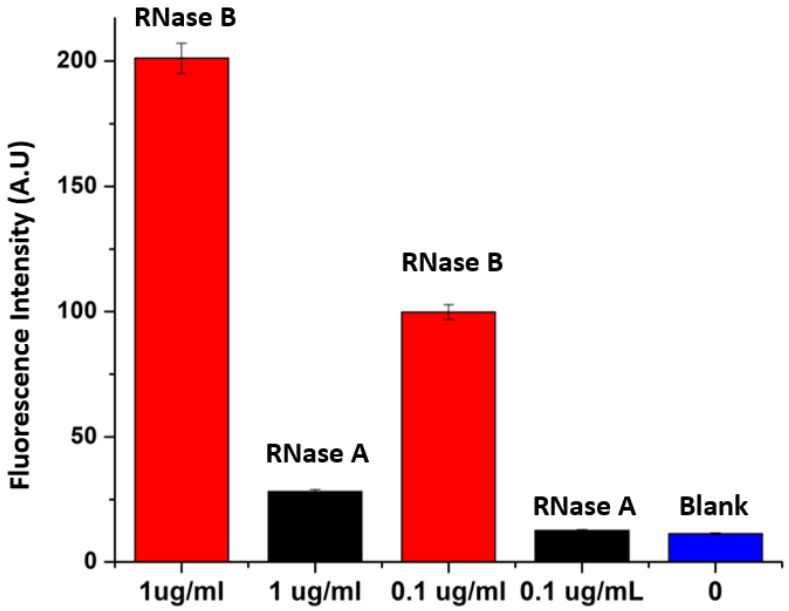

Figure 42: RNase assay results with RNase B as positive control, RNase A as negative control and their fluorescence intensities.

3.3.2 PSA assay

PSA assay was performed as mentioned in the above protocol and various concentrations of target antigen were used in the assay starting from 0, 0.1, 1, 10 and 100 pg/mL. As an example, the typical fluorescence image for 1 pg/mL was displayed in Figure 43, which showed a very low background level for the blank control and the percentage of positive microwells increased along with the PSA concentration. The assay performance was pretty good by resulting in low background and high detection limit of 10 fg/mL. The percentage of positive microwells increased with that of the PSA concentration. As shown in the Figure 43 we saw a clear straight increase after the assay reached a saturation point. The working range of the digital assay was between 0.1 – 1 pg/mL concentrations of PSA whereas from 10 pg/mL the assay slightly deviated from the linear increase to saturation phase where it was no more a digital signal as most of the wells were having fluorescent signal. We also compared the log % active wells and log concentration of PSA which showed a semi linear increase as shown in Figure 44. As shown in the Figure 45 we clearly experienced a linear increase in the percentage of positive wells within the concentration range of 0.1 -1 pg/mL with R^2 value = 0.9815. The λ value which is the average number of molecules per well was calculated using (eq.4) for each concentration based on the positive wells as shown in Table 8. The Table clearly showed that the λ increased with the increase in positive wells which increased along with the concentration of PSA.

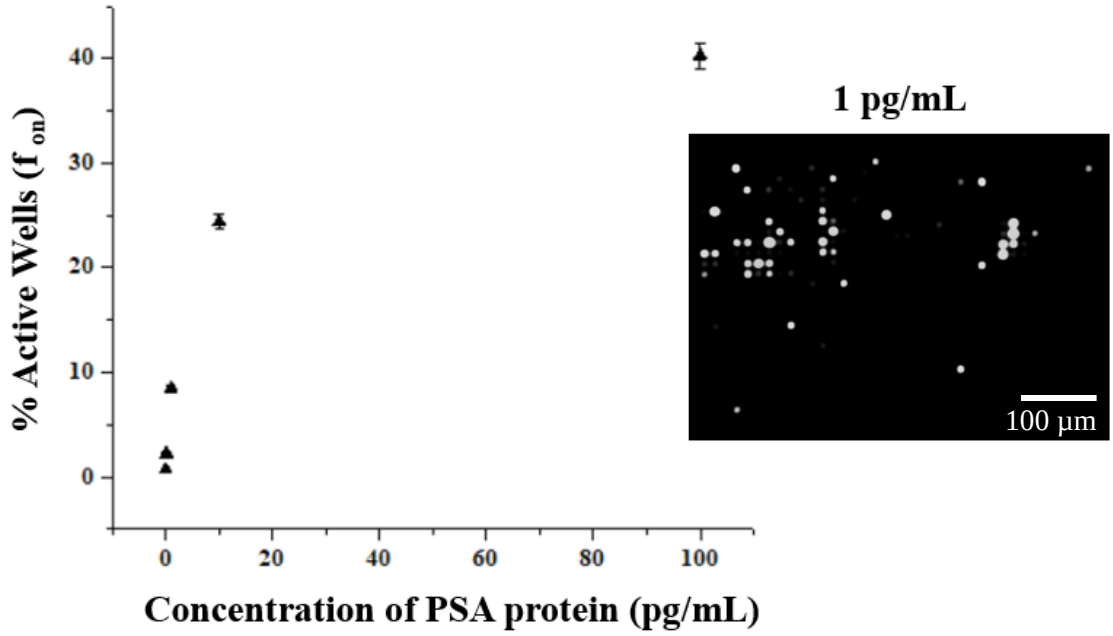

Figure 43: Quantitative detection of PSA was achieved over a dynamic range of 0.1 pg/mL to 100 pg/mL with a theoretical LOD of 10 fg/mL calculated from the value of blank signal plus three standard deviations. Error bars are standard deviations of three replicate experiments. Typical fluorescence image of 1 pg/mL was shown as an example of digital image.

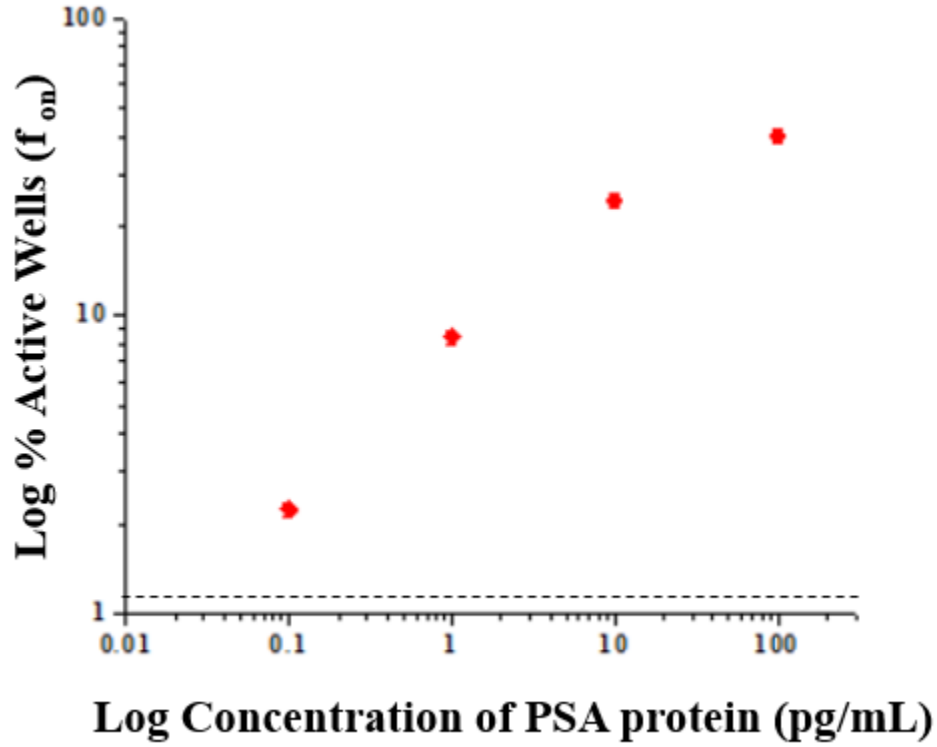

Figure 44: Comparison with log % active wells with log concentration of PSA range 0.1 – 100 pg/mL with a theoretical LOD of 10 fg/mL calculated from the value of blank signal plus three standard deviations. Error bars are standard deviations of three replicate experiments.

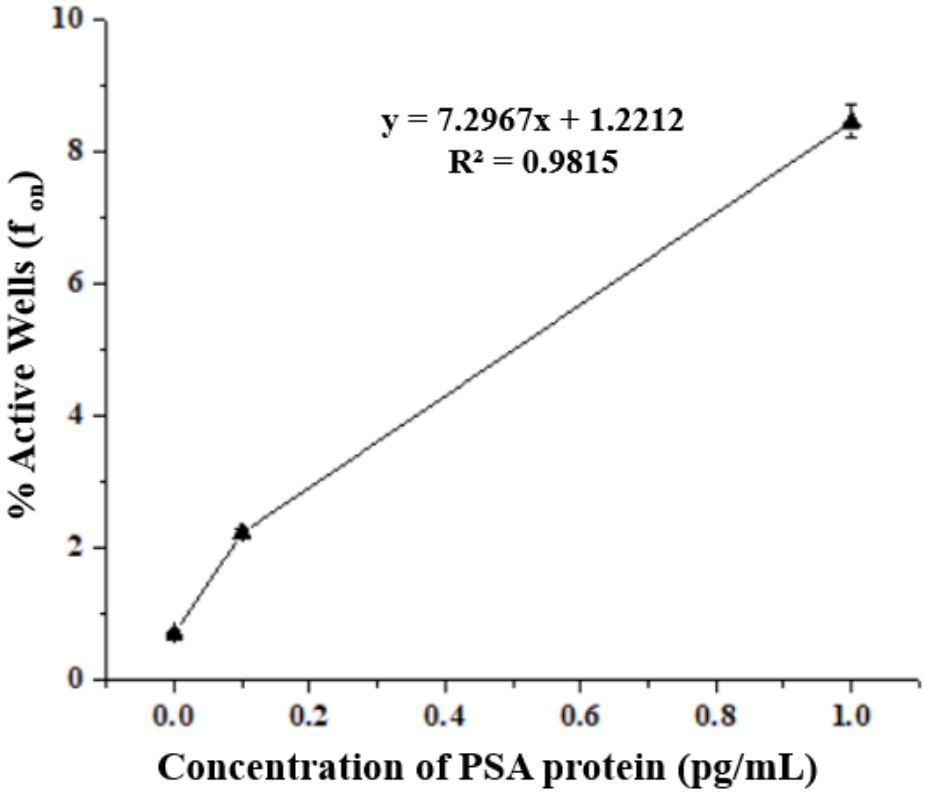

Figure 45: A working concentration range of PSA for digital assay was between 0.1 to 1 pg/mL. Error bars are standard deviations of three replicate experiments.

Table 8: Calculation of λ (average number of molecules per well) values from % active wells for PSA concentration range. The Table clearly showed that the λ increased with the increase in positive wells which increased along with the concentration of PSA.

Concentration of PSA protein (pg/mL)	% Active wells (f_{on})	λ
0	0.7	0.007
0.1	2.53	0.02
1	8.46	0.08
10	24.4	0.27
100	40.29	0.5

3.3.3 Detection of PSA with different biotinylated lectins

Table 9: Different lectins with their origin and specificities for glycans

Lectin	Origin	Specificity
SNA	*Sambucus Nigra*	Sialic Acid
Jacalin	*Artocarpus Integrifolia*	Galactose
AAL	*Aleuria Aurentia*	Fructose
DSL	*Datura Stramonium*	[GluNAc] 1-3, N Acetyl glucosamine
Con A	*Canavalia Ensiformis*	Mannose and glucose

Different biotinylated lectins were used to detect PSA. PSA assay with biotinylated SNA lectin which has specificity for sialic acid was performed as mentioned in the above protocol and various concentrations of target antigen were used in the assay starting from 0, 0.1, 1, 10 and 100 pg/mL. As an example, the typical fluorescence image for 0.1 pg/mL was displayed in Figure 46, which showed a very low background level for the blank control and the percentage of positive microwells increased along with the PSA concentration. The assay performance was pretty good

by resulting in low background and high detection limit of 9.5 fg/mL. The percentage of positive microwells increased with that of the PSA concentration. As shown in the Figure 46 we saw a clear straight increase after the assay reached a saturation point. The working range for the digital assay was between 0.1 – 1 pg/mL concentrations of PSA whereas from 10 pg/mL the assay slightly deviated from the linear increase to saturation phase where it was no more a digital signal as most of the wells were having fluorescent signal. We also compared the log % active wells and log concentration of PSA which showed a semi linear increase as shown in Figure 47. As shown in the Figure 48 we clearly experienced an increase in the percentage of positive wells within the concentration range of 0.1 -1 pg/mL with R^2 value = 0.9902. The λ value which is the average number of molecules per well was calculated using (eq.4) for each concentration based on the positive wells as shown in Table 10. The Table clearly showed that the λ increased with the increase in positive wells which increased along with the concentration of PSA.

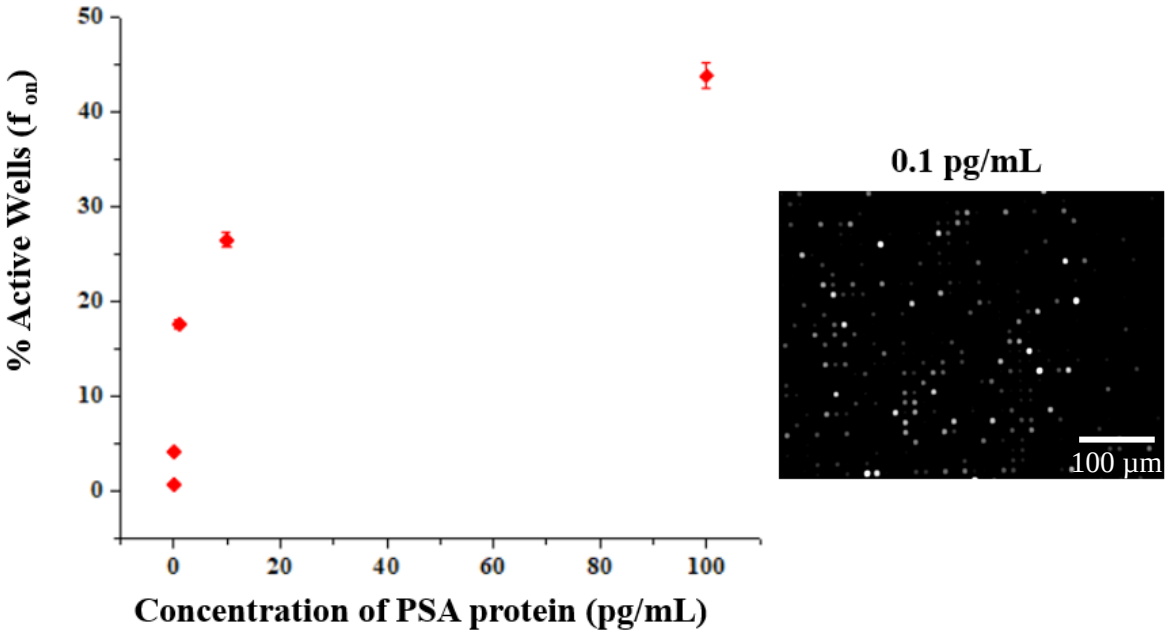

Figure 46: Quantitative detection of PSA using biotinylated SNA lectin was achieved over a dynamic range of 0.1 pg/mL to 100 pg/mL with a theoretical LOD of 9.5 fg/mL calculated from the value of blank signal plus three standard deviations. Error bars are standard deviations of three

replicate experiments. Typical fluorescence image of 0.1 pg/mL was shown as an example of digital image.

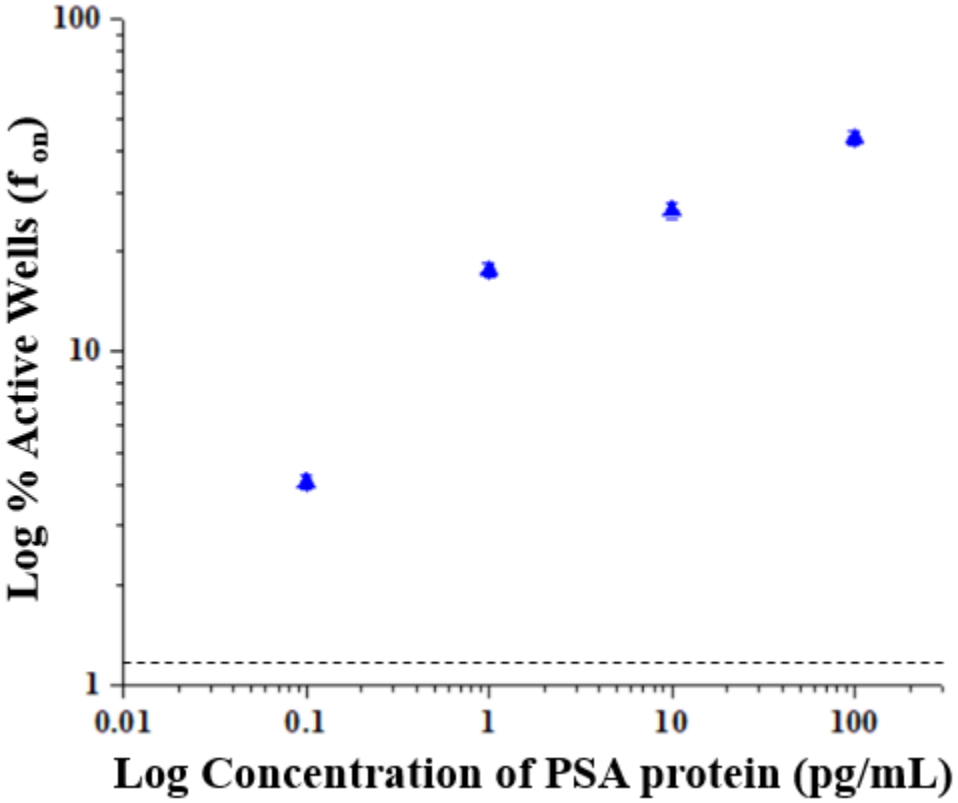

Figure 47: Comparison with log % active wells with log concentration of PSA range 0.1 – 100 pg/mL with a theoretical LOD of 9.5 fg/mL calculated from the value of blank signal plus three standard deviations. Error bars are standard deviations of three replicate experiments.

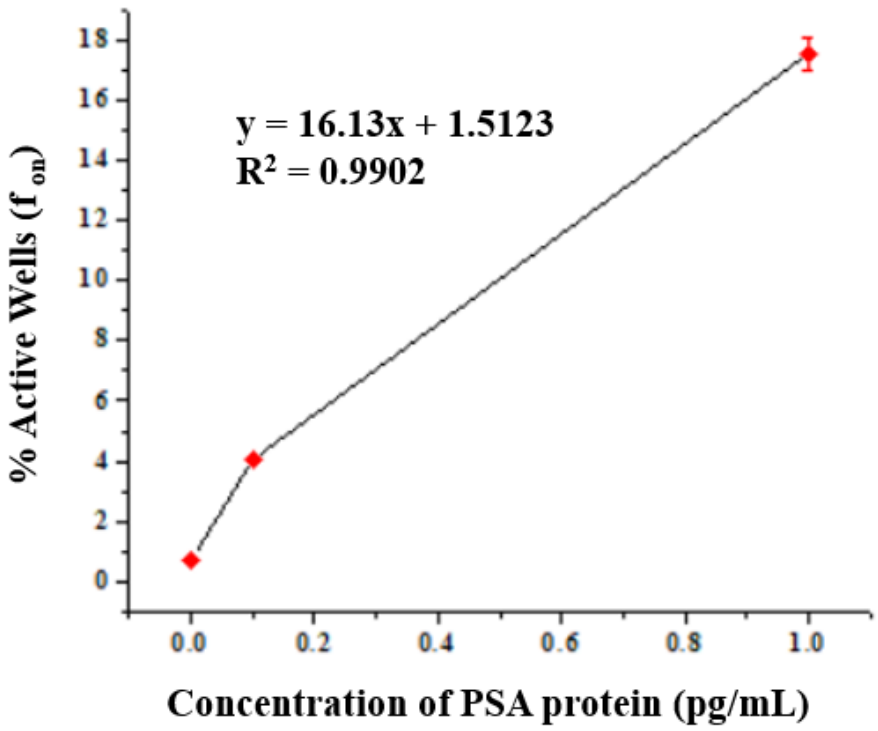

Figure 48: A working concentration range of PSA for digital assay was between 0.1 to 1 pg/mL. Error bars are standard deviations of three replicate experiments.

Table 10: Calculation of λ (average number of molecules per well) values from % active wells for PSA concentration range. The Table clearly showed that the λ increased with the increase in positive wells which increased along with the concentration of PSA detected with SNA.

Concentration of PSA protein (pg/mL)	% Active wells (f_{on})	λ
0	0.68	0.003
0.1	4.05	0.04
1	17.55	0.19
10	26.5	0.3
100	43.82	0.57

PSA assay with biotinylated Jacalin lectin which has specificity for galactose was performed as mentioned in the above protocol and various concentrations of target antigen were used in the assay starting from 0.1 – 100 pg/mL. As an example, the typical fluorescence image for 0.1 pg/mL was displayed in Figure 49, which showed a very low background level for the blank control and the percentage of positive microwells increased along with the PSA concentration. The assay performance was pretty good by resulting in low background and high detection limit of 9.05 fg/mL. The percentage of positive microwells increased with that of the PSA concentration. As shown in the Figure 49 we saw a clear straight increase after the assay reached a saturation point. The linear range was between 0.1 – 1 pg/mL concentrations of PSA whereas from 10 pg/mL the assay slightly deviated from the linear increase to saturation phase where it was no more a digital signal as most of the wells were having fluorescent signal. We also compared the log % active wells and log concentration of PSA which showed a semi linear increase as shown in Figure 50. As shown in the Figure 51 we clearly experienced a linear increase in the percentage of positive wells within the concentration range of 0.1 -1 pg/mL with R^2 value = 0.9898. The λ value which is the average number of molecules per well was calculated using (eq.4) for each concentration based on the positive wells as shown in Table 11. The Table clearly showed that the λ increased with the increase in positive wells which increased along with the concentration of PSA.

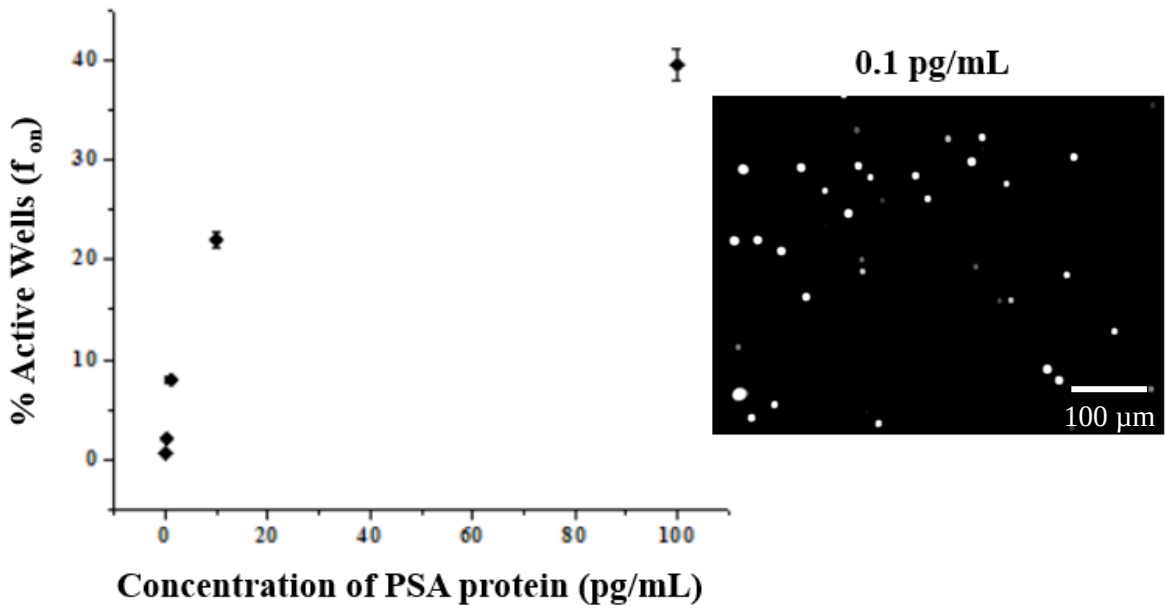

Figure 49: Quantitative detection of PSA using biotinylated jacalin lectin was achieved over a dynamic range of 0.1 pg/mL to 100 pg/mL with a theoretical LOD of 9.05 fg/mL calculated from the value of blank signal plus three standard deviations. Error bars are standard deviations of three replicate experiments. Typical fluorescence image of 0.1 pg/mL was shown as an example of digital image.

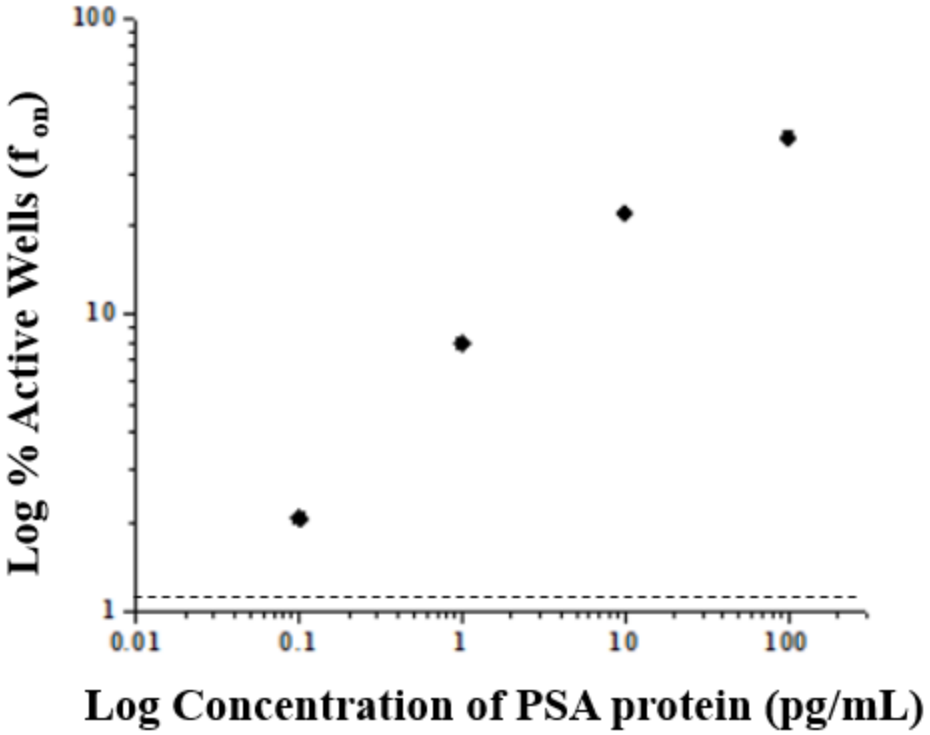

Figure 50: Comparison with log % active wells with log concentration of PSA range 0.1 – 100 pg/mL with a theoretical LOD of 9.05 fg/mL calculated from the value of blank signal plus three standard deviations. Error bars are standard deviations of three replicate experiments.

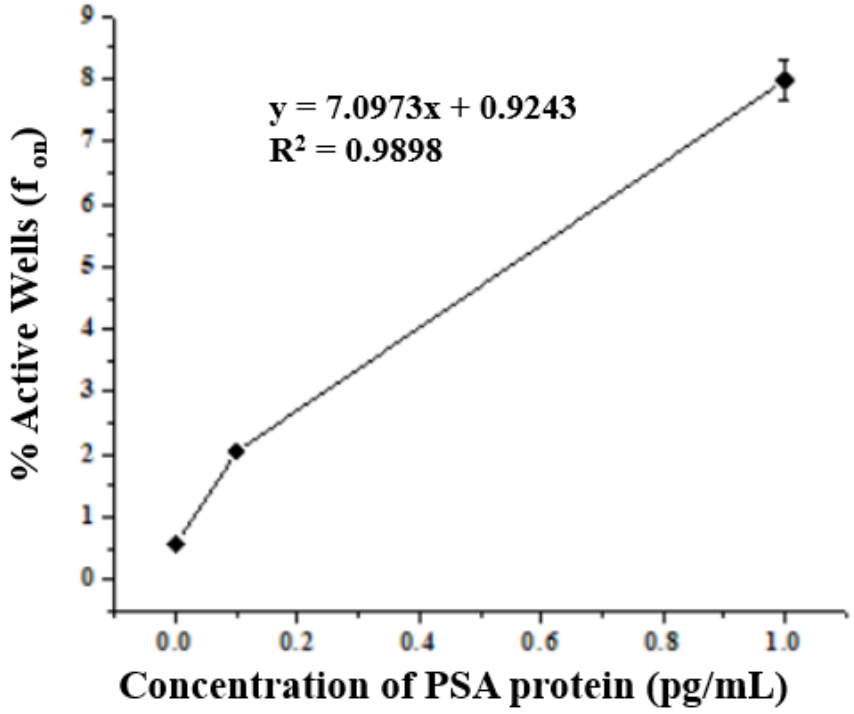

Figure 51: A working concentration range of PSA for digital assay was between 0.1 to 1 pg/mL. Error bars are standard deviations of three replicate experiments.

Table 11: Calculation of λ (average number of molecules per well) values from % active wells for PSA concentration range. The Table clearly showed that the λ increased with the increase in positive wells which increased along with the concentration of PSA detected with Jacalin lectin.

Concentration of PSA protein (pg/mL)	% Active wells (f_{on})	λ
0	0.55	0.005
0.1	2.05	0.02
1	7.98	0.08
10	21.96	0.24
100	39.5	0.5

PSA assay with biotinylated AAL lectin which has specificity for fructose was performed as mentioned in the above protocol and various concentrations of target antigen were used in the assay starting from 0.1 – 100 pg/mL. As an example, the typical fluorescence image for 1 pg/mL was displayed in Figure 52, which showed a very low background level for the blank control and the percentage of positive microwells increased along with the PSA concentration. The assay performance was pretty good by resulting in low background and high detection limit of 8.78 fg/mL. The percentage of positive microwells increased with that of the PSA concentration. As shown in the Figure 52 we saw a clear straight increase after the assay reached a saturation point. The linear range was between 0.1 – 1 pg/mL concentrations of PSA whereas from 10 pg/mL the assay slightly deviated from the linear increase to saturation phase where it was no more a digital signal as most of the wells were having fluorescent signal. We also compared the log % active wells and log concentration of PSA which showed a semi linear increase as shown in Figure 53. As shown in the Figure 54 we clearly experienced a linear increase in the percentage of positive wells within the concentration range of 0.1 -1 pg/mL with R^2 value = 0.9843. The λ value which is the average number of molecules per well was calculated using (eq.4) for each concentration based on the positive wells as shown in Table 12. The Table clearly showed that the λ increased with the increase in positive wells which increased along with the concentration of PSA.

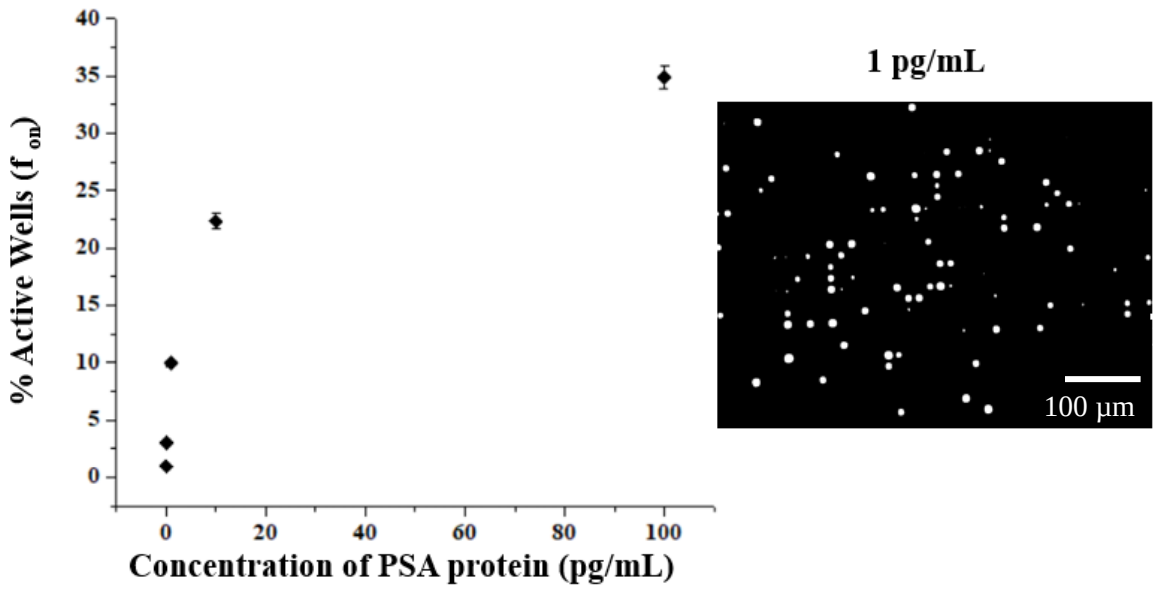

Figure 52: Quantitative detection of PSA using biotinylated AAL lectin was achieved over a dynamic range of 0.1 pg/mL to 100 pg/mL with a theoretical LOD of 8.78 fg/mL calculated from the value of blank signal plus three standard deviations. Error bars are standard deviations of three replicate experiments. Typical fluorescence image of 1 pg/mL was shown as an example of digital image.

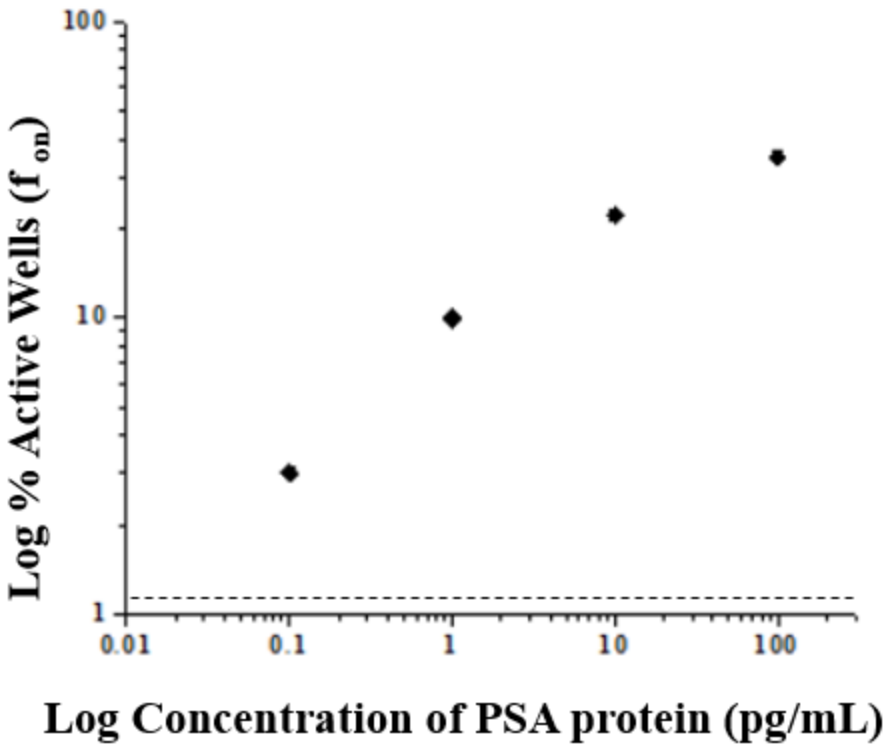

Figure 53: Comparison with log % active wells with log concentration of PSA range 0.1 – 100 pg/mL with a theoretical LOD of 8.78 fg/mL calculated from the value of blank signal plus three standard deviations. Error bars are standard deviations of three replicate experiments.

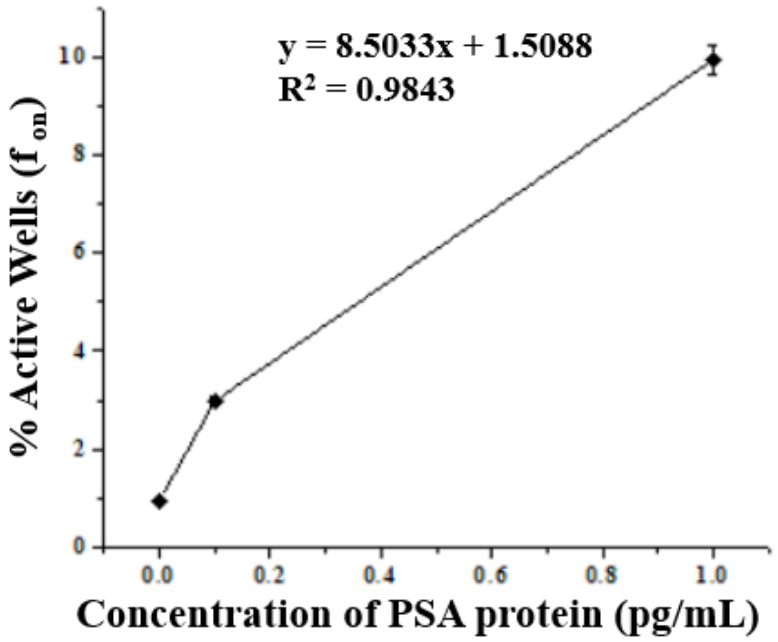

Figure 54: A working concentration range of PSA for digital assay was between 0.1 to 1 pg/mL. Error bars are standard deviations of three replicate experiments.

Table 12: Calculation of λ (average number of molecules per well) values from % active wells for PSA concentration range. The Table clearly showed that the λ increased with the increase in positive wells which increased along with the concentration of PSA detected with AAL.

Concentration of PSA protein (pg/mL)	% Active wells (f_{on})	λ
0	0.95	0.004
0.1	2.98	0.03
1	9.95	0.07
10	22.3	0.25
100	34.9	0.49

PSA assay with biotinylated DSL lectin which has specificity for glucosamine was performed as mentioned in the above protocol and various concentrations of target antigen were used in the assay starting from 0.1 – 100 pg/mL. As an example, the typical fluorescence image for 1 pg/mL was displayed in Figure 55, which showed a very low background level for the blank control and the percentage of positive microwells increased along with the PSA concentration. The assay performance was pretty good by resulting in low background and high detection limit of 11.05 fg/mL. The percentage of positive microwells increased with that of the PSA concentration. As shown in the Figure 55 we saw a clear straight increase after the assay reached a saturation point. The linear range was between 0.1 – 1 pg/mL concentrations of PSA whereas from 10 pg/mL the assay slightly deviated from the linear increase to saturation phase where it was no more a digital signal as most of the wells were having fluorescent signal. We also compared the log % active wells and log concentration of PSA which showed a semi linear increase as shown in Figure 56. As shown in the Figure 57 we clearly experienced a linear increase in the percentage of positive wells within the concentration range of 0.1 -1 pg/mL with R^2 value = 0.9857. The λ value which is the average number of molecules per well was calculated using (eq.4) for each concentration based on the positive wells as shown in Table 13. The Table clearly showed that the λ increased with the increase in positive wells which increased along with the concentration of PSA.

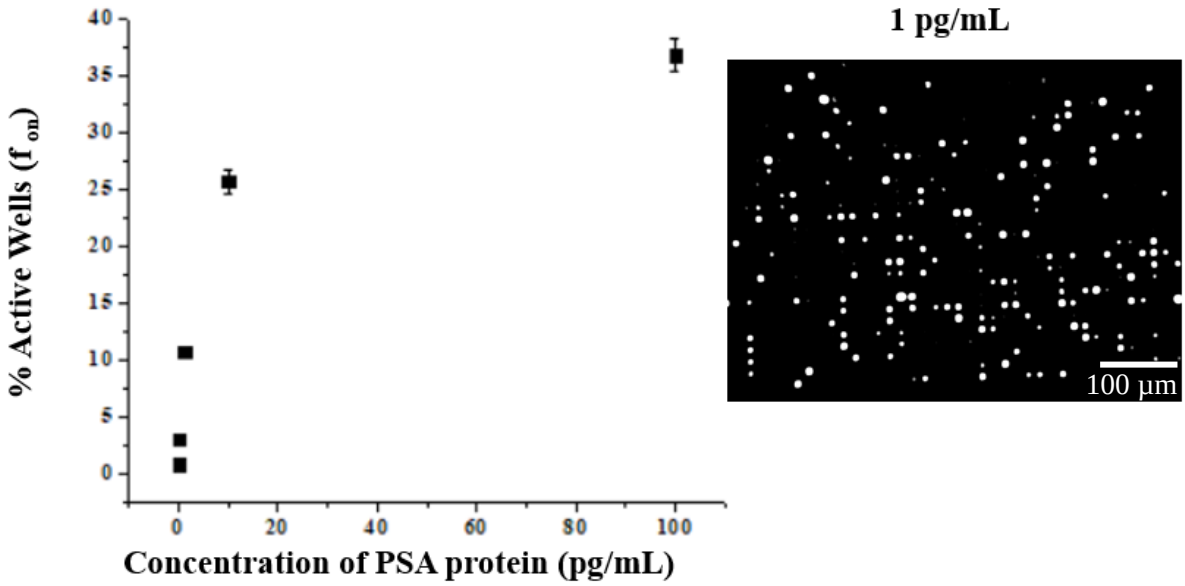

Figure 55: Quantitative detection of PSA using biotinylated DSL lectin was achieved over a dynamic range of 0.1 pg/mL to 100 pg/mL with a theoretical LOD of 11.05 fg/mL calculated from the value of blank signal plus three standard deviations. Error bars are standard deviations of three replicate experiments. Typical fluorescence image of 1 pg/mL was shown as an example of digital image.

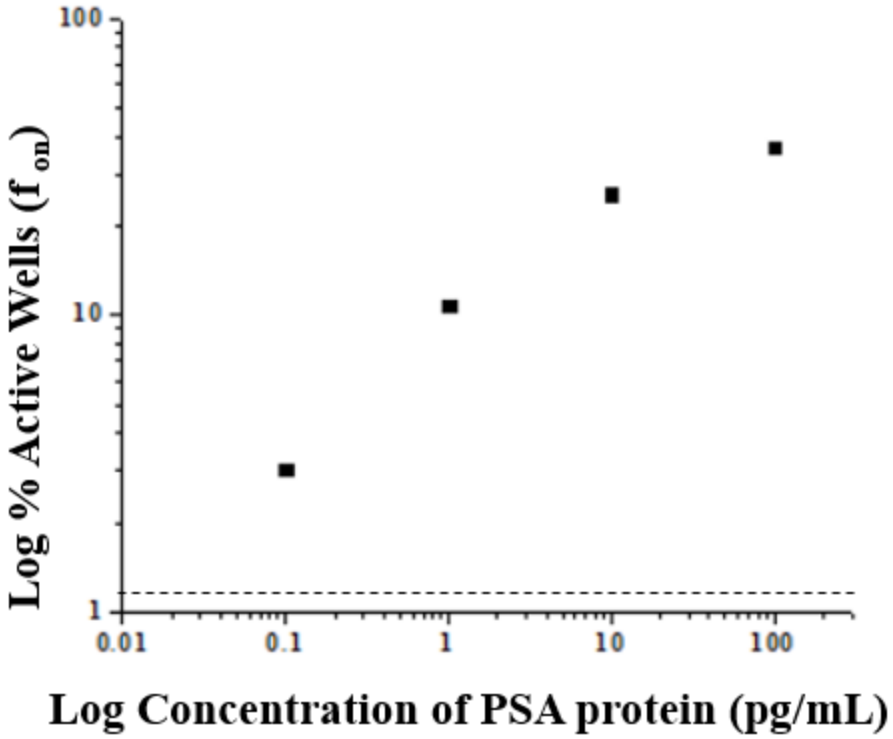

Figure 56: Comparison with log % active wells with log concentration of PSA range 0.1 – 100 pg/mL with a theoretical LOD of 11.05 fg/mL calculated from the value of blank signal plus three standard deviations. Error bars are standard deviations of three replicate experiments.

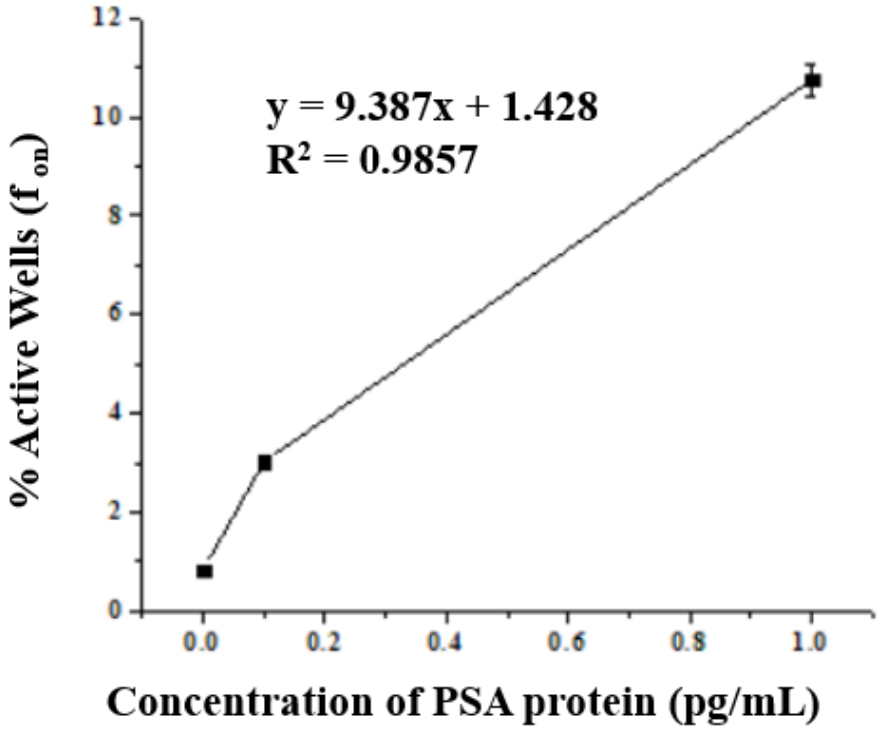

Figure 57: A working concentration range of PSA for digital assay was between 0.1 to 1 pg/mL. Error bars are standard deviations of three replicate experiments.

Table 13: Calculation of λ (average number of molecules per well) values from % active wells for PSA concentration range. The Table clearly showed that the λ increased with the increase in positive wells which increased along with the concentration of PSA detected with DSL lectin.

Concentration of PSA protein (pg/mL)	% Active wells (f_{on})	λ
0	0.84	0.005
0.1	3.02	0.02
1	10.75	0.08
10	25.68	0.27
100	36.8	0.52

PSA assay with biotinylated Con A lectin which has specificity for mannose and glucose was performed as mentioned in the above protocol and various concentrations of target antigen were used in the assay starting from 0.1 – 100 pg/mL. As an example, the typical fluorescence image for 0.1 pg/mL was displayed in Figure 58, which showed a very low background level for the blank control and the percentage of positive microwells increased along with the PSA concentration. The assay performance was pretty good by resulting in low background and high detection limit of 11.75 fg/mL. The percentage of positive microwells increased with that of the PSA concentration. As shown in the Figure 58 we saw a clear straight increase after the assay reached a saturation point. The linear range was between 0.1 – 1 pg/mL concentrations of PSA whereas from 10 pg/mL the assay slightly deviated from the linear increase to saturation phase where it was no more a digital signal as most of the wells were having fluorescent signal. We also compared the log % active wells and log concentration of PSA which showed a semi linear increase as shown in Figure 59. As shown in the Figure 60 we clearly experienced a linear increase in the percentage of positive wells within the concentration range of 0.1 -1 pg/mL with R^2 value = 0.9897. The λ value which is the average number of molecules per well was calculated using (eq.4) for each concentration based on the positive wells as shown in Table 14. The Table clearly showed that the λ increased with the increase in positive wells which increased along with the concentration of PSA.

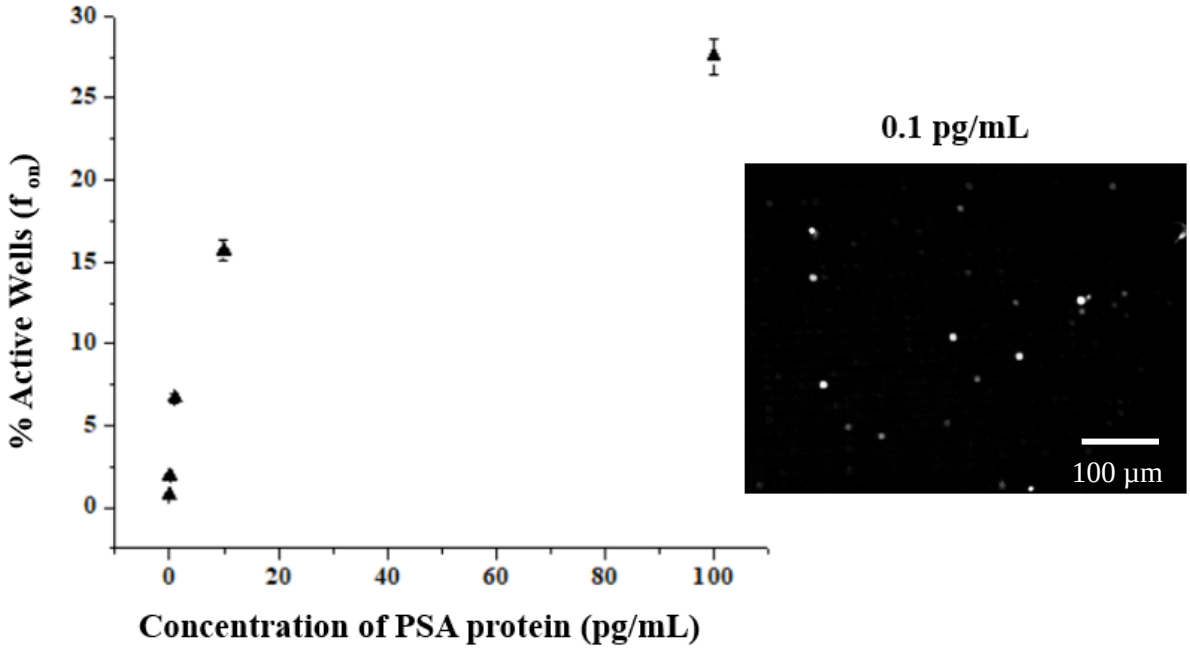

Figure 58: Quantitative detection of PSA using biotinylated Con A lectin was achieved over a dynamic range of 0.1 pg/mL to 100 pg/mL with a theoretical LOD of 11.75 fg/mL calculated from the value of blank signal plus three standard deviations. Error bars are standard deviations of three replicate experiments. Typical fluorescence image of 0.1 pg/mL was shown as an example of digital image.

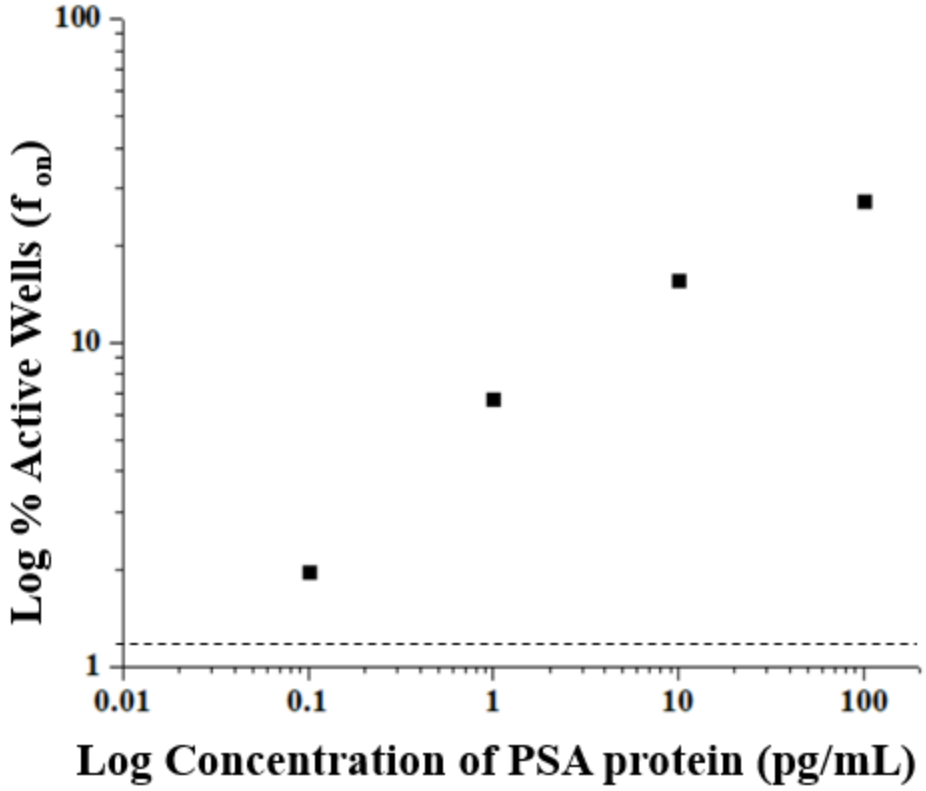

Figure 59: Comparison with log % active wells with log concentration of PSA range 0.1 – 100 pg/mL with a theoretical LOD of 11.75 fg/mL calculated from the value of blank signal plus three standard deviations. Error bars are standard deviations of three replicate experiments.

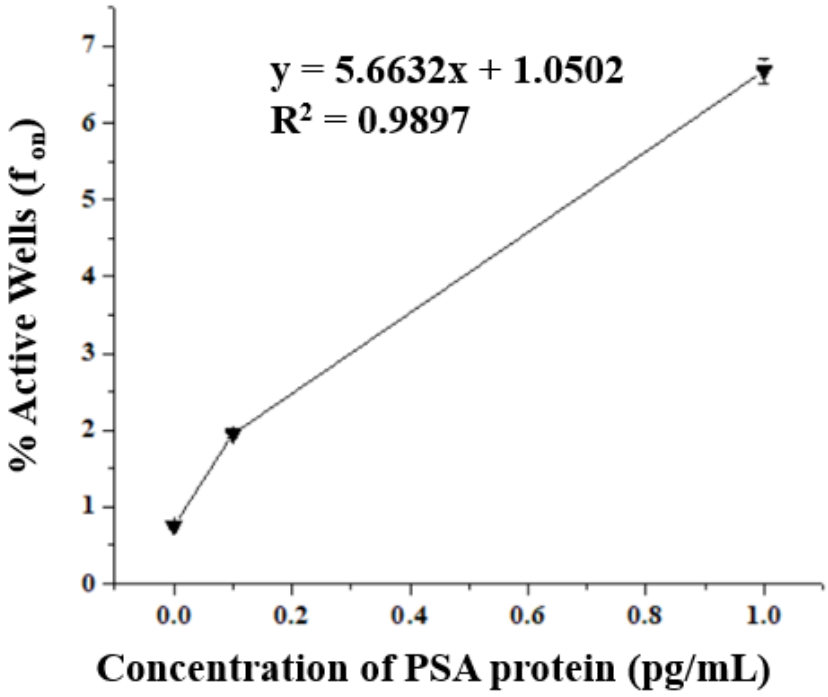

Figure 60: A working concentration range of PSA for digital assay was between 0.1 to 1 pg/mL. Error bars are standard deviations of three replicate experiments.

Table 14: Calculation of λ (average number of molecules per well) values from % active wells for PSA concentration range. The Table clearly showed that the λ increased with the increase in positive wells which increased along with the concentration of PSA detected with Con A lectin.

.

Concentration of PSA protein (pg/mL)	% Active wells (f_{on})	λ
0	0.75	0.004
0.1	1.95	0.03
1	6.68	0.05
10	15.69	0.32
100	27.54	0.42

As shown in Figure 61 PSA aptamer was detected with biotinylated PSA antibody and five biotinylated lectins. Various concentrations from 0.1 – 100pg/mL were used, and percentage of positive wells were compared between PSA antibody and five lectins. Among the five lectins SNA showed more percentage of positive wells as it has the specificity for sialic acid which is present in high quantities and Con A showed a low percentage of positive wells which had specificity for mannose and glucose.

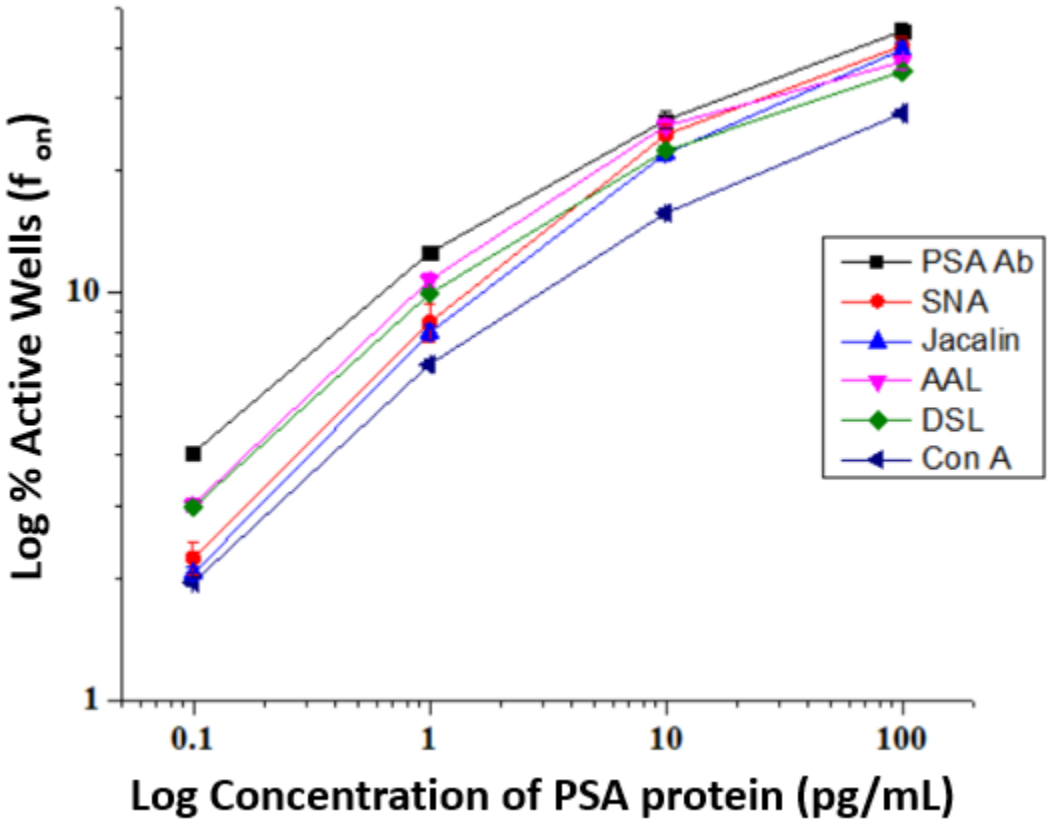

Figure 61: Detection of PSA aptamer with PSA antibody and biotinylated lectins SNA, DSL, Jacalin, AAL and Con A. Error bars are standard deviations of three replicate experiments.

3.4 Conclusion

Here we successfully developed an integrated microfluidic system for rapid and ultrasensitive PSA antigen detection with biotinylated lectins. When compared with other existing microfluidic devices for solid-phase immunoassays, our system was able to perform flow through

immuno-capture in an open channel and subsequently chemifluorescence detection in a reduced volume, by improving the analytical sensitivity. Using this novel method, we demonstrated the quantitative detection of PSA using aptamers and biotinylated lectins, which showed better performance than the commercial ELISA kits. The ability of our assay to quantitatively detect highly glycosylated protein biomarkers across a broad dynamic range will be beneficial for the clinical utilities as the target concentration can vary significantly in patients at different disease states. Moreover, the adaptation of the femtoliter microwell pattern in our design opens opportunity to develop the next-generation microfluidic platforms that integrate and automate both digital and analog immunoassays to facilitate the advance of proteomics.

3.5 References

1. Hirabayashi, J., Concept, Strategy and Realization of Lectin-based Glycan Profiling. *The Journal of Biochemistry* **2008,** *144* (2), 139-147.
2. Yang, Z.; Hancock, W. S., Approach to the comprehensive analysis of glycoproteins isolated from human serum using a multi-lectin affinity column. *Journal of Chromatography A* **2004,** *1053* (1), 79-88.
3. Sun, S.; Shah, P.; Eshghi, S. T.; Yang, W.; Trikannad, N.; Yang, S.; Chen, L.; Aiyetan, P.; Hoti, N.; Zhang, Z.; Chan, D. W.; Zhang, H., Comprehensive analysis of protein glycosylation by solid-phase extraction of N-linked glycans and glycosite-containing peptides. *Nat Biotech* **2016,** *34* (1), 84-88.
4. Nishimura, S.-I., Chapter 5 - Toward automated glycan analysis. In *Advances in Carbohydrate Chemistry and Biochemistry*, Horton, D., Ed. Academic Press: 2011; Vol. 65, pp 219-271.
5. Lauc, G.; Rudan, I.; Campbell, H.; Rudd, P. M., Complex genetic regulation of proteinglycosylation. *Molecular BioSystems* **2010,** *6* (2), 329-335.
6. Xu, C.; Ng, D. T. W., Glycosylation-directed quality control of protein folding. **2015,** *16*, 742.
7. Shang, Y.; Zeng, Y.; Zeng, Y., Integrated Microfluidic Lectin Barcode Platform for High-Performance Focused Glycomic Profiling. **2016,** *6*, 20297.
8. Hirabayashi, J.; Yamada, M.; Kuno, A.; Tateno, H., Lectin microarrays: concept, principle and applications. *Chemical Society Reviews* **2013,** *42* (10), 4443-4458.
9. Ghazarian, H.; Idoni, B.; Oppenheimer, S. B., A glycobiology review: carbohydrates, lectins, and implications in cancer therapeutics. *Acta histochemica* **2011,** *113* (3), 236-247.
10. Kuno, A.; Uchiyama, N.; Koseki-Kuno, S.; Ebe, Y.; Takashima, S.; Yamada, M.; Hirabayashi, J., Evanescent-field fluorescence-assisted lectin microarray: a new strategy for glycan profiling. *Nat Meth* **2005,** *2* (11), 851-856.
11. Roy, B.; Das, T.; Maiti, T. K.; Chakraborty, S., Effect of fluidic transport on the reaction kinetics in lectin microarrays. *Analytica Chimica Acta* **2011,** *701* (1), 6-14.
12. Pilobello, K. T.; Krishnamoorthy, L.; Slawek, D.; Mahal, L. K., Development of a Lectin Microarray for the Rapid Analysis of Protein Glycopatterns. *ChemBioChem* **2005,** *6* (6), 985-989.
13. Gilgunn, S.; Conroy, P. J.; Saldova, R.; Rudd, P. M.; O'Kennedy, R. J., Aberrant PSA glycosylation[mdash]a sweet predictor of prostate cancer. *Nat Rev Urol* **2013,** *10* (2), 99-107.
14. Jolly, P.; Damborsky, P.; Madaboosi, N.; Soares, R. R. G.; Chu, V.; Conde, J. P.; Katrlik, J.; Estrela, P., DNA aptamer-based sandwich microfluidic assays for dual quantification and multi-glycan profiling of cancer biomarkers. *Biosensors and Bioelectronics* **2016,** *79* (Supplement C), 313-319.
15. Meany, D. L.; Zhang, Z.; Sokoll, L. J.; Zhang, H.; Chan, D. W., Glycoproteomics for Prostate Cancer Detection: Changes in Serum PSA Glycosylation Patterns. *Journal of proteome research* **2009,** *8* (2), 613-619.
16. George, D. J.; Halabi, S.; Shepard, T. F.; Sanford, B.; Vogelzang, N. J.; Small, E. J., The prognostic significance of plasma interleukin-6 levels in patients with metastatic hormone-refractory prostate cancer: results from cancer and leukemia group B 9480. *Clin Cancer Res* **2005,** *11*.
17. Munkley, J.; Mills, I. G.; Elliott, D. J., The role of glycans in the development and progression of prostate cancer. *Nature Reviews Urology* **2016,** *13*, 324+.

18. Toh, S. Y.; Citartan, M.; Gopinath, S. C. B.; Tang, T.-H., Aptamers as a replacement for antibodies in enzyme-linked immunosorbent assay. *Biosensors and Bioelectronics* **2015,** *64* (Supplement C), 392-403.
19. Liu, W.; Wei, H.; Lin, Z.; Mao, S.; Lin, J.-M., Rare cell chemiluminescence detection based on aptamer-specific capture in microfluidic channels. *Biosensors and Bioelectronics* **2011,** *28* (1), 438-442.
20. Lou, K.-J., Imaging with aptamers. *Sci BX* **2011,** *4* (11).
21. Jayasena, S. D., Aptamers: An Emerging Class of Molecules That Rival Antibodies in Diagnostics. *Clinical Chemistry* **1999,** *45* (9), 1628-1650.

Chapter 4
Summary and Future Directions

4.1 Summary

To envision our single cell analysis of genotypic and phenotypic changes associated with cancer at the systems level we have developed simple and portable microfluidic tools. Microfluidic digital ELISA is a very powerful tool which is useful to detect different biomarkers at low level concentrations up to femtomolar to attomolar range. As discussed in Chapter 1 microfluidic platforms offer various advantages in handling different biomolecules.

Tracking the protein expression in single cells is in great need as they enable the study of heterogeneous behaviors, but the main challenges are the requirement of the methodologies that are sensitive enough to detect low copy number of protein molecules within a dynamic range.[1] Low copy proteins cannot be neglected as they can provide information about the phenotypic responses involved. Moreover, traditional analog methods are not suitable for detecting such small numbers as they give an average measurement, differentiating unique cells and quantifying population distributions would be problematic.[2] Digital immunoassays have emerged as a robust technology for sub picomolar detection of proteins. To detect the low copy numbers of protein molecules in single cells using digital methods, cross communication between individual reactions, diffusing of reagents into bulk solutions and evaporation of solvents could be critical as mentioned in Chapters 2 and 3.[3] To address this concern, we have developed a portable, automated instrument for sealing the microwells in the chambers with high pressure for conducting chemi- fluorescent reactions with increased resolution and sensitivity. Here we engineered a multiplexed microfluidic digital ELISA platform with microarray structures for analyzing multiple proteins with low sample volume and high sensitivity. With our developed platform, we can detect up to fifteen biomarkers.

At the same time, we also developed an aptamer-lectin based assays for the digital detection of highly glycosylated biomarkers as a replacement of capture antibodies due to their drawbacks as discussed in chapter 3. When compared with other existing microfluidic devices for solid-phase immunoassays, our system could perform flow through immuno-capture in an open channel and subsequently chemifluorescence detection in a reduced volume, by improving the analytical sensitivity.[4] Using this novel method, we demonstrated the quantitative detection of PSA aptamers using biotinylated lectins, which showed better performance than the commercial ELISA kits. The ability of our assay to quantitatively detect highly glycosylated protein biomarkers across a broad dynamic range will be beneficial for the clinical utilities as the target concentration can vary significantly in patients at different disease states.[5] Moreover, the adaptation of the femtoliter microwell pattern in our design opens opportunity to develop the next-generation microfluidic platforms that integrate and automate both digital and analog immunoassays to facilitate the advance of proteomics. Therefore, our microfluidic system is able to substantially enhance the pace of lectin-based assay for high-throughput glycomic profiling. The valve and pump structures hold the complete potential for full automation of the microsystem.[6]

4.2 Future Work

4.2.1 Single Cell Analysis

With the successful results from both the projects the next step would be analyzing the single cells. Ideally, the cell behaves in a system and processes input factors into output behaviors using these internal signaling pathways like diffusion, active transport. The principle processes in each cell is same but the behavior of individual cells can vary significantly. These cell-to-cell interactions and differences play a key role in understanding their signaling pathways associated with several diseases such as cancer. Cells under identical conditions often display a distribution of heterogeneous behaviors.[7] But the response and interaction are not known. So, analyzing single

cells is important. It is the study of individual cells there by provides better resolution of the components involved in the biology. In an ensemble analysis, it is not possible to distinguish between a state in which all cells have an intermediate phenotype (pink cells) and one in which half are on (red cells), half are off (white cells) as shown in the Figure 62.[8-9] Whereas, in single cell analysis we can clearly differentiate the distribution between positive events and negative events. Also results from averaged populations could result in incorrect interpretations of regulatory and physiological mechanisms. To determine the actual mechanism in the disease states, analysis at the single cell level is required. Studying single cells is useful for analyzing various diseases such as cancer.[10]

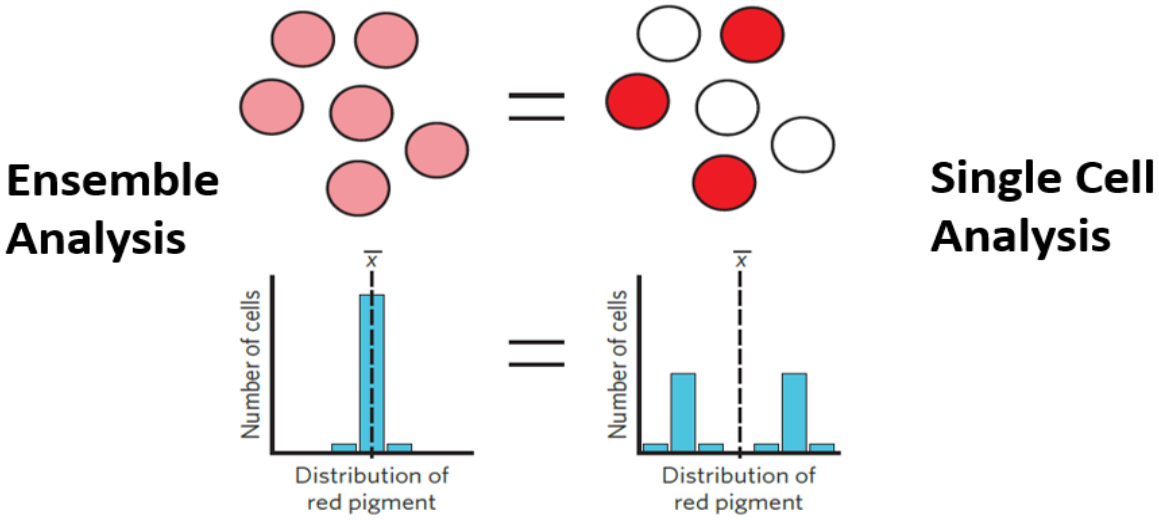

Figure 62: Single cell analysis vs ensemble analysis[9]

Protein expression drives cellular functions like cell development and activity. Changes in the protein concentration can affect the cell phenotype, metabolism, growth and disease progression. Tracking protein expression in single cells enables the study of cellular pathways and cell-cell variations inside the tumor cells. In the pooled sample analysis, we cannot differentiate all the cell types but in the single cell analysis we can clearly see how well they are distributed which thereby

helps to understand the heterogenic behaviors as shown in Figure 63. Single cell technology induces a straightforward process that can detect both high and low protein expression levels which enables both earlier disease detection and targeted therapy.[11]

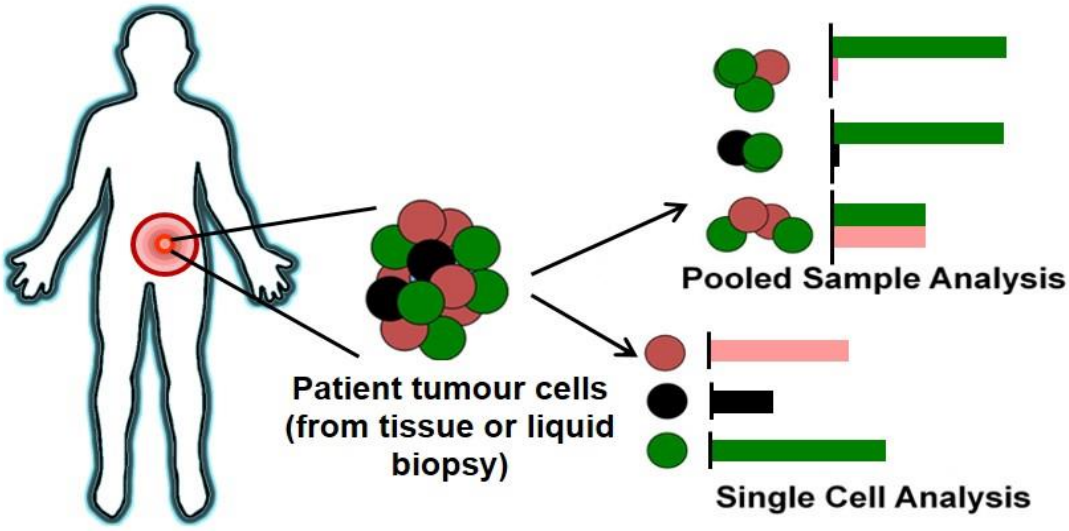

Figure 63: Role of single cell analysis in studying tumor heterogeneity[12]

4.2.2 Methods for trapping single cells

a) Flow Cytometry

There are few methods available for single cell analysis. One of them is flow cytometry which is widely used. It is a cell-based bioanalytical tool for analyzing hundreds of thousands of individual cells according to their size, granularity and fluorescence properties in a wide range of applications, e.g. viability, protein expression and localization, gene expression. It usually uses fluorescent probes to highlight cellular constituents or functions and measures the single cells flowing through the fluorescence detectors as shown in Figure 64.[13-14] However, there are few downsides of using flow cytometry because it is not possible to have large volume of sample always. For example, a blood sample from patient or sample with rare cell types where the volume of the sample is highly limited. Also, it does not provide information about cell to cell interactions

and cell subpopulations with similar biomarker expression levels. The sensitivity is too low as it can detect only 500 copies per cell.[15] The main challenge for tracking the heterogeneous behaviors at the single cell level is the requirement of the methodologies that are sensitive enough to detect low copy number of protein molecules within a dynamic range. These low copy numbers of proteins cannot be neglected as they can provide information about the phenotypic responses involved. It is not well suitable for point of care diagnostics as it is not portable in size and not cost effective.[16]

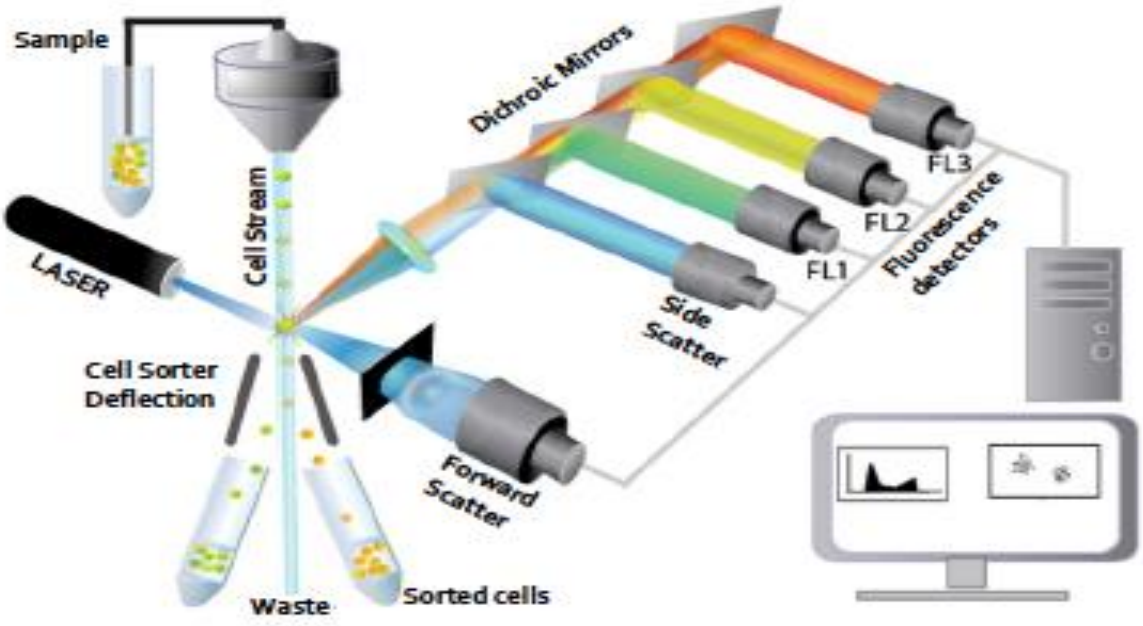

Figure 64: Flow cytometry with different fluorescence detectors.[14]

b) Our Strategy for trapping single cells
Method 1:

One of the methods we plan to design for trapping single cells is shown in Figure 65. The cells can be trapped in micro sized hurdle like structures in the center of a microchamber and they can be repeatedly treated and washed before lysis. The device consists of two layers of PDMS which

are finally bonded on a microscope glass slide. The core features are the chambers with the two central hurdles made of PDMS to physically trap the cells. In the current design, 60 of these chambers are ordered in alternate rows of seven or eight chambers on one microchip and each row is connected via a microchannel. The height of the channels and chambers is 20 μm, which is sufficiently high to allow most mammalian cell types to pass and prevent cellular stress due to shear forces.[17] A ring-shaped valve (200 μm in diameter) surrounds the hurdles. When actuated, it isolates the trapped cells from the surrounding solution in a volume of 625 pL. Every microchamber within a row can be opened and closed individually, which enables a sequential supply of reagents to every single microchamber along the microchannel with virtually no cross-contamination. After the lysis step, and the addition of the immunoassay compounds, the small volume of the microchambers prevents dilution of the target molecules and the fluorescent product, hence guaranteeing a high sensitivity.[18]

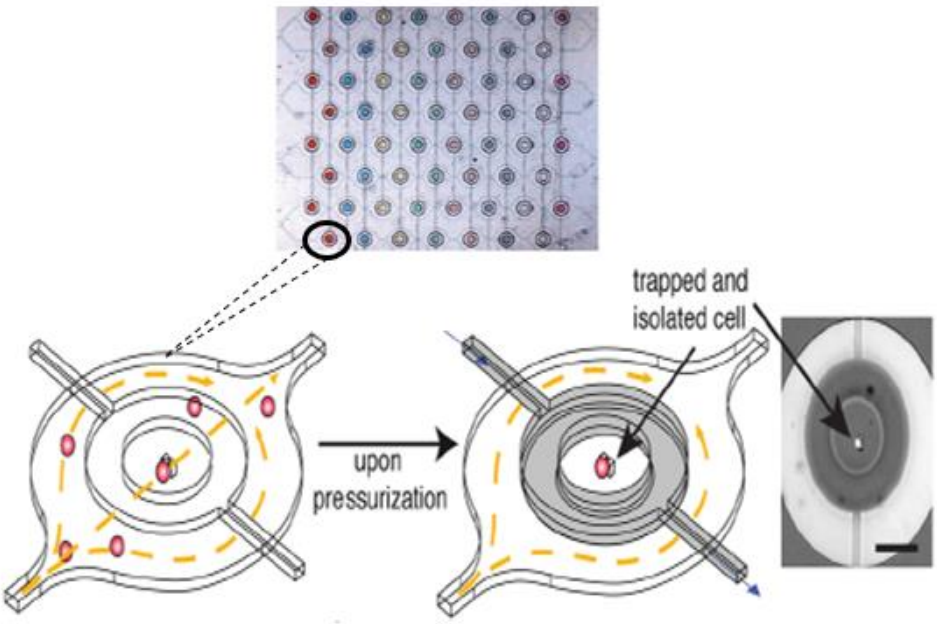

Figure 65: Schematic of a microchamber which is used to introduce and trap a cell inside the micro hurdle feature and to deliver compounds to the cell. The trapped cell can be isolated from the environment by hydraulic actuation of a ring-shaped valve (gray color). The image on the right is a fluorescent micrograph. the device consists of 60 hurdles and chambers. As shown by the different trapped food dyes, the chambers of one row can be actuated individually, thereby avoiding cross-contamination.[17]

Method 2:

The second method includes the fabrication of a microarray that can capture single cells inside an array without using pumps or tubing to help the fluid flow within the device. The passive-flow microfluidic device consists of physical traps which are embedded in a center channel, connecting an inlet and an outlet reservoir. Fluid flow through the channel could be achieved by altering the surface of the channel.[19] By treating the glass surface and the inner walls of the PDMS microchannel with oxygen plasma polar functional groups could be introduced on PDMS, thus providing the hydrophilic surface. The basic trap shapes could be in S-shaped square pillars with

approximate dimensions of 10 mm-10 mm and V-shaped rectangular pillars could be 10 mm - 7 mm both with sides inclined at 30°C and separated by a 5mm gap as shown in Figure 66.

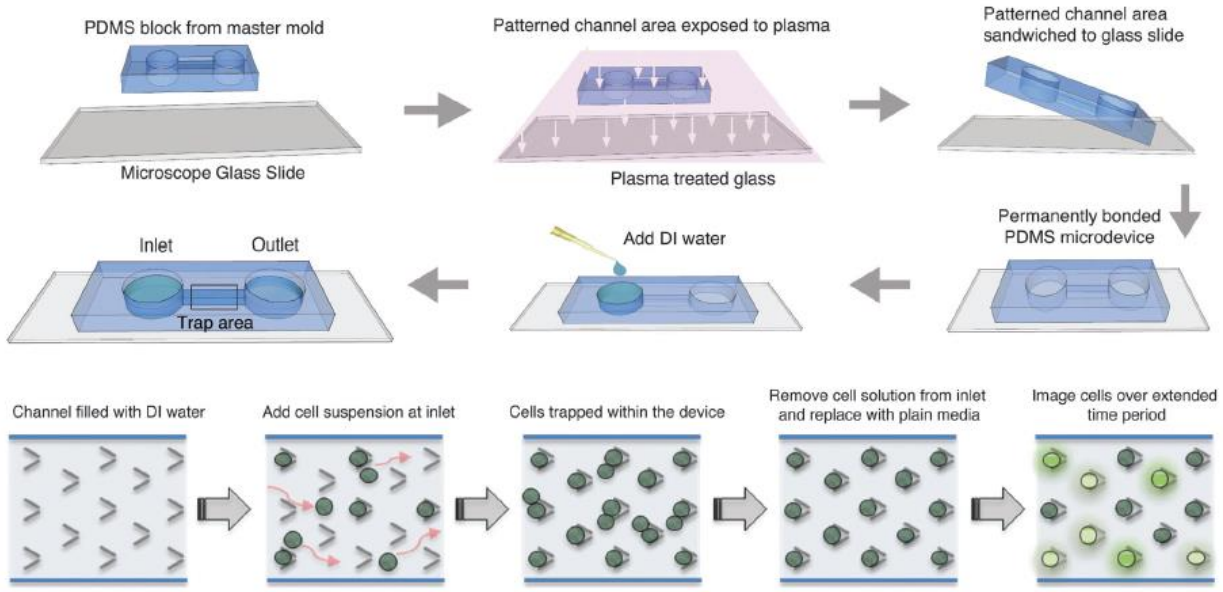

Figure 66: Design and operation of the passive-flow microfluidic device with schematic diagram of the microfluidic device fabrication process and a brief protocol to trap single cells in the passive-flow microfluidic device.[19]

Therefore, lysis chip will be designed as shown in Figure in which the cells will be lysed and then the target antigens will be detected with digital ELISA devices.

4.3 References

1. Spiller, D. G.; Wood, C. D.; Rand, D. A.; White, M. R. H., Measurement of single-cell dynamics. *Nature* **2010,** *465* (7299), 736-745.
2. Liu, Y.; Singh, A. K., Microfluidic Platforms for Single-Cell Protein Analysis. *Journal of Laboratory Automation* **2013,** *18* (6), 446-454.
3. Cai, L.; Friedman, N.; Xie, X. S., Stochastic protein expression in individual cells at the single molecule level. *Nature* **2006,** *440* (7082), 358-362.
4. Fan, R.; Vermesh, O.; Srivastava, A.; Yen, B. K. H.; Qin, L.; Ahmad, H.; Kwong, G. A.; Liu, C.-C.; Gould, J.; Hood, L.; Heath, J. R., Integrated barcode chips for rapid, multiplexed analysis of proteins in microliter quantities of blood. *Nat Biotechnol* **2008,** *2*.
5. Nishimura, S.-I., Chapter 5 - Toward automated glycan analysis. In *Advances in Carbohydrate Chemistry and Biochemistry*, Horton, D., Ed. Academic Press: 2011; Vol. 65, pp 219-271.
6. Jayasena, S. D., Aptamers: An Emerging Class of Molecules That Rival Antibodies in Diagnostics. *Clinical Chemistry* **1999,** *45* (9), 1628-1650.
7. Di Carlo, D.; Wu, L. Y.; Lee, L. P., Dynamic single cell culture array. *Lab Chip* **2006,** *6*.
8. Pan, X., Single Cell Analysis: From Technology to Biology and Medicine. *Single cell biology* **2014,** *3* (1), 106.
9. Lidstrom, M. E.; Konopka, M. C., The role of physiological heterogeneity in microbial population behavior. **2010,** *6*, 705.
10. Wu, M.; Singh, A. K., Single-Cell Protein Analysis. *Current Opinion in Biotechnology* **2012,** *23* (1), 83-88.
11. Wills, Q. F.; Mead, A. J., Application of single-cell genomics in cancer: promise and challenges. *Human Molecular Genetics* **2015,** *24* (R1), R74-R84.
12. Brown, J. M.; Attardi, L. D., The role of apoptosis in cancer development and treatment response. *Nat Rev Cancer* **2005,** *5*.
13. Di Carlo, D.; Aghdam, N.; Lee, L. P., Single-cell enzyme concentrations, kinetics, and inhibition analysis using high-density hydrodynamic cell isolation arrays. *Anal Chem* **2006,** *7*.
14. Han, Y.; Lo, Y.-H., Imaging Cells in Flow Cytometer Using Spatial-Temporal Transformation. **2015,** *5*, 13267.
15. Gawad, C.; Koh, W.; Quake, S. R., Single-cell genome sequencing: current state of the science. *Nat Rev Genet* **2016,** *17* (3), 175-188.
16. Lu, Y.; Chen, J. J.; Mu, L.; Xue, Q.; Wu, Y.; Wu, P.-H.; Li, J.; Vortmeyer, A. O.; Miller-Jensen, K.; Wirtz, D.; Fan, R., High-Throughput Secretomic Analysis of Single Cells to Assess Functional Cellular Heterogeneity. *Analytical Chemistry* **2013,** *85* (4), 2548-2556.
17. Eyer, K.; Stratz, S.; Kuhn, P.; Küster, S. K.; Dittrich, P. S., Implementing Enzyme-Linked Immunosorbent Assays on a Microfluidic Chip To Quantify Intracellular Molecules in Single Cells. *Analytical Chemistry* **2013,** *85* (6), 3280-3287.
18. Oshima, Y.; Yajima, S.; Yamazaki, K.; Matsushita, K.; Tagawa, M.; Shimada, H., Angiogenesis-related factors are molecular targets for diagnosis and treatment of patients with esophageal carcinoma. *Ann Thorac Cardiovasc Surg* **2010,** *16*.
19. Ramji, R.; Wong, V. C.; Chavali, A. K.; Gearhart, L. M.; Miller-Jensen, K., A passive-flow microfluidic device for imaging latent HIV activation dynamics in single T cells. *Integrative Biology* **2015,** *7* (9), 998-1010.